AD NUMBER
AD324796
CLASSIFICATION CHANGES
TO: **unclassified**
FROM: **confidential**
LIMITATION CHANGES
TO: **Approved for public release; distribution is unlimited.**
FROM: **Controlling Organization: British Embassy, 3100 Massachusetts Avenue, NW, Washington, DC 20008.**
AUTHORITY
DSTL, DSIR 23/28861, 11 Dec 2008; DSTL, DSIR 23/28861, 11 Dec 2008

ROYAL AIRCRAFT ESTABLISHMENT

(FARNBOROUGH)

REPORT No: G.W. 24

THE BLACK KNIGHT TEST VEHICLE CONTROL SYSTEM

by

A. P. MACLAREN, B.S.c. and

Squadron Leader G. E. THIRLWALL, R.A.F.

FEBRUARY, 1961

MINISTRY OF AVIATION

U.D.C. No. 621-52 : 623.451-519

Report No. G.W.24

February, 1961

ROYAL AIRCRAFT ESTABLISHMENT

(FARNBOROUGH)

THE BLACK KNIGHT TEST VEHICLE CONTROL SYSTEM

by

A. P. MacLaren, B.Sc.
and
Squadron Leader G. E. Thirlwall, R.A.F.

SUMMARY

In this Report the closed-loop control system for the ballistic test vehicle Black Knight is described and an account is given of the theory underlying its design. Attitude control of the vehicle is achieved by swivelling the four rocket motor combustion chambers in response to gyroscope and command guidance signals. The effects of propellent sloshing, aerodynamic instability and flexibility of the vehicle structure are among the factors taken into account in determining transfer functions, relating combustion chamber movements to gyroscope signals, which satisfy the conditions for stable flight.

In the final section a brief account is given of ground tests, which resulted in some alterations to the roll stabilisation system, and of early flight trial results. The control system has performed very satisfactorily in all flights to date.

Report No. G.W.24

LIST OF CONTENTS

LIST OF TABLES

LIST OF ILLUSTRATIONS

LIST OF ILLUSTRATIONS (Cont'd)

LIST OF ILLUSTRATIONS (Cont'd)

1 INTRODUCTION

Black Knight[1] is a ballistic test vehicle intended for research into problems associated with ballistic missiles, especially that of high speed re-entry into the atmosphere. The development of Black Knight is also expected to yield useful experience in the design and operation of the type of control system used in ballistic missiles.

The layout of Black Knight is shown in Fig.1. Four swivelling rocket motors, burning kerosene and hydrogen peroxide (H.T.P.), are used for propulsion and attitude control of the vehicle. Each motor has a sea-level thrust of 4000 lb and can be rotated through $\pm 10^{\circ}$ about a single axis by an electro-hydraulic position control servo-mechanism. Opposite pairs are deflected together to provide pitch and yaw attitude control and all four differentially for roll stabilisation. The motor pivot axes are so inclined that the direction of thrust makes an angle of $5\frac{3}{4}^{\circ}$ with the vehicle centre line, in order to reduce disturbances which might arise if the motor thrusts were unequal, particularly near all-burnt. The swivelling combustion chambers are supported by a composite structure which transmits thrust and other loads to the base of the H.T.P. tank. Propellents are pumped in through the trunnion mountings, kerosene through the outer bearing and H.T.P. through the inner. The 3 ft diameter body, of welded* aluminium alloy construction, is fitted with fixed fins at the rear to improve the aerodynamic characteristics of the vehicle. To minimise the weight penalty, however, the fins are not large enough to make the airframe aerodynamically stable throughout flight. At take-off a typical vehicle weighs about 12,800 lb, of which propellents comprise approximately 11,400 lb. The initial acceleration is thus 1.25g (0.25g excess) and the velocity and altitude at all-burnt, after 145 sec of powered flight, are about 11,500 ft per sec and 400,000 ft respectively. During the ballistic phase peak altitudes of about 500 miles are attained.

Guidance[20] is by radio command link. Deviations from the desired flight path, in the form of displacement and velocity components in two orthogonal planes, corresponding to the pitch and yaw planes when the vehicle is correctly roll stabilised, are derived from radar or optical sources and displayed on cathode ray tubes to two operators. The latter are able to vary the vehicle heading to keep it on course by transmitting, when necessary, discrete correction signals via a radio link. In the early part of flight, when the desired trajectory is vertical, guidance information is obtained from two M2 optical trackers situated respectively 8000 yards behind and to the left of the launcher. Above 20,000 ft the desired flight path is a straight line inclined at 1° 50' to the vertical in order that re-entry may take place over the impact area 50 to 60 miles down range. For this part of the powered ascent phase, guidance information is obtained either from a modified S.C.R.584 radar, with its aerial dish fixed at a Q.E. of 88° 10', or from an optical telescope system in which the rocket motor flame is tracked manually. A transponder is carried in one of the vehicle fin pods to enable sufficient radar range with good signal to noise ratio to be obtained. Filters with 1, 2 and 4 sec time constants, which can be inserted as required by the operators between the radar resolvers and the displays, are provided to smooth the error and rate signals.

Command signals are transmitted over the 79 Mc/s radio link in the form of short pulses of audio frequency modulation. Four audio frequency tones, which correspond to left, right, up and down command signals respectively, are available. These tones may also be transmitted continuously together to command self destruction in the event of the vehicle behaving in a dangerous manner. Discrimination between tones is accomplished by means of tuned filters in the receiver. Each command pulse is converted by the command units shown in

---

*Prototype design was riveted.

Fig.2 into a demand for 0.25° change of heading in the pitch or yaw plane. Fig.3 shows the circuit diagram of the command units; these effectively integrate the heading changes commanded in the two planes of control, their output voltages at any time being proportional to the algebraic sum of the heading changes demanded since take-off. The relay shown is used to short circuit the integrator capacitors until a few seconds before take-off. To limit the rate of turn demanded by the guidance system to one degree per second, the rate at which pulses can be transmitted, via any one audio frequency channel, is fixed at four per second. The operators guide the vehicle by controlling the duration of the pulse trains transmitted from time to time.

A schematic block diagram of the control system is shown in Fig.2. Roll error and heading angle signals are obtained from two free gyroscopes fitted with A.C. angular displacement pick-offs[12] on each gimbal axis. Signals from the inner gimbal pick-offs are used for pitch and yaw control and from both outer gimbal pick-offs for roll stabilisation. Any change of roll datum after the gyroscopes are uncaged is thus equal to the average drift of both gyros about their outer gimbal axes. The vehicle is roll stabilised by feeding signals which are functions of roll error and roll rate, derived from a phase advance network and associated amplifier, to the four motor servos. For pitch and yaw control the demodulated gyro signals are passed through a phase advance network and amplifier and, in a parallel branch, added to the command unit output signals by means of a summing amplifier. The outputs from the phase advance and summing amplifiers are passed through the gain programming unit and combined with the roll control signals in the summing networks of the motor servo amplifiers. The gain programming unit consists essentially of four motor driven potentiometers which vary the lateral control feedback loop gains in a predetermined manner as the flight proceeds.

The theoretical design and analysis of the control system should take into account all the factors which influence the stability of the system. The following are the main ones which have been considered.

(i) The vehicle airframe is aerodynamically unstable in pitch and yaw during the greater part of the powered flight period. In other words its centre of pressure is then situated ahead of its centre of gravity.

(ii) The vehicle has a flexible structure and hence the control gyroscopes sense local deflections of the structure in addition to the desired motion of the vehicle as a whole.

(iii) The mass, moments of inertia etc of the vehicle and the aerodynamic forces and moments acting on it change greatly during the powered flight period.

(iv) Liquid propellents with free surfaces form a large proportion of the total mass and give rise to "sloshing" effects.

In general these factors increase the difficulty of designing a satisfactory control system. For instance, when the vehicle is aerodynamically unstable, the heading control feedback loops can only maintain stability if the gain exceeds a certain minimum value which depends on the aerodynamic moment derivative. Otherwise any disturbance, e.g. a gust or wind shear, would cause the vehicle to overturn since the disturbing moment would increase more rapidly than the restoring moment. Hence the condition of maximum aerodynamic instability is one of the critical design cases. On the other hand, if the loop gain is too high the system will be oscillatory, as with any feedback control system. In the case of a flexible missile the value of gain which

makes the system oscillate depends not only on the response of the control system components but also on the body bending and torsional modes, location of the gyroscopes etc.

The purpose of the analysis which follows is to determine what response the control system components should have and what values of gain should be specified to ensure that the system will remain stable under all conditions likely to occur in flight. The analysis is based mainly on the original estimates of aerodynamic and other vehicle parameters but the effect of later modifications is referred to where appropriate. Linear servo-mechanism theory and frequency response methods are used throughout. Quasi-static stability only is investigated; in other words the vehicle parameters such as mass, speed etc are assumed constant for each instant of flight considered although in reality they vary continuously with time. This assumption that stability depends on instantaneous values of parameters and not on their rates of change, is not thought likely to lead to grossly erroneous conclusions, as the rates of change are generally relatively small, but it should be borne in mind especially when very low frequencies (below say 0.5 c/s) are considered. Motor servo non-linearities are allowed for, to some extent, by using experimentally determined frequency response curves for four different amplitudes of input signal. As the vehicle is roll-stabilised and symmetrical, apart from the fin pods, cross-coupling effects are neglected and the stability of the heading control system in one plane (yaw) only is investigated. The pitch plane control system is assumed to be identical since the aerodynamic estimates used are based on the original configuration which had no pods. These were introduced as a modification to avoid unacceptable losses in the transponder aerial feeder cable. Since the pods actually make the airframe somewhat more stable in yaw than in pitch, their effect is to give the yaw control system a greater margin of stability than is indicated by the analysis. The gyroscopes are assumed to be located in the electronics bay at approximately 28 ft from the base datum. This position was chosen, after preliminary consideration of the stability problem, mainly for reasons of convenience of installation and because it was thought that the vibration environment would be less severe than for locations nearer the rocket motors. Since it was found that a stable system could be obtained for this gyroscope position alternative locations have not been seriously considered.

The first part of the Report is concerned with the stability of the heading control system which may be represented, for this purpose, by the simplified block diagram shown in Fig.4. In designing a closed loop control system it is necessary to obtain an expression for the open loop, or feedback, transfer function. To this end it is convenient to regard the system as consisting of an arbitrary number of interconnected blocks the transfer functions of which can be determined fairly readily. The transfer function of a transmission path through a system component is defined as the ratio of the Laplace transform of the output signal to the Laplace transform of the input signal. The Laplace transform of a function $f(t)$ of the real variable t is given by

$$F(p) = \int_0^\infty e^{-pt} f(t)\, dt \qquad (1)$$

where p is a complex variable $\sigma + j\omega$. The transfer function of any block or component will be denoted by $Y_n(p)$, or simply Y_n as in Fig.4, and the corresponding frequency response function by $Y_n(j\omega)$, the suffix indicating the block concerned. Transfer functions are also expressed in the form

$Y_n(p) = K_n G_n(p)$ where K_n is a gain factor which is independent of frequency and $G_n(p)$ or $G_n(j\omega)$ denotes the frequency dependent part. Having determined the transfer functions of the individual blocks, the open loop transfer function is obtained simply by adding or multiplying these as indicated by the block diagram. This implies that no appreciable interaction, which would alter their transfer functions, occurs between blocks when they are connected together such as, for example, loading of the output circuit of one by the input circuit of the next. This has been taken into account in drawing the block diagram and in the design of the components. Section 2 is devoted to the missile dynamics transfer function $Y_2(p)$, which relates the yaw gyroscope pick-off output to movements of the yaw motors and section 3 deals briefly with the response characteristics of the rocket motor servos and gyroscope signal demodulators. In sections 4, 5 and 6 the stability of the heading control system is examined, first at the critical time of maximum aerodynamic instability and then at other times. Propellent sloshing effects and the design of the roll stabilisation system are dealt with in sections 7 and 8 and finally, in section 9, a brief account is given of ground test and flight trial results.

2 DERIVATION OF THE MISSILE DYNAMICS TRANSFER FUNCTION IN THE YAW PLANE

It has been shown by Graham and Rodrigne[2] that, for the purpose of calculating the forces and moments due to small oscillations of an incompressible, inviscid liquid in a vertical rectangular tank, an equivalent mechanical system may be used. This consists of a fixed mass plus an infinite set of moving masses attached to the tank walls by means of springs and constrained to move horizontally. Each spring-mass combination represents one of the characteristic modes of oscillation or sloshing. The analysis of Ref.2 has been extended to the case of a vertical cylindrical tank by Stafford[3] and numerical values for the masses, spring rates etc for Black Knight have been calculated[4]. In the case of Black Knight it is only necessary to consider the fundamental sloshing mode for each tank since the moving masses associated with the overtone modes are small enough to be negligible. For instance in the early part of flight the moving masses associated with the fundamental H.T.P. and kerosene sloshing modes are 13.0 and 7.4 slugs, respectively, whereas the corresponding second mode masses are only 0.4 and 0.2 slugs. Fig.5 shows diagrammatically the equivalent missile based on this mechanical analogue. As the propellents are consumed during flight the locations and magnitudes of the masses etc vary with time. The curves of Fig.6 show the estimated variation of the "effective" mass, lateral moment of inertia and centre of gravity position compared with corresponding values calculated on the assumption that, at any instant, the propellents remaining in the tanks are solidified. The "effective" values are calculated from the mass etc of the empty vehicle plus the "fixed" part of both propellents. Sprung masses are not included; thus the difference between the total mass and the "effective" mass at any time is equal to total of the sloshing mode moving masses. The curves of Fig.6 are based on original estimates[4] of the vehicle parameters, rates of propellent consumption etc.

The complete missile dynamics transfer function, including aerodynamic body flexure and propellent sloshing effects all together, is complicated and inconvenient to use. To show more clearly their influence on the stability of the control system these effects have been treated separately as far as possible. It has been assumed, for example, that body flexure effects are independent of aerodynamic and sloshing forces and depend only on rocket motor thrust and inertia forces. Similarly propellent sloshing effects are ignored at this stage, though "effective" values of centre of gravity position, mass etc, as defined above, have been used throughout in calculating numerical values of aerodynamic parameters and transfer function coefficients.

Neglecting propellent sloshing, the equations of motion in yaw of a rigid missile may be written in the form

$$m(\dot{v} + ur) = Y_v v + Y_r r + \frac{T}{2}\delta + mg\psi \qquad (2)$$

$$C\dot{r} = N_v v + N_r r - \frac{T\ell}{2C}\delta \qquad (3)$$

where the dot denotes differentiation with respect to time,

ψ = the heading angle of the missile with respect to a fixed vertical datum;

r = $\dot{\psi}$ = the rate of turn of the missile;

δ = the deflection of the two rocket motors used for control in yaw (see Figs.1 and 5), δ and ψ are assumed small such that $\sin\delta \doteq \delta$ and $\cos\delta \doteq 1$ etc;

T = $T_T \cos 5\frac{3}{4}^{\circ}$, where T_T is the total thrust of the motors,

= the component of thrust of four undeflected rocket motors along the missile axis;

u, v = respectively the forward and lateral components of velocity (see Fig.5);

m, C = respectively the mass and lateral moment of inertia of the missile;

ℓ = the distance of the centre of gravity from the motor pivot station;

g = the acceleration due to gravity;

Y_v, Y_r = the aerodynamic normal force derivatives with respect to v and r

N_v, N_r = the corresponding aerodynamic moment derivatives.

Expressing equations (2) and (3) in terms of Laplace transforms, assuming all the above parameters, except ψ, δ and v and their derivatives, to be constant, and eliminating $\bar{v}$ yields the rigid missile dynamics transfer function

$$\frac{\bar{\psi}}{\bar{\delta}} = \frac{-\frac{T\ell}{2C}p + \frac{T}{2mC}(N_v + \ell Y_v)}{p^3 - \left(\frac{Y_v}{m} + \frac{N_r}{C}\right)p^2 + \left(\frac{uN_v}{C} + \frac{Y_v N_r - N_v Y_r}{mC}\right)p - \frac{gN_v}{C}} \qquad (4)$$

where $\bar{\psi}$, $\bar{\delta}$ and $\bar{v}$ denote Laplace transforms of ψ, δ and v.

The aerodynamic derivatives N_v, N_r and Y_v for the original Black Knight configuration at zero incidence have been estimated by Stafford[5] and their variation with time, for the assumed standard trajectory, is shown in Fig.7. Y_r is assumed to be negligible. It is evident that these derivatives vary considerably during the powered flight period, the airframe being unstable (N_v negative) after the first 24 sec. In calculating the aerodynamic yawing moments about the C.G. the "effective" centre of gravity (Fig.6) has been used as this gives a greater yawing moment than would have been obtained if the C.G. based on instantaneously solidified propellents had been used. The results of wind tunnel tests[6] to measure normal force and pitching moment of the Black Knight configuration at various values of Mach number and incidence became available after the control system had been designed on the basis of Stafford's estimates. As the tunnel tests indicated that the airframe was less unstable than had been estimated it was decided that no alterations to the system were necessary. Fig.8 shows the estimated variation with time of total motor thrust, missile acceleration, velocity and altitude assumed when the aerodynamic derivatives of Fig.7 were calculated. Numerical values for the coefficients of expression (4) can be computed as required from the data given in Figs.6, 7 and 8. For example, the variation with time of the coefficient $T\ell/2C$, which gives the angular acceleration per unit deflection of the yaw motors in the absence of aerodynamic forces, is shown in Fig.8 also.

Since the missile is flexible the angle ψ_G detected by the yaw gyroscope includes a component ψ_F proportional to the angular deflection of the body at the gyroscope station in addition to the desired rigid body heading angle ψ. Near the body resonance frequencies the unwanted feedback due to this body flexure component may be sufficient to cause control system instability and precautions may be necessary to prevent this. Thus we have

$$\psi_G = \psi + \psi_F \qquad (5)$$

where ψ_F is a function of the vehicle mass and stiffness distribution, the location of the gyroscope, the lateral force F and reaction couple L at the motor pivot. It is assumed that ψ_F is independent of ψ and that aerodynamic forces do not contribute materially towards exciting oscillations at the body resonance frequencies. For small δ the exciting force and couple are given by

$$F = \tfrac{1}{2} T \delta + 2 M_c d \ddot{\delta} \qquad (6)$$

and

$$L = 2 I_c \ddot{\delta} \qquad (7)$$

where I_c and M_c = respectively the moment of inertia about its pivot and the mass of one combustion chamber.

d = the distance of the combustion chamber centre of mass behind the pivot axis.

In the case of Black Knight the combustion chambers are pivoted about axes which pass very close to their centres of mass ($d \doteq 0$) and hence the term $2 M_c d \delta$ in equation (6) can be neglected.

It is assumed that the Laplace transform of the body flexure angle ψ_F is given by

$$\bar{\psi}_F = \sum_{n=1}^{\infty} \frac{H_{nF}\bar{F} + H_{nL}\bar{L}}{1 + \frac{2\zeta_n}{\omega_n}p + \frac{1}{\omega_n^2}p^2} \qquad (8)$$

where $\omega_n = 2\pi f_n$ where f_n is the nth mode resonance frequency

ζ_n = the damping factor associated with the nth mode

H_{nF} and H_{nL} = constants for the nth mode equal to $2\zeta_n \times$ the angular deflection amplitude (in radians) at the gyro station at resonance per lb lateral exciting force and per lb ft couple, respectively, applied at the motor pivot axis.

Combining equations (6), (7) and (8) we obtain the body flexure part of the missile dynamics transfer function[7]

$$\frac{\bar{\psi}_F}{\bar{\delta}} = \sum_{n=1}^{\infty} \frac{\frac{1}{2}H_{nF}T + 2H_{nL}I_c p^2}{1 + \frac{2\zeta_n}{\omega_n}p + \frac{1}{\omega_n^2}p^2} \cdot \qquad (9)$$

Bending mode shapes, values of the resonance frequencies f_n and angular amplitudes of missile deflection at the gyro station due to lateral forces and couples at these frequencies applied at the motor pivots have been calculated by Donno[8]. The numerical values are given in Table 1 and Fig.9 shows the estimated variation with time of the first four resonance frequencies. For these calculations the missile was assumed to be an elastic free-free beam and, in the absence of more precise information, the damping factor ζ_n was taken as 0.01 (i.e. 1% of critical) for all modes. Damping of vibrating structures is usually assumed to be hysteretic, the damping force being proportional to displacement and in phase with velocity. As it is not feasible to express this in transfer function form, viscous damping has been assumed. It has been shown by Bishop[9] that, when hysteretic damping is small, the frequency response of a single degree of freedom system is very similar to that obtained on the assumption of viscous damping.

Equation (9) may be written in the form

$$\frac{\bar{\psi}_F}{\bar{\delta}} = \sum_{n=1}^{\infty} \frac{h_n\left(1 + \frac{p^2}{u_n^2}\right)}{1 + \frac{2\zeta_n}{\omega_n}p + \frac{1}{\omega_n^2}p^2} \qquad (10)$$

where $h_n = \frac{1}{2} T H_{nF}$ and $u_n^2 = \frac{T H_{nF}}{4 I_c H_{nL}}$. $\frac{u_n}{2\pi}$ is the frequency of motor oscillation at which excitation of the nth mode by motor thrust forces is cancelled by that due to the inertia reaction couple L. The magnitude and sign of h_n depend on the mode shape and the position of the gyroscope relative to the nodes. h_n is positive if positive motor deflection δ, shown in Fig.5, tends to produce positive ψ_F for the mode considered. Since the proposed gyro position is forward of the foremost node for the first four modes, h_n is positive for the first and third and negative for the second and fourth modes. Curves are given in Figs.10 and 11 which show how the factors h_1 and h_2 and the frequencies $u_1/2\pi$ and $u_2/2\pi$ for the first and second bending modes vary during the powered flight period. The higher modes have been omitted as they have been found to have negligible influence. These curves are based on the data given in Table 1, the thrust/time curve of Fig.8 and an estimated combustion chamber moment of inertia of 0.7* slug ft^2. General frequency response curves corresponding to the functions $(1 + p^2/u_n^2)$ and $\frac{1}{1 + \frac{2\zeta_n}{\omega_n} p + \frac{1}{\omega_n^2} p^2}$ for $\zeta_n = 0.01$ are given in Figs.12 and 13.

Specific transfer functions for particular times and the corresponding frequency response curves can be obtained as required from equation (10) by substituting the appropriate values of h_n, u_n and ω_n from the data given in the figures. Examples are given in sections 4 and 5.

By equation (5), the general form of the missile dynamics transfer function Y_2, neglecting propellent sloshing effects, is given by the sum of expressions (4) and (10). Thus

$$\frac{\psi_G}{\delta} = \frac{-\frac{T\ell}{2C} p + \frac{I}{2mC}(N_v + \ell Y_v)}{p^3 - \left(\frac{Y_v}{m} + \frac{N_r}{C}\right) p^2 + \left(\frac{uN_v}{C} + \frac{Y_v N_r - N_v Y_r}{mC}\right) - g\frac{N_v}{C}} + \sum_{n=1}^{\infty} \frac{h_n\left(1 + \frac{p^2}{u_n^2}\right)}{1 + \frac{2\zeta_n}{\omega_n} p + \frac{1}{\omega_n^2} p^2} \quad \ldots.(11)$$

3 CHARACTERISTICS OF THE MOTOR SERVOS AND GYROSCOPE DEMODULATORS

Before the stability of the heading control system as a whole is considered a brief description of these components is necessary. The motor servos are designed to operate at a hydraulic pressure of 3000 lb per sq in. and to have a stall torque of 450 lb ft. This latter figure was chosen to make the servo performance insensitive to trunnion friction and thrust misalignment torques, which at the time were not accurately known, and to meet a frequency response specification that the servos should be capable of moving the motors approximately sinusoidally at a frequency of 10 c/s with an amplitude of 5°. Hydraulic power is obtained in flight from two oil pumps, driven by two of the four propellent pump turbines, in conjunction with an hydraulic accumulator. When

---

*Actual value 0.63 slug ft^2.

the latter is fully charged the pressure rises to 3,300 p.s.i. and the pump delivery is by-passed to the reservoir through an off-loading valve. Oil for the servos is then supplied from the accumulator until the pressure drops to 2,700 p.s.i. when recharging of the accumulator commences.

The layout of the hydraulic servo is shown diagrammatically in Fig.14.

Oil flow to the cylinders is controlled by a single stage 5/32" diameter spool valve connected by a torque arm to the shaft of an E.12 torque motor (commonly known as the Laws relay)[10] which is totally enclosed and immersed in oil. The valve stem profile and the valve liner are shaped to reduce the flow reaction forces to a low level and the torque motor is fitted with a restoring spring to give optimum loading of this component and to make its performance insensitive to variations in pressure and flow conditions[11,12]. The actuator cylinders are connected by a low leakage bleed pipe, not shown in Fig.14, to minimise peak pressures and improve servo stability. Motion of the actuator pistons is transmitted to the rocket motor combustion chamber via a torque arm and two struts with ball joints at each end. Backlash and wear are automatically taken up with this arrangement.

Angular position feedback is derived from an A.C. pick-off[13] the rotor of which is turned through twice the combustion chamber angle by a mechanical linkage. The pick-off output is demodulated and fed back to one of the servo amplifier input summing resistors as indicated in Fig.2. Circuit diagrams of the demodulator and servo amplifier are shown in Figs.15 and 16. These components and the 36 volt 1,300 c/s inverter, which supplies the pick-offs and demodulators, are located in the electronics bay near the front of the vehicle. Primary electrical power supplies are obtained from batteries. The gain of each servo demodulator is set, in conjunction with its associated pick-off, to give 1 volt (D.C.) per degree of motor deflection and the gain of the servo amplifiers is adjusted to give a differential current of 16 mA through the torque motor coils per volt input. Thus a D.C. signal to any of the servo amplifier 1 MΩ summing resistors results in a steady motor deflection of one degree per volt input. Hence K_1 = 1 degree per volt.

Since the dynamic behaviour of the motor servos is rather non-linear, a describing function based on experimentally determined frequency response characteristics of a prototype unit has been used for system design purposes instead of an approximate analytical expression for the servo transfer function Y_1. This describing function $G_1(j\omega)$ is illustrated in Fig.17 as a family of gain and phase curves for constant amplitude sinusoidal input signals of 0.5, 1, 2 and 5 volts with frequencies from 1 to 100 c/s. At low frequencies these inputs give motor deflection amplitudes of approximately 0.5, 1, 2 and 5 degrees respectively. At higher frequencies when the motor angle waveform is not sinusoidal the gain and phase curves are based on the fundamental component of the output waveform. It can be seen from Fig.17 that for frequencies below 7 c/s the phase lag increases as the amplitude decreases. This is due to the use of circular ports in the valve liner and to valve lap and stiction effects. Acceleration and velocity saturation are responsible for the increased attenuation and phase lag which are apparent for the larger amplitude signals at higher frequencies. Reduction of the feedback gain from the specified figure of 16 mA per degree of motor error has the effect of increasing the phase lag, especially for small amplitude low frequency input signals.

The gyroscope demodulator circuit is similar to that of the servo demodulator shown in Fig.15. The transformer ratios are different, however, since the gain is higher. The gain of the pitch and yaw demodulators is set, in conjunction with their respective gyroscopes, to 1.75 volts per degree of pick-off rotation and that of the roll demodulator, which is fed from two pick-offs in parallel, to 2.0 volts per degree. To avoid inaccuracy in gain setting due

to gyro drift effects the gyroscopes are oscillated at a low frequency with known angular amplitude while the gain potentiometer RV2 (Fig.15) is adjusted until the correct demodulator output voltage amplitude is obtained. The demodulators have a transfer function of the form

$$\frac{\bar{e}_3}{\bar{\psi}_G} = \frac{K_3}{1 + T_3 p} = K_3 G_3(p) = Y_3 \qquad (12)$$

where K_3 is the gain in volts per degree and T_3 is a time constant between 1 and 2 milliseconds. The larger value has been used in this analysis and Fig.18 shows the corresponding frequency response curves for $G_3(j\omega)$.

4 STABILITY OF THE HEADING CONTROL SYSTEM AT THE TIME OF MAXIMUM AERODYNAMIC INSTABILITY

The stability of the heading control system may now be examined using the transfer and describing functions from the previous sections. The object is to establish the required gains and frequency characteristics of the remaining control system components shown in the block diagram of Fig.4, the phase advance and summing amplifiers. For a system of this type, the most convenient method to use for this purpose is the Nyquist diagram and stability criterion[14]. The latter enables the number of roots with positive real parts in the characteristic equation of a closed loop control system to be determined from the open loop frequency response and transfer functions. The Nyquist diagram is a complex-plane plot, or vector locus, of the open loop transfer function, as the complex variable p is allowed to assume values on a contour which encloses the entire right-hand half of the p-plane. If N is the number of counter-clockwise encirclements of the point (-1,j0) by this locus the Nyquist stability criterion states that

$$N = Z - P \qquad (13)$$

where P = the number of poles of the open loop transfer function in the right half of the p-plane (i.e. with positive real parts)

and Z = the number of roots of the closed loop characteristic equation with positive real parts.

For a stable system Z must be zero. Inspection of the Nyquist diagram also gives useful information about the relative stability, or damping, of the closed loop system and about what increase or decrease of loop gain, for example, would be permissible. This margin of stability can be expressed numerically in terms of the gain and phase margins associated with specific values of loop gain etc. If these margins are reasonably large (say 6 db and 30°) the closed loop response of the system will normally be adequately damped.

Before a Nyquist diagram can be drawn it is necessary to derive an expression for the open loop transfer function. As the required phase advance and summing amplifier transfer functions Y_4 and Y_5 are unknown at this stage, the assumption is made that they have the simple forms $K_4 p$ and K_5, respectively, where K_4 and K_5 are gain factors to be determined. This is equivalent to assuming that the deflection of the rocket motors is proportional to heading error plus rate of change of heading gyro output. To

avoid making the first Nyquist diagram too complicated, the body flexure terms in the missile dynamics transfer function (11) have been omitted. The rigid missile transfer function at t = 80 sec, when uN_v, the aerodynamic moment per unit incidence, has its maximum value, is given by

$$Y_2 = - \frac{8.36p + 0.696}{p^3 + 0.316p^2 - 9.45p + 0.16} \qquad (14)$$

This expression, which is derived from equation (4) and the data given in Figs.6 to 8, has two poles in the right hand half of the p-plane. The corresponding open loop transfer function for t = 80 sec is

$$Y_1Y_2Y_3(Y_4 + Y_5) = - \frac{K_1K_3G_1(p)\ (K_4p + K_5)\ (8.36p + 0.696)}{(1 + 0.002p)\ (p^3 + 0.316p^2 - 9.45p + 0.16)} \qquad (15)$$

where $G_1(p)$ is defined by the family of gain and phase curves shown in Fig.17. Curve A of Fig.19 shows the Nyquist diagram corresponding to expression (15) for the 1° amplitude motor servo frequency response $G_1(j\omega)$ and the arbitrary gain values of $K_1K_3K_4 = 1$ and $K_1K_3K_5 = 4$. These assumed gain factors are equivalent to 4 degrees of motor deflection per degree of heading error and 1 degree of motor deflection per degree per second rate detected by the gyro. From the complete Nyquist diagram, shown as inset A in Fig.19, it can be seen that the vector locus encircles the point (-1,j0) twice in the clockwise direction. Thus N = -2 and, since P = 2 for the open loop transfer function (15), Z = 0 by equation (13). Hence for the rigid body case the system is stable with these values of gain. It can be seen from curve A that the phase margin is 47° at 1.3 c/s and the gain margins are -10.5 db at 0.107 c/s and 22.4 db at 17.5 c/s. This implies that if the error loop gain were reduced by more than 10.5 db, i.e. a factor of 3.35, the system would become unstable due to aerodynamic moment increasing more rapidly than the restoring moment from thrust deflection. Alternatively if the gain were increased by more than 22.4 db, a factor of 13.2, the system would become unstable in an oscillatory manner.

Curve B of Fig.19 and the corresponding inset show the effect of neglecting the gravity term gN_v/C in equation (4). The open loop transfer function then becomes, for the same gain factors

$$Y_1Y_2Y_3(Y_4 + Y_5) = - \frac{G_1(p)(P + 4)\ (8.36p + 0.696)}{p(1 + 0.002p)(p^2 + 0.316p - 9.45)} \ . \qquad (16)$$

This function has one pole in the right half of the complex plane (P = 1) and one at the origin. The complete Nyquist diagram, inset B, shows one negative encirclement of (-1,j0) and hence Z = 0 which indicates that the system is stable, as would be expected. The gain and phase margins are practically the same as for locus A since the loci differ appreciably only for frequencies lower than 0.1 c/s. Locus B tends to $\infty \angle -270°$ as ω tends to zero from the

positive direction. In plotting the loci A and B a logarithmic (db) scale has been used for magnitudes greater than 2 and a linear scale for smaller magnitudes. This has been done to enable the low frequency part to be shown more fully without using an unduly small linear scale. It does not affect the number of encirclements of $(-1,j0)$ nor the gain and phase margins, though it does distort the shape of the loci.

The effect of including the first two body flexure modes is illustrated by Fig.20 which shows the Nyquist diagram for t = 80 sec corresponding to the open loop transfer function

$$Y_1Y_2Y_3(Y_4+Y_5) = -\frac{G_1(p)\,(p+4)}{(1+0.002p)}\left\{\frac{8.36p+0.696}{p^3+0.316p^2-9.45p+0.16} - \frac{6.15\times10^{-3}\left[1+\dfrac{p^2}{(2\pi\times28.0)^2}\right]}{\dfrac{p^2}{(2\pi\times10.5)^2}+\dfrac{0.02p}{2\pi\times10.5}+1}\right.$$

$$\left. + \frac{1.25\times10^{-3}\left[1+\dfrac{p^2}{(2\pi\times24.0)^2}\right]}{\dfrac{p^2}{(2\pi\times29.3)^2}+\dfrac{0.02p}{2\pi\times29.3}+1}\right\} \qquad \ldots.(17)$$

This expression is derived from equations (11) and (15) and the data given in Figs.6 to 11. The same arbitrary values of gain, 4 and 1 sec^{-1}, have been used and the 1° amplitude case of Fig.17 has been used for $G_1(j\omega)$. In this case the system is unstable since the open loop transfer function has two poles in the right half plane as before but the net number of encirclements of the point $(-1,j0)$ is zero. The number of zeros is therefore 2, by equation (13), indicating that the closed loop characteristic equation would have two roots with positive real parts.

One way of stabilising the system is to change the simple functions initially assumed for Y_4 and Y_5 to obtain considerably more phase lag at the fundamental body flexure frequency. Examination of the effects on system stability of a number of possible filters indicated that the insertion of a third order low pass filter with a break frequency of 9 c/s would give acceptable stability throughout flight. Frequency response curves of such a filter are shown in Fig.21. The open loop transfer function with this filter included becomes

$$Y_1Y_2Y_3(Y_4+Y_5) = -\frac{(p+4)\,G_1(p)}{(1+0.002p)\,(1+0.018p)^3} \quad \{\text{Missile dynamics transfer function as in (17)}\} \qquad \ldots.(18)$$

Curve A of Fig.22 shows part of the Nyquist diagram, corresponding to this function, plotted for frequencies above 0.01 c/s. The lower frequency part is the same as that of Fig.20. It is evident from this diagram that the system is now stable since the complete Nyquist diagram encircles the point (-1, j0) twice in the negative sense, as for the rigid body case shown in Fig.19 (curve A). Comparison with the latter, however, indicates that insertion of the filter has resulted in substantial reduction of the phase and gain margins. The phase margin is now 29° at 1.25 c/s and the gain margins are 7.1 db at 3.25 c/s and -10.7 db at 0.12 c/s

Since at body resonance frequencies the gain of the phase advance amplifier is much larger than that of the summing amplifier, it is not necessary to include the filter in the latter and, in practice, it is simpler and more convenient to insert it in the phase advance amplifier only. The open loop transfer function then becomes

$$Y_1Y_2Y_3(Y_4 + Y_5) = -\frac{G_1(p)}{(1 + 0.002p)}\left[4 + \frac{p}{(1 + 0.018p)^3}\right]\left\{\begin{matrix}\text{Missile dynamics}\\ \text{transfer function}\\ \text{as in (17)}\end{matrix}\right\} \quad \ldots.(19)$$

Locus B of Fig.22 is the Nyquist diagram for this case. The system is stable with a phase margin of 32° at 1.45 c/s and gain margins of 6.0 db at 3.5 c/s and -10.7 db at 0.12 c/s. The transfer function Y_4 of the actual phase advance amplifier differs slightly from that incorporated in expression (19) since A.C. coupling is used throughout to avoid saturation by the D.C. component of the gyro demodulator signal and to minimise amplifier drift effects. The actual open loop transfer function is

$$Y_1Y_2Y_3(Y_4 + Y_5) = -\frac{G_1(p)}{(1 + 0.002p)}\left[4 + \frac{16.8\,p^3}{(1 + 4.1p)^2\,(1 + 0.018p)^3}\right]\left\{\begin{matrix}\text{Missile dynamics}\\ \text{transfer function}\\ \text{as in (17)}\end{matrix}\right\} \quad \ldots.(20)$$

The 4.1 sec time constants associated with the interstage coupling networks shown in the circuit of Fig.23 affect the gain and phase at low frequencies as indicated in Fig.24. Curves A correspond to the transfer function Y_4 in expression (19) and curves B to that in (20). Locus C of Fig.22 shows how the Nyquist diagram is affected. The phase margin is now 34° at 1.45 c/s and the gain margin at 3.5 c/s is unchanged at 6.0 db but the low frequency gain margin is 1.1 db less at -9.6 db at 0.11 c/s. The latter would be still further reduced if the coupling network time constants were made smaller. As they stand these values of gain and phase margin are large enough to assure satisfactory closed loop stability and adequate damping but further reduction would be undesirable.

Comparing the Nyquist diagrams of Figs.20 and 22, it is evident that introduction of the stabilising filter has resulted in a considerable reduction in the magnitude of feedback at the second body flexure mode frequency of 29.3 c/s. The gain margin associated with this mode is about 16 db which should

be more than adequate even if the structural damping factor were lower than the assumed value of 1%. A lower fundamental mode damping factor would not affect the stability of the system since the phase angle at 10.5 c/s is such that feedback is negative at this frequency. The influence of higher bending modes on the stability of the system appears to be negligible.

Finally the effect of motor servo non-linearities must be considered. The Nyquist diagrams shown in Figs.19, 20 and 22 are based on servo frequency response measurements for 1° amplitude. For $\frac{1}{2}$° demanded amplitude, however, the measured phase lag at 1.5 and 3 c/s is 4° and 5° greater than for the 1° case though the gain is unchanged. This extra phase lag reduces the phase margin to 30° at 1.45 c/s and the gain margin to 5.2 db at 3.2 c/s. It is clear from Fig.17 that at low frequencies the servo phase lag increases as the input signal amplitude decreases. If the system stability margins were inadequate this could result in small amplitude limit cycle hunting. For input signal amplitudes larger than 1 volt (i.e. 1° demand) the low frequency gain and phase margins will be greater than those indicated in Fig.22 but at higher frequencies the attenuation and phase lag are greater. For instance, at the fundamental flexure frequency of 10.5 c/s the phase lag is 56° greater for 5° than for 1° demanded amplitude. It can be seen from the Nyquist diagram that this extra phase lag does not make the proposed system unstable nor the stability margin inadequate. In any case it is very unlikely that such large amplitudes and rates of motor movement will ever be demanded in normal flight. It is therefore concluded that the proposed system will be satisfactory for the conditions expected to occur at the time of maximum aerodynamic instability.

5 HEADING CONTROL SYSTEM STABILITY AT OTHER TIMES

Practical considerations make it desirable that control system changes in flight should be restricted to variations of the gain factors K_4 and K_5; changes of filter time constants etc would involve greater complexity and hence potentially decreased reliability. It will now be shown that the system arrived at in the previous section is satisfactory from this point of view.

Stability immediately before all-burnt (t = 145 sec) and immediately after clearing the launcher (t = 0) are considered first as these are the times at which the vehicle mass, inertia etc have their minimum and maximum values. Since the dynamic pressure is very small for both these cases, aerodynamic forces and moments have negligible influence on control system stability. Thus the rigid body transfer function (4) reduces to

$$\frac{\bar{\psi}}{\bar{\delta}} = - \frac{T\ell}{2Cp^2} \qquad (21)$$

where $T\ell/2C = 16.7$ sec^{-2} at t = 145 and 5.85 at t = 0 as shown in Fig.8. Since the angular acceleration of the rigid missile per unit motor deflection at t = 145 sec is approximately double that at t = 80 sec it is necessary to reduce the internal control system gain by a factor of two to obtain the same margin of stability. As the latter is not excessive at t = 80 sec it was decided to increase the gain and phase margin at all-burnt by reducing K_4 and K_5 by a factor of four since, in the absence of aerodynamic moments there is no sharply defined lower limit to the gain which can be used. Too low a value of gain would, however, make the response of the vehicle to guidance command signals sluggish and poorly damped and this would adversely affect guidance accuracy. Fig.25 shows the Nyquist diagram for t = 145 sec, plotted from the open loop transfer function

$$Y_1Y_2Y_3(Y_4 + Y_5) = -\frac{G_1(p)}{(1+0.002p)}\left[1+\frac{4.2p^3}{(1+4.1p)^2(1+0.018p)^3}\right]\left\{\frac{16.7}{p^2} - \frac{2.15\times10^{-3}\left[1+\frac{p^2}{(2\pi\times14.3)^2}\right]}{1+\frac{0.02p}{2\pi\times34.9}+\frac{p^2}{(2\pi\times34.9)^2}}\right\} \quad \ldots.(22)$$

where $G_1(p)$ denotes the motor servo transfer function for 1° amplitude.

Higher body flexure modes are omitted as they do not affect stability significantly. It is evident from Fig.25 that the system is stable with a phase margin of 38° at 0.9 c/s and a gain margin of 14.8 db at 3.4 c/s. If the internal gain were kept the same as at t = 80 sec the phase margin would be 10° and the gain margin 2.8 db which would be quite inadequate. There appears to be no danger of instability at the fundamental flexure frequency even if the structural damping should be less than has been assumed.

The Nyquist diagram for conditions immediately after take-off, shown in Fig.26, has been plotted for the same values of internal gain as those selected for t = 80 sec from the open loop transfer function

$$Y_1Y_2Y_3(Y_4 + Y_5) = -\frac{G_1(p)}{1+0.002p}\left[4+\frac{16.8p^3}{(1+4.1p)^2(1+0.018p)^3}\right]\times$$

$$\times\left\{\frac{5.85}{p^2} - \frac{6.35\times10^{-3}\left[1+\frac{p^2}{(65\pi)^2}\right]}{1+\frac{0.02p}{15.1\pi}+\frac{p^2}{(15.1\pi)^2}} + \frac{1.85\times10^{-3}\left[1+\frac{p^2}{(52.4\pi)^2}\right]}{1+\frac{0.02p}{33\pi}+\frac{p^2}{(33\pi)^2}}\right\} \quad \ldots.(23)$$

It can be seen that the system is stable with a phase margin of 37° at 1.1 c/s and gain margins of 7.8 and 7.5 db at 3.3 and 16.5 c/s respectively. Feedback at the fundamental body flexure frequency is predominantly negative and at the first overtone frequency the phase angle is such that neither motor servo non-linearity nor a moderate reduction in structural damping will make the system unstable. Feedback at the higher mode frequencies is negligible.

From the three cases considered so far it appears likely that stable flight would be obtained if the internal gain factors $K_1K_3K_5$ and $K_1K_3K_4$ were kept constant at 4 and 1 respectively until shortly after t = 80 sec and were then gradually reduced to 1 and 0.25 at 145 sec. In practice, however, lower values of gain at take-off are preferable and it can be seen from Fig.26 that the gain at t = 0 could be reduced by 5 db without any reduction in phase margin. Such a reduction would have the effect of reducing the motor deflections at launch due to gyro and amplifier drifts and, in the event of the gain

programme motor failing to run after take-off, the lower gain would be a better compromise for a fixed gain system and would give stable flight throughout. Immediately after release a transient disturbance, involving lateral motion of the vehicle rear, is likely to occur due to the combined effects of wind, thrust inequalities and misalignments, motor deflections at take-off etc. This is unimportant provided that the lateral movement is less than the available launcher clearance and, to ensure that this requirement is met, limit switches are incorporated which prevent the vehicle being released if the deflection of any motor exceeds 3°. Reducing the gain at take-off thus reduces the probability of this limit being reached. The gain programme shown in Fig.27 was therefore selected. The heading error gain $K_1K_3K_5$ increases linearly from 2.25 at t = 0 to 4 at t = 75, remains constant until t = 85 and then decreases uniformly to 1 at t = 145 sec. The rate gain $K_1K_3K_4$ varies similarly being always one quarter of the above figures. Due to the characteristics of the linkage connecting the potentiometer wipers to the driving shaft the actual gain programme differs slightly from that shown in Fig.27.

Although it is fairly obvious from the way in which the aerodynamic and other parameters vary with time that, for a rigid vehicle, the proposed gain programme will give a stable and well damped system throughout the powered flight period it is not immediately obvious that instability due to body flexure will be avoided. To show this, vector loci have been plotted in Fig.28 which give the variation with time of the magnitude and phase of the feedback at body flexure frequencies. Loci A_1 and A_2 are drawn for the fundamental mode for the 1° and 5° servo amplitude cases respectively and B for the first overtone 1° servo case. As before a structural damping factor of 1% of critical has been assumed. To find out if the system is unstable due to the body flexure mode considered at any particular time it is necessary to determine the approximate shape of the Nyquist diagram for frequencies close to the body resonance. This can be done by simply drawing a circle with the vector for the time of interest as diameter[31]. For example, circle C_1 gives the approximate shape of the Nyquist diagram near frequency f_1 at t = 109 sec for the 5° amplitude case. The system is stable provided that this circle does not enclose the point (-1,j0). This procedure does not give the exact shape of the Nyquist diagram but, as can be seen from the second mode in Fig.26 for example, it gives reasonable accuracy near the resonance frequency when the damping is low and when feedback due to body flexure is large compared with that due to rigid body motion. It can be seen from curve A_1 that for the 1° amplitude case the system is stable and would remain so even if the structural damping factor were considerably lower than the assumed value. For the 5° case locus A_2 shows that the system is stable but that if the damping factor were less than half the assumed value instability might occur between 100 and 115 sec. However, since such large amplitudes or rates of motor movement and such small values of structural damping are very unlikely, the risk of instability is very small. The worst case for the second mode (curve B) appears to be t = 0 which has already been specifically dealt with (Fig.26) and shown to be stable. It is therefore concluded that with the system proposed instability due to body flexure should not occur.

6 THE EFFECT OF CHANGES IN THE BODY BENDING MODES

After the basic theoretical design of the lateral control system had been completed, as outlined in the previous sections, substantial alterations to the vehicle structure were introduced. These involved, inter alia, replacement of the original riveted body with stringers by a heavier gauge welded version without stringers. It was therefore necessary to re-assess the effects of body flexure on the control system on the basis of revised

estimates of bending mode frequencies etc. Table 2 gives the revised figures, which are reproduced from Table 3 of Ref.15. Comparison with Table 1 shows that in the early part of flight the bending frequencies have increased but towards all-burnt they are considerably lower. The forced vibration amplitudes at the gyro station are generally somewhat less than for the original structure.

Fig.29 shows the Nyquist diagram for the tanks full case (t = 0) based on these revised estimates, the other elements of the control system being the same as before. As it was thought that the welded vehicle might have lower structural damping than the riveted one a damping factor of 0.3% was assumed for this case. It is clear from the Nyquist diagram that even with this low value of damping the system is stable with an ample margin. In particular it may be observed that the increase in the first overtone frequency has resulted in a substantially increased gain margin for this mode (c.f. Fig.26).

To show that the system is stable throughout flight, loci similar to those of Fig.28 have been plotted in Fig.30 using the revised estimates for the fundamental bending mode. A structural damping factor of 0.5% has been assumed. These loci, the interpretation of which has been discussed in the previous section, indicate that the system should remain stable throughout the powered flight period. Hence it was concluded that no alteration to the proposed control system was necessary on account of the improved structure.

7 THE EFFECTS OF PROPELLENT SLOSHING

Expressions for the transfer function relating rigid body heading angle to rocket motor deflection with sloshing effects included have been derived for two-tank ballistic missiles by Smith[16] and Ward[17] on the basis of the mass-spring mechanical analogue referred to in section 2. To keep the order of the transfer function low only the fundamental sloshing mode for each tank has been included; the effect of the overtone modes is considered negligible. In the absence of aerodynamic forces the transfer function has the form

$$\frac{\bar{\psi}}{\bar{\delta}} = -\frac{T\ell}{2Cp^2}\left\{\frac{p^4 + \alpha_1 p^2 + \alpha_2}{p^4 + \beta_1 p^2 + \beta_2}\right\} \qquad (24)$$

where

$$\alpha_1 = \frac{k_1}{m_1}\left\{1 + \frac{m_1}{M_o}\left(1 - \frac{\ell_1}{\ell}\right)\right\} + \frac{k_2}{m_2}\left\{1 + \frac{m_2}{M_o}\left(1 - \frac{\ell_2}{\ell}\right)\right\} + \frac{a(m_1 + m_2)}{M_o \ell}$$

$$\alpha_2 = \frac{k_1 k_2}{m_1 m_2}\left\{1 + \frac{m_1}{M_o}\left(1 - \frac{\ell_1}{\ell}\right) + \frac{m_2}{M_o}\left(1 - \frac{\ell_2}{\ell}\right)\right\} + \frac{a}{M_o \ell}\left\{\frac{k_1 m_2}{m_1} + \frac{k_2 m_1}{m_2}\right\}$$

$$\beta_1 = \frac{k_1}{m_1}\left\{1 + \frac{m_1}{M_o}\left(1 + \frac{\ell_1^2}{R_o^2}\right)\right\} + \frac{k_2}{m_2}\left\{1 + \frac{m_2}{M_o}\left(1 + \frac{\ell_2^2}{R_o^2}\right)\right\} - \frac{a(\ell_1 m_1 + \ell_2 m_2)}{M_o R_o^2}$$

$$\beta_2 = \frac{k_1 k_2}{m_1 m_2}\left\{1 + \frac{m_1}{M_o}\left(1 + \frac{\ell_1^2}{R_o^2}\right) + \frac{m_2}{M_o}\left(1 + \frac{\ell_2^2}{R_o^2}\right) + \frac{m_1 m_2}{M_o^2}\left(\frac{\ell_1 - \ell_2}{R_o}\right)^2\right\}$$

$$+ \frac{a}{M_o R_o^2}\left\{m_1 k_2\left(\frac{\ell_2 - \ell_1}{M_o} - \frac{\ell_1}{m_2}\right) + m_2 k_1\left(\frac{\ell_1 - \ell_2}{M_o} - \frac{\ell_2}{m_1}\right)\right\}$$

m_1 and k_1 = respectively the mass and spring rate associated with the fundamental sloshing mode for the H.T.P. tank

m_2 and k_2 = the mass and spring rate for the fundamental kerosene tank mode

ℓ_1 and ℓ_2 = distances of masses m_1 and m_2 behind the effective centre of gravity

M_o and R_o = mass and radius of gyration of empty missile plus "fixed" part of both propellents. ($M_o R_o^2$ = effective lateral moment of inertia C)

a = component of acceleration along missile axis (assumed vertical).

The variation with time of the fundamental H.T.P. and kerosene sloshing frequencies f_P and f_K is shown in Fig.31, from Ref.4, where

$$f_P = \frac{1}{2\pi}\sqrt{\frac{k_1}{m_1}} \quad \text{and} \quad f_K = \frac{1}{2\pi}\sqrt{\frac{k_2}{m_2}} \; . \tag{25}$$

In the early part of flight f_P and f_K are nearly equal, varying from 1.13 c/s at t = 0 to 1.3 c/s at 60 sec. Thereafter they diverge slowly, f_P rising to a peak of 2.8 c/s at 135 sec whereas f_K reaches its maximum of 1.9 c/s at 120 sec. Towards all-burnt f_P and f_K fall rapidly towards zero.

The transfer function of expression (24) can be factorised to give

$$\frac{\bar{\psi}}{\bar{\delta}} = -\frac{K_2}{p^2}\left\{\frac{(p^2+\omega_a^2)\,(p^2+\omega_b^2)}{(p^2+\omega_c^2)\,(p^2+\omega_d^2)}\right\} \tag{26}$$

where $K_2 = T\ell/2C$ as before and ω_a, ω_b, etc are respectively 2π x frequencies f_a, f_b and f_c, f_d at which this function has zeros and poles. The variation of these with time from launch is shown in Fig.32. It can be seen that f_a and f_c are nearly equal throughout powered flight and vary in a similar manner to f_P while f_b and f_d follow closely the variation of f_K. Since in deriving the spring-mass analogue the propellents have been assumed inviscid, the transfer function (26) becomes infinite at frequencies f_c and f_d and the Nyquist diagram consists of two infinite semi-circles. It can be seen from the shape of the Nyquist diagrams obtained[17] that, in the absence of propellent damping, the stability of the system depends on the order of frequencies f_a, f_b, f_c and f_d. Referring to Fig.32 there are three cases:-

(1) $f_b < f_d < f_a < f_c$ (i.e. zero, pole, zero, pole). System stable.
t = 0 to 85 sec and 113 to 140 sec

(2) $f_b < f_d < f_c < f_a$ (i.e. zero, pole, pole, zero). System unstable.
t = 85 to 113 sec

(3) $f_d < f_b < f_a < f_c$ (i.e. pole, zero, zero, pole). System unstable.
t = 140 to 145 sec.

To obtain quantitative information about the damping of the sloshing modes under closed loop conditions it is necessary to evaluate the roots of the characteristic equation derived from the closed loop transfer function. Since the fundamental sloshing frequencies are rather low, it was thought that the lags associated with the motor servo, filter, gyro demodulator etc could be neglected in the first instance. Then, to confirm this and to obtain some indication of the effects, if any, of these lags, a simple second order transfer function, having about the same total gain and phase over the sloshing frequency band, was included and the roots again evaluated.

Neglecting component lags the open loop transfer function is

$$Y_o = Y_1 Y_2 Y_3 (Y_4 + Y_5) = - \frac{K_1 K_2 K_3 (K_4 p + K_5)}{p^2} \left\{ \frac{(p^2 + \omega_a^2)\ (p^2 + \omega_b^2)}{(p^2 + \omega_c^2)\ (p^2 + \omega_d^2)} \right\} \qquad (27)$$

and the characteristic equation, from the denominator of the closed loop transfer function $Y_o/(1 - Y_o)$, is

$$p^2 (p^2 + \omega_c^2)\ (p^2 + \omega_d^2) + K_1 K_2 K_3 (K_4 p + K_5)\ (p^2 + \omega_a^2)\ (p^2 + \omega_b^2) = 0 . \qquad (28)$$

The roots of equation (28) have been obtained, by means of a digital computer, for parameter values at intervals of ten seconds or less, assuming the parameters to be constant for each instant considered. The gain factors K_2, $K_1 K_3 K_4$ and $K_1 K_3 K_5$ were assumed to vary as shown in Figs.8 and 27 and the frequencies f_a, f_b, f_c and f_d as in Fig.32. Six complex roots, corresponding to three oscillatory modes with frequencies f_x, f_y and f_z and damping factors ζ_x, ζ_y and ζ_z were obtained for each instant considered. Fig.33 shows how these frequencies and damping factors vary as the propellents are used up. f_x, which is the natural frequency of the heading control system in the absence of aerodynamics and component lags, increases from 0.57 c/s at take-off to 0.9 c/s at 80 sec diminishing again to 0.56 c/s at 145 sec due to the programmed gain reduction. The corresponding damping factors ζ_x are 0.44, 0.69 and 0.51. The other two are closed loop sloshing modes and it can be seen that f_y and f_z vary in a similar manner to f_K and f_P respectively. The damping factor ζ_y of what may be loosely called the closed loop kerosene sloshing mode starts very small (0.1% of critical) and positive, increases to 0.027 at 100 sec and then falls to zero at 140 sec. During the last five seconds it is negative, as would be expected since $f_d < f_b$, but very small (> -0.003) which implies a slowly diverging oscillation. The H.T.P. closed loop sloshing mode damping factor ζ_z is positive and greater than 0.01 until 66 sec. As would be expected there is a period of instability from 83 to 113 sec but it can be seen from Fig.33 that the greatest negative damping factor is 0.005 at 100 sec. From 113 sec to all-burnt this mode is stable.

The effect of including control system component lags is illustrated in Fig.34. In this case the open loop transfer function was taken as

$$Y_o = - \frac{K_1 K_2 K_3 (K_4 p + K_5)}{p^2 (1 + 0.0487p + 0.00196p^2)} \left\{ \frac{(p^2 + \omega_a^2)(p^2 + \omega_b^2)}{(p^2 + \omega_c^2)(p^2 + \omega_d^2)} \right\} \quad (29)$$

which gives an eighth order characteristic equation. The additional second order term in expression (29) was chosen to represent the effective lag of the control system components as it has about the same total gain and phase lag for frequencies from 1 to 3 c/s. Comparison of Figs.33 and 34 shows that with this extra lag included the closed loop sloshing frequencies f_Y and f_Z are practically the same as f_y and f_z in the early part of flight but are slightly higher after about 100 sec. The damping factor ζ_Y of the kerosene mode varies in a similar manner to ζ_y and is generally somewhat larger. The period of instability associated with the H.T.P. mode occurs slightly later, between 90 and 117 sec and the maximum negative value of ζ_Z (-0.006) occurs at 110 sec. Between 120 and 140 sec ζ_Z is appreciably less than ζ_z and a second very short period of instability occurs around 135 sec (ζ_Z = -0.0006) when f_Z has its maximum value of 3.27 c/s. As this is the main difference between the results obtained from the sixth and eighth order equations it is reasonable to conclude that only when the sloshing mode frequency exceeds 2.5 c/s is its closed loop damping factor affected adversely to an appreciable extent by control system component lags.

When the closed loop sloshing mode damping factor remains negative for a period any disturbance will result in oscillations of increasing amplitude. For instance at 100 sec, when ζ_Z = -0.005, oscillations at 2.1 c/s would build up to double their initial amplitude in 10.5 sec, if the parameters remained constant. The amplitude would continue to increase until either the damping factor became positive or some non-linear effect, such as wave-breaking, caused amplitude limiting to occur. Even when the sloshing mode damping is positive it is evident that if propellent oscillations were excited, by aerodynamic disturbances or guidance commands, these would take a long time to decay as the damping factors are so small especially ζ_Y in the early part of flight. In view of this it was decided that the guidance command repetition frequency should be changed from two per second, as originally proposed, to four, since periodic disturbances at or near one of the sloshing frequencies might cause forced oscillations to build up to large amplitude. The frequency of four per second was chosen as it is above the highest fundamental sloshing frequency and below the lowest body flexure frequency.

The effects of aerodynamic forces and of propellent viscosity have so far been ignored in the discussion of sloshing. Ward[17] has shown that, although the influence of aerodynamic forces on the frequency and damping of the closed loop sloshing modes is small, they tend to make the system more unstable when one of the sloshing modes is already unstable in the absence of aerodynamics. Some idea of the effect of propellent viscosity may be obtained by assuming each spring-mass to be associated with a

viscous damper, although the mechanical analogy is strictly applicable only for inviscid fluid. It has been shown by Smith[18] that if at 100 sec either the H.T.P. or kerosene fundamental sloshing mode is assumed to have a damping factor of 0.05 associated with it, the other being undamped, the unstable (z) mode becomes positively damped with a damping factor of +0.010 or +0.006. Thus it appears that, while viscous damping in either tank is beneficial, the increase in closed loop damping factor is less than that of the open loop mode and that damping in the H.T.P. tank is slightly more effective for this particular unstable mode. The Black Knight tanks are not smooth-walled but contain stiffening rings spaced about 18" apart in the H.T.P. tank and 12" apart in the kerosene tank. Experimental measurements by Lineham[19] have shown that in water such a ring gives a damping factor of 0.02 when at the surface and 0.003 when 9" below it. For a smooth 3 ft diameter tank the damping factor was found to be 0.001. In flight the damping would be less than this due to the effect of acceleration but this would be partly counterbalanced by the kinematic viscosity of kerosene being greater than that of water.

The case for additional anti-sloshing devices in Black Knight is thus rather inconclusive as the period of instability is fairly short and the rate of divergence of sloshing oscillations appears likely to be slow. However, to ensure the greatest chance of success in the early flight trials, it was decided that seven equally spaced rows of fourteen baffle plates, each 3" square, should be welded to the H.T.P. tank walls between 42" and 79" from the lower datum to increase the sloshing mode damping between 88 and 117 sec. Consideration was also given to the possibility of increasing the sloshing mode damping under closed loop conditions by modifying the heading control system transfer function electrically but this did not appear to be practicable without the use of extra feedback transducers such as lateral accelerometers. Such extra complication was considered to be unjustified. After all, even if heading angle oscillations of moderate amplitude did occur for a period during the ascent they would be unlikely to result in catastrophic failure. At a later stage in the trials programme it may be considered desirable to flight test a Black Knight without anti-slosh baffles, which involve a small weight penalty, to determine experimentally if they can be safely left out.

8 THE ROLL STABILISATION SYSTEM

If large deviations from the correct roll attitude were to occur in flight, due to aerodynamic and other disturbing torques acting on the vehicle, cross-coupling between the azimuth and elevation guidance channels would make accurate guidance difficult. It has been shown[20] that a total phasing error of 15° can be tolerated without serious effects on the performance of the guidance system though considerably less than this is obviously desirable. Allowing a somewhat pessimistic total of 10° for gyro drift and phasing error in the guidance radar set, it appears that up to 5° roll error with respect to the gyro datum would be acceptable. To minimise the effects of gyro drift, signals from the outer gimbal pick-offs of both gyroscopes are used to feed a common demodulator. In addition to averaging the drift of the two gyros, this arrangement has the advantage that the system would still function, with reduced gain, if the roll pick-off of one gyro became inoperative due to an open-circuit fault.

The maximum transient disturbing torque due to motor thrust inequalities, fin misalignments etc was originally estimated to be 1000 lb ft, the bulk of this being due to aerodynamic forces at the time of maximum dynamic pressure. Since the motor thrust acts at a radius of 0.81 ft the control moment available in roll varies from 226 lb ft per degree of motor deflection at sea level to 256 above 100,000 ft. Thus the maximum motor deflection likely to be required to overcome the estimated disturbing torque is about 4° and hence, to keep the

error within 5°, a control system stiffness of not less than 0.8° of motor deflection per degree of roll error is desirable. The possibility of using integral of error control was considered but it was decided that the possible benefit would be insufficient to justify the extra complication involved. There should be no steady state rolling moment and it was felt that an integrator would be another potential source of drift.

In analysing the stability of the roll stabilisation system the procedure adopted is similar to that used for the heading control system. The aim is to determine what transfer functions should be inserted between the gyro demodulator and the rocket motor servos to ensure that the system remains stable throughout the powered flight period. The problem is simpler than for the heading control system since it has been shown[21] that the bulk of the propellents do not rotate when the vehicle rolls. It may therefore be assumed that the moment of inertia in roll remains constant at the value for the empty vehicle. This was estimated to be 57.2 slug ft^2. The maximum value of the aerodynamic roll damping coefficient L_p was estimated to be 75 lb ft per radian per sec, at 50 sec after take-off, while the propellents contribute a small amount of viscous damping. For practical purposes this is almost negligible since with tanks full it amounts to about 3.5 lb ft per radian per sec.

Considering first the vehicle as a rigid body, the equation of rolling motion is

$$A\ddot{\phi} + L_p \dot{\phi} = - TR\delta_R + L_o \qquad (30)$$

where ϕ = roll angle with respect to roll datum

A = moment of inertia in roll

L_p = roll damping coefficient

R = radius at which motor thrust acts

δ_R = component of motor deflection tending to roll the vehicle

L_o = roll disturbing torque.

The rigid missile transfer function relating roll angle to motor deflection is therefore

$$\frac{\bar{\phi}}{\bar{\delta}_R} = - \frac{\frac{TR}{A}}{p^2 + \frac{L_p}{A} p} \qquad (31)$$

where TR/A = 227, 242 and 257 sec^{-2} and L_p/A = 0.06, 1.35 sec^{-1} and zero for t = 0, 50 and >120 sec respectively.

Assuming that $\delta_R = Y_1 Y_3 (K_6 \phi + K_7 \dot{\phi})$ where K_6 and K_7 are roll error and rate gain factors at our disposal and Y_1 and Y_3 are the motor servo and gyro demodulator transfer functions, the open loop transfer function becomes

$$Y_o = - \frac{Y_1 K_3 \frac{TR}{A} (K_6 + K_7 p)}{(1 + 0.002p)\left(p^2 + \frac{L_P}{A} p\right)} \qquad (32)$$

assuming the gyro demodulator transfer function to be the same as before. Fig.35 shows part of the Nyquist diagram, plotted from expression (32), for four cases which illustrate the effects of the variation of motor servo response with input amplitude and of the rigid body transfer function with time. In all four cases the assumed gain factors are $K_1K_3K_6 = 1.7$ (degrees of motor deflection per degree roll error) and $K_1K_3K_6 = 0.1$ sec^{-1} which give the maximum possible stiffness consistent with an adequate margin of stability. Curves A, B and C are drawn for the $\frac{1}{2}^o$, 1^o and 5^o servo amplitude cases with the maximum value of TR/A (i.e. t > 120 sec) while curve D shows the effect of L_P at 50 sec for the $\frac{1}{2}^o$ amplitude case. Comparison of curves A and D shows that L_P only affects the shape of the Nyquist diagram significantly at frequencies below 2 c/s. If plotted to a smaller scale, it would be seen that curve D becomes asymptotic to the negative imaginary axis as the frequency tends to zero. In all four cases the system is stable with adequate gain and phase margins. For the 1^o amplitude case the gain margin is 10.1 db and the phase margin 32^o. The latter is reduced to 25^o (curve A) or 27^o (curve D) for the $\frac{1}{2}^o$ amplitude case but the gain margin is increased slightly. For the 5^o amplitude case the phase margin is 43^o and the gain margin 7.9 db.

Since torques applied to the vehicle by the rocket motors will produce torsional deflections of the structure, it is necessary to investigate to what extent these affect the stability of the roll stabilisation system. For small motor deflections the applied torque is $TR\delta_R$ due to thrust and the component of torsional couple due to angular acceleration of the combustion chambers is $4I_c \ddot{\delta}_R \sin 5\frac{3}{4}^o$. The transfer function relating roll gyro output ϕ_G to motor deflection δ_R may be written in the form

$$\frac{\bar{\phi}_G}{\bar{\delta}_R} = - \frac{\frac{TR}{A}}{p^2 + \frac{L_P}{A} p} + \sum_{n=1}^{\infty} \frac{J_n (TR + 4I_c p^2 \sin 5\frac{3}{4}^o)}{1 + \frac{2\zeta_{Tn}}{\omega_{Tn}} p + \frac{1}{\omega_{Tn}^2} p^2} \qquad (33)$$

where the first term is the rigid body transfer function and the subsequent ones the effects of torsional modes;

$\omega_{Tn} = 2\pi f_{Tn}$ where f_{Tn} is the nth mode torsional frequency

ζ_{Tn} = the damping factor associated with the nth torsional mode

J_n = a constant for the nth torsional mode equal to $2\zeta_{Tn}$ × the angular amplitude of torsional deflection (in radians) at resonance at the gyro station per lb ft amplitude of torsional couple applied at the motor pivot station.

The fundamental torsional frequency f_{T1} was originally estimated[22] to be 50 c/s with $J_1 = 15.6 \times 10^{-6}$ assuming ζ_{T1} to be 1% and the system was designed on this basis. Curve A of Fig.36 shows the Nyquist diagram including this mode; it is directly comparable with curve A of Fig.35, being drawn for the same assumed values of gain and the $\frac{1}{2}^{o}$ servo amplifier case, and corresponds to the open loop transfer function

$$Y_o = - \frac{(1.7 + 0.1p)\, G_1(p)_{(\delta_R = \frac{1}{2}^{o})}}{(1 + 0.002p)} \left[\frac{257}{p^2} - \frac{4.6 \times 10^{-3} \,(1 + 0.19 \times 10^{-4}\, p^2)}{1 + \frac{0.02}{314.2}\, p + \frac{1}{(314.2)^2}\, p^2} \right] \quad \ldots.(34)$$

The feedback amplitude at higher torsional mode frequencies was assumed to be negligible. It is evident from the Nyquist diagram that the system is stable as the point (-1,j0) is not encircled and the margin of stability near the fundamental torsional frequency is considerable. This is increased for larger servo amplitudes due to the greater servo phase lag at 50 c/s. Referring to expression (34), the term $(1 + 0.19 \times 10^{-4}\, p^2)$ is zero at 36.6 c/s; in other words at this frequency the torsional excitation due to motor thrust is cancelled by that due to combustion chamber inertia effects. At lower frequencies thrust forces provide the main excitation and at higher frequencies, such as we are concerned with here, inertial effects are the most important.

To avoid troubles due to noise, especially demodulator ripple, it is necessary to limit the bandwidth of the phase advance amplifier by means of low pass filters. The larger the time constants of these filters the smaller the bandwidth will be and the less noisy the output but the greater the extra phase lag. A compromise is necessary therefore and time constants of 3 and 1.5 milliseconds were chosen to give adequate rejection of demodulator ripple and a still acceptable phase margin. Curve B of Fig.36 shows the effect of these filters on the Nyquist diagram and Fig.37 gives the frequency response and transfer function of the proposed roll phase advance amplifier. The phase margin is only 20^{o} for the $\frac{1}{2}^{o}$ amplitude case, though for larger servo amplitudes it is greater, and the gain margin is 6.3 db. If larger time constants were used greater noise rejection would be obtained but it would be necessary to reduce the stiffness of the system. It was concluded, on the basis of the original torsional mode estimates that a maximum stiffness of 1.7^{o} of motor deflection per degree of roll error could be used if the frequency response of the phase advance amplifier was as shown in Fig.37.

The torsional modes were subsequently re-calculated[23] to allow for the effects of fin bending and of changing to the welded tank structure referred to in section 6. The fundamental torsional mode for this was estimated to be 63.4 c/s, with $J_1 = 4.3 \times 10^{-6}$, and the fin modes to be 39 and 41 c/s. The effect of these changes on the stability of the system was re-assessed by calculating the magnitude and phase of the feedback vector at the resonance frequencies. The fin modes were found to have negligible effect and the magnitude of the feedback vector at 63.4 c/s was found to be 0.208 with a phase angle of -356^{o}. It was therefore concluded that no instability due to body torsion was to be expected.

9 GROUND TEST AND FLIGHT TRIAL RESULTS

It has been shown in the preceding sections how the main features of the control system were arrived at by using linear servo-mechanism theory and the best available estimates of vehicle parameters. To complete this acoount it is relevant to include a brief summary of the control system tests subsequently carried out and to indicate their influence on the evolution of the system.

While design and manufacture of prototype test vehicles and components were proceeding, a series of single-plane fixed-parameter simulator studies of the heading control and roll-stabilisation systems was carried out using an electronic analogue computer and a prototype hydraulic servo. In these studies, which have been reported in detail elsewhere[21,24,25], the dynamic performance of both systems was examined for a number of points on the standard trajectory over a range of gain factors and their responses to a variety of stimuli were recorded. No major design changes were found to be necessary as a result of these simulator studies.

At a later stage closed loop tests of the control system were carried out using complete vehicles on a static firing test stand with and without the motors thrusting. The object of these tests was to determine whether any undesirable effects, due to structural constraints etc, would occur if the gyro feedback loops were closed prior to take-off. In the first series of tests, with the motors not thrusting, the heading control systems were found to be satisfactory but, when the roll-stabilisation loop was closed, the motors oscillated with small amplitude at about 65 c/s. In an attempt to ascertain the cause of these, open loop measurements were made in which the rocket motors were oscillated and the resultant motion of the vehicle in the vicinity of the gyros was measured by accelerometer type pick-ups. Comparison of the angular amplitudes indicated by the latter and by gyroscopes showed that at 65 c/s the gyro outputs were very much larger. The nutation frequency of the gyros then in use (Reid and Sigrist type GW5 Mk.I) was measured and found to be about 65 c/s with a damping factor of less than 0.5%. It was therefore suggested that an alternative gyroscope (Smiths Series 7 Mod.4) with a nutation frequency of 112 c/s should be tried in the hope that this would cure the trouble. In the first series of tests with the new gyroscope both heading control and roll-stabilisation systems functioned satisfactorily in the absence of motor thrust. Subsequently the roll-stabilisation system again became noisy, the rocket motors tending to buzz at about 40 c/s. Although this was probably caused by deterioration of the gyro performance under vibration, it was apparent that a reduction in the gain of the roll rate amplifier at frequencies between 20 and 100 c/s (see Fig.37) would be beneficial provided that this could be obtained without excessive low frequency phase lag. To meet these requirements a tuned L.C. filter giving more than 20 db attenuation between 40 and 50 c/s and a small low frequency phase lag was designed and inserted between the roll phase advance and motor servo amplifiers. The small increase in low frequency phase lag due to the filter made it necessary to reduce the stiffness of the roll-stabilisation system ($K_1K_3K_6$) to 0.8 to maintain adequate gain and phase margins. As mentioned in section 8, this lower stiffness is still sufficient to give acceptable performance even if the maximum estimated roll disturbing torque occurs.

Insertion of the filter was found to give satisfactory control system performance in the test stand both in the absence of thrust and during static firing of the motors. During pre-launch testing of the first flight vehicle (BK01) at Woomera, however, audible 60 c/s noise was found to occur and it was decided that increased attenuation at this frequency would be desirable. A two-stage L.C. filter, the circuit and frequency response of which are shown in Fig.38 was made and inserted. At first the trouble seemed to have

been cured but next day noise again occurred. This was found to be due to one of the gyroscopes having become noisy and after this had been replaced no further noise trouble was experienced. BK.01 was fired on 7th September, 1958 and the control system performed satisfactorily in flight[26].

Fig.39 shows the Nyquist diagram for the roll stabilisation system with the two-stage filter included and the stiffness reduced to 0.8. It can be seen that the system is stable with gain and phase margins of 5.0 db and 27° respectively for the $\frac{1}{2}$° servo amplitude case. For the 1° case these increase to 6.0 db and 34°. No change was made in the rate gain factor $K_1K_3K_7$ though this could well have been reduced by 3.5 db without appreciably affecting the dynamic performance of the system.

To check the bending and torsional mode estimates a series of full-scale resonance tests has been carried out on a Black Knight vehicle with welded tanks (BK.02)[30]. With tanks full the measured bending mode resonance frequencies[27], were generally in quite good agreement with the estimates but the amplitudes at the gyro station were lower. The fundamental mode (9.83 c/s) damping factor was about 1% but for the second and third modes values of 1.6% and 3.1% were obtained. These damping factors were calculated from energy balance considerations; the corresponding figures derived from polar plots of amplitude and phase from selected pick-ups were 0.9%, 1.1% and 1.3%. With tanks empty the fundamental resonance frequency (23.5 c/s) agreed quite well with the estimate (Table 2) but the associated damping factor was found to be 6.7% from energy balance considerations and 2.5% from a polar plot[28]. Higher modes were found at 32.2, 60.0 and 66.7 c/s whereas the estimated first overtone was 59.7 c/s. The damping factors associated with these modes were considerably higher than the assumed value of 1% and the amplitudes at the gyro station correspondingly lower. For example, for the fundamental mode the forced vibration amplitude was found to be only 15% of the estimate.

In November 1958 revised estimates of the torsional mode frequencies etc were issued[29] as comparison of the resonance test results with the earlier estimates had shown unexpected discrepancies. These were due to the effect of flexibility in the fin root fittings which made the fin bending frequencies much lower than had been anticipated. Static tests on a single fin attached to a motor bay structure were carried out to confirm this theory. The revised estimates gave the fundamental torsional mode frequency as 56.8 c/s with $J_1 = 1.09 \times 10^{-6}$, podded fin modes at 22.3 and 25.55 c/s with gyro amplitude factors of 0.92×10^{-6} and 5.60×10^{-6} respectively and a plain fin mode at 73.0 c/s with an amplitude factor of 4.64×10^{-6} assuming 1% critical damping. The effect of these on the modified roll stabilisation system, i.e. with L.C. filter included, was examined but in no case is instability indicated. The worst case occurs for the 25.55 c/s mode which gives a feedback vector magnitude of 0.63 at this frequency with a phase lag of 289°. It appears however that the assumption of 1% damping is pessimistic. The resonance tests did not give results from which the torsional mode damping could be satisfactorily determined[30], due to impurity of the modes excited, but the polar plots suggested that it was appreciably more than this. Torsional resonances were found at 19.7 c/s, 22.8 c/s 26.0 c/s, 45.6 c/s, 54.1 c/s, 64.5 c/s, 65.4 c/s, 71.2 c/s with tanks empty and 19.2 c/s, 21.6 c/s, 48.2 c/s, 55.8 c/s and 66.3 c/s with tanks full. The modes with frequencies below 30 c/s are predominantly fin modes and those above 50 c/s have mode shapes similar to the fundamental torsional mode.

The results from these resonance tests did not provide a satisfactory explanation of the roll stabilisation system noise troubles which had led to the insertion of the L.C. filter. In the hope of obtaining further elucidation direct measurements have been made of the gyro demodulator outputs resulting from small amplitude motor oscillations in a freely suspended vehicle. These measurements have been made over a wide range of frequencies

at 1 c/s intervals with tanks full and empty. The results obtained have not yet been fully analysed, as they are very complex, but it appears that the gyro outputs do not agree well especially at higher frequencies with what had been expected. Possible reasons for this disagreement are the effects of vibration on the gyroscopes, local resonances in the structure on which they are mounted, play in the gyro bearings etc. It has been found, for example, that the increase in roll rate amplifier gain necessary to make the system unstable on the launcher varies to a marked degree from one gyro to another. Modified G.W.5 gyroscopes, whose nutation frequency had been increased to over 100 c/s by fitting a heavier rotor, were found to give a larger gain margin, in the absence of thrust, than the Series 7 type used in BK.01. Subsequent vehicles have therefore been fitted with modified G.W.5 gyroscopes.

Eight Black Knight test vehicles have been fired to date and in all of these the control system has functioned satisfactorily in flight. In every case the telemetry records show small amplitude pitch and yaw oscillations at about 1.8 c/s between 75 and 105 sec after take-off. These are presumed to be due to propellent sloshing, in view of their frequency and time of occurrence, but there is no evidence that they are in any way harmful. Roll errors have been very small.

10 CONCLUSIONS

The analysis has shown that, in the absence of propellent sloshing, adequate control system stability margins can be obtained with the parameters selected. Hence it was concluded that the response of the vehicle to guidance signals and aerodynamic disturbances would be stable and adequately damped. This has been confirmed in flight. Due to the low values of damping factor associated with the propellent sloshing modes, however, pitch and yaw oscillations of low frequency and small amplitude are likely to occur. Small baffles have been fitted to part of the oxidant tank to increase the damping of these modes.

Ground tests have shown that the higher frequency effects of structural flexibility on the control system are not in accordance with expectation based on the simple theory used in the analysis. In consequence it was found necessary to modify the roll stabilisation system by inserting an additional filter.

Up to date eight Black Knight test vehicles have been fired and in all of them the control system has functioned correctly in flight. It is therefore concluded that the system is basically sound and reliable.

11 FURTHER DEVELOPMENTS

Development work is well advanced on a transistorised version of the control system described in this Report. Appreciable saving of weight will be obtained.

For stabilising the vehicle attitude after the rocket motors have stopped thrusting, a bang-bang jet control system with dead space has been developed. The jet efflux will be steam generated from catalytic decomposition of hydrogen peroxide. This system has not yet been tested in flight but single plane ground rig tests have been successfully carried out.

LIST OF SYMBOLS

A	slug ft^2	The roll moment of inertia of the vehicle
a	ft per sec^2	longitudinal acceleration of the vehicle
C	slug ft^2	moment of inertia of the vehicle in yaw
d	ft	distance of the combustion chamber centre of mass behind the pivot axis
e		the exponential function
e_1	volts	output signal from the yaw command unit
e_2	"	output signal from yaw summing amplifier variable gain potentiometer
e_3	"	output signal from yaw gyro demodulator
e_4	"	output signal from yaw phase advance amplifier variable gain potentiometer
f	cycles per sec	frequency
$f_1 \ldots f_n$	"	body bending mode frequencies
$f_{T1} \ldots f_{Tn}$	"	body torsional mode frequencies
f_P and f_K	"	fundamental H.T.P. and kerosene sloshing frequencies
f_a, f_b, f_c, f_d	"	frequencies at which the missile transfer function, including propellent sloshing, has zeros and poles
f_x and f_X	"	approximate natural frequencies of closed loop heading control system
f_y and f_Y	"	frequencies associated with the kerosene sloshing mode under closed loop conditions
f_z and f_Z	"	frequencies associated with the H.T.P. sloshing mode under closed loop conditions
$G_n(p)$		frequency dependent part of the transfer function $Y_n(p)$
g	ft per sec^2	acceleration due to gravity
H_{nF}, H_{nL} and h_n		constants for the nth bending mode defined in section 2
J_n		constant for the nth torsional mode defined in section 8
j		$\sqrt{-1}$

LIST OF SYMBOLS (Cont'd)

K_n		gain factor, which is independent of frequency, associated with transfer function $Y_n(p)$
k_1, k_2	lb per ft	spring rates associated respectively with H.T.P. and kerosene fundamental sloshing modes
L	lb ft	reaction couple at motor pivot due to angular acceleration of combustion chamber
L_o	lb ft	roll disturbing torque
L_p	lb ft per radian/sec	roll damping coefficient
ℓ	ft	distance of effective centre of gravity from motor pivot station
ℓ_1, ℓ_2	ft	distances of sloshing masses m_1 and m_2 behind effective centre of gravity
M_o	slugs	mass of empty vehicle plus "fixed" part of both propellents
M_c	slugs	mass of one combustion chamber
m	slugs	mass of vehicle
m_1, m_2	slugs	moving masses associated respectively with fundamental H.T.P. and kerosene sloshing modes
N		number of encirclements of the point (-1,j0)
N_v	lb ft per ft per sec	aerodynamic yawing moment derivative with respect to sideslip velocity
N_r	lb ft per radian per sec	aerodynamic yawing moment derivative with respect to rate of yaw
n		suffix denoting number of bending or torsional mode
P		number of poles of feedback transfer function in right hand half of p-plane
P1, P2		rocket motors controlling vehicle in pitch plane
p		Laplace transform complex variable $\sigma + j\omega$
R	ft	radius at which motor thrust acts
R_o	ft	radius of gyration of empty vehicle plus fixed part of propellents
r	radians per sec	rate of yaw (also = $\dot{\psi}$)

LIST OF SYMBOLS (Cont'd)

T	lb	longitudinal component of motor thrust = $T_T \cos 5\frac{3}{4}^{\circ}$
T_T	lb	total thrust from four motors
T_3	sec	gyro demodulator time constant
t	sec	time (from launch)
u	ft per sec	longitudinal component of missile velocity
u_n	rad per sec	2π × frequency of motor oscillation at which excitation of the nth bending mode due to motor thrust is cancelled by the inertia reaction couple
v	ft per sec	sideslip velocity in the yaw plane
$Y_o(p)$		open loop transfer function (or feedback transfer function)
$Y_1(p) = K_1G_1(p)$		rocket motor servo mechanism transfer function
$Y_2(p) = K_2G_2(p)$		missile dynamics transfer function (yaw plane)
$Y_3(p) = K_3G_3(p)$		gyro demodulator transfer function
$Y_4(p) = K_4G_4(p)$		yaw phase advance amplifier transfer function
$Y_5(p) = K_5G_5(p)$		yaw summing amplifier transfer function
$Y_6(p) = K_6G_6(p)$		roll summing amplifier transfer function
$Y_7(p) = K_7G_7(p)$		roll phase advance amplifier transfer function
$Y(j\omega) = KG(j\omega)$		frequency response function corresponding to transfer function Y(p)
Y_v	lb per ft per sec	aerodynamic normal force derivative with respect to sideslip velocity
Y_r	lb per radian per sec	aerodynamic normal force derivative with respect to yate of yaw
Y1, Y2		rocket motors controlling vehicle in yaw
y_1, y_2	ft	lateral displacements of masses m_1 and m_2 with respect to vehicle centre line

LIST OF SYMBOLS (Cont'd)

Z		number of zeros in denominator of closed loop transfer function in right hand half of p-plane
δ	radians	deflection of rocket motors used for yaw plane control
δ_R	radians	differential rocket motor defleotion giving rolling moment
ζ		damping factor
ζ_n etc		damping factor associated with frequency f_n etc
ϕ	radians	angle of roll of vehicle with respect to roll datum
ϕ_G	radians	angle detected by roll gyroscopes
ψ	radians	vehicle heading angle in yaw plane with respeot to vertical
ψ_F	radians	angular deflection in yaw at gyro station due to body flexure
ψ_G	radians	angle detected by yaw gyroscope
ω	radians per sec	angular frequency = $2\pi f$
ω_n etc	radians per sec	$2\pi f_n$ etc

NOTATION

Dot denotes derivative with respect to time e.g. $\dot{v} = \frac{dv}{dt}$.

Bar denotes Laplace transform e.g. $\bar{\psi} = \int_0^\infty e^{-pt}\, \psi(t)\, dt$.

LIST OF REFERENCES

Ref. No.	Author	Title, etc.
1	Robinson, H.G.R.	The ballistic test vehicle Black Knight. R.A.E. Technical Note No. G.W.503, December, 1958.
2	Graham, E.W. Rodriguez, A.M.	The characteristics of fuel motion which affect airplane dynamics Douglas Aircraft Co. Report No.SM-14212 November, 1951.
3	Stafford, J.	The oscillations of liquid in a circular cylindrical tank with a vertical axis. Saunders-Roe Publication No. T.P.183. June, 1956.

LIST OF REFERENCES (Cont'd)

Ref. No.	Author	Title, etc.
4	Stafford, J.	Black Knight - a spring mass system representing the fuel. Saunders-Roe Memo JCS/JS/RPD/530, March,1956.
5	Stafford, J.	Black Knight - aerodynamic derivatives. Saunders-Roe Memo JCS/JS/RPD/537, March, 1956.
6	Huntley, E.	Normal force and pitching moment measurements at transonic and supersonic speeds on a 1:22.5 scale model of the test missile Black Knight. R.A.E. Technical Note No. Aero 2549. February, 1958.
7	Beharrell, J.L. Friedrich, H.R.	The transfer function of a guided missile with consideration of its structural elasticity. Journal of Aeronautical Sciences Vol.21, July, 1954.
8	Donno, G.F.	Black Knight - normal modes and response to excitation from rocket motors. Saunders-Roe Technical Memo No. SR/G2/28(issue 2) March, 1956.
9	Bishop, R.E.D.	The treatment of damping forces in vibration theory. Journal of Royal Aero. Soc. November, 1955.
10	Laws, A.E.	An electro-mechanical transducer with permanent magnet polarisation. R.A.E. Technical Note No. G.W.202. July, 1952.
11	Eynon, G.T.	The Black Knight motor servo. R.A.E. Technical Note to be issued.
12	Eynon, G.T.	Developments in high performance electro-mechanical servo-mechanisms at R.A.E. Farnborough. Inst. of Mech. Engineers Symposium on Automatic Control. January, 1960.
13	Roehr, H.W.	A new type of a.c. angular displacement pick-off. R.A.E. Technical Note No. G.W.321. June, 1954.
14	James, H.M. Nichols, N.B. Phillips, R.S.	Theory of servo-mechanisms. M.I.T. Radiation Laboratory Series Vol.25 1947.
15	Donno, G.F.	Lateral bending modes and response to excitation from rocket motors. Saunders-Roe Tech. Memo No.SR/G2/71. August, 1957.
16	Smith, K.W.	Present work on the effect of fuel sloshing on the control of ballistic missiles. (unpublished internal Memo). R.A.E. File Ref. G.W./S5027/KWS, June, 1956.
17	Ward, B.	Fuel sloshing effects in a two tank ballistic missile with reference to Blue Streak. R.A.E. Technical Note No. G.W.466, August, 1957.

LIST OF REFERENCES (Cont'd)

Ref. No.	Author	Title, etc.
18	Smith, K.W.	Effects of fuel damping on the sloshing modes in the control loop. (Unpublished internal Memo.) R.A.E. File Ref. G.W./S5027/KWS, September, 1957.
19	Lineham, E.F.	Details of experimental work on damping of fuel sloshing in missiles with particular reference to Black Knight. (Unbublished internal Memo.) R.A.E. File Ref. G.W./S5027/EFL, September, 1957.
20	Robertson, A.C.C.	The Black Knight guidance simulator and proposed automatic guidance system. R.A.E. Technical Memo. No. G.W.375, June, 1960.
21	Kerry, B.A. Burgess, A. Buchan, A.L.	Analogue computer investigations of Black Knight control system - response and stability characteristics in roll. Saunders-Roe Report No. Comp./A/Comp./13, March, 1956.
22	Donno, G.F.	Black Knight torsional vibration. Saunders-Roe Technical Memo. No. SR/G2/31 March and August, 1956.
23	Donno, G.F.	Black Knight torsional modes and frequencies. Saunders-Roe Technical Memo No. SR/G2/68, July, 1957.
24	Oulsnam, G. Kerry, B.A. Pennelegion, L. Buchan, A.L.	Analogue computer investigation of Black Knight roll control system using a missile hydraulic servo unit. Saunders-Roe Report No. Comp./A/Comp./15, August, 1956.
25	Burgess, A. Pennelegion, L. Oulsnam, G. Buchan, A.L.	Black Knight - analogue computer investigation of dynamic pitch and yaw characteristics using the A-6 hydraulic rig. Saunders-Roe Report No. Comp./A/Comp./16, January, 1957.
26	-	Black Knight - summary of results for BK.01 firing. R.A.E. Technical Memo No. G.W.353, July, 1959.
27	Donno, G.F.	Black Knight lateral bending modes in tanks full condition: comparison of experimental and theoretical forced vibration amplitudes. Saunders-Roe Technical Memo No. SR/G2/82, June, 1958.
28	Donno, G.F.	Black Knight lateral bending modes in tanks empty condition: comparison of experimental and theoretical results. Saunders-Roe Technical Memo No. SR/G2/98, April, 1959.
29	Donno, G.F.	Black Knight torsional modes and frequencies. Saunders-Roe Technical Memo. No. SR/G2/87, November, 1958.

LIST OF REFERENCES (Cont'd)

Ref. No.	Author	Title, etc.
30	Jones, D.R.D.	Black Knight resonance tests on production vehicle; Phase I. Saunders-Roe Report No. SR/G2/1474, June, 1960.
31	Kennedy, C.C. Pancu, D.P.	Use of vectors in vibration measurement and analysis. Jour. Aero. Sciences Vol.14, No.11 (November, 1947), p.603.

ATTACHED:-

Tables 1 and 2
Drgs. Nos. GW/P/9909 to 9946
Detachable Abstract Cards

ADVANCE DISTRIBUTION:-

Ministry of Aviation

Chief Scientist
CGWL
DGBM
GW(G&C)5 90 copies
DGLRD (TA)
TIL 90 copies

R.A.E.

Director
DD(E)
DD(A)
RPE 3
Aero 2
Radio
Structures
Arm 2
IAP 3
Instn.
Maths
Trials
Aberporth
NGTE
Patents
Bedford Library
Library

TABLE 1

Estimated bending mode natural frequencies and forced vibration amplitudes at gyro station for excitation at motor pivot for riveted Black Knight structure (G4/2000 Series)[8]

Missile condition; time of flight on nominal trajectory; bending mode	Bending mode frequency c/s	Angular amplitude in radians of forced vibration at gyro station at resonance due to excitation at motor pivot of (a) 1 lb lateral force and (b) 1 lb ft couple assuming 1% of critical damping (ζ_n = 0.01).	
		(a) Lateral force of 1 lb	(b) 1 lb ft couple
Tanks full. t = 0 sec			
Fundamental (f_1)	7.55	39.8×10^{-6}	5.7×10^{-6}
1st overtone (f_2)	16.5	11.4 "	2.5 "
2nd " (f_3)	25.7	5.03 "	1.27 "
3rd " (f_4)	32.9	2.98 "	0.87 "
50% burnt. t = 72.5 sec			
Fundamental (f_1)	9.68	35.6 "	6.23 "
1st overtone (f_2)	27.6	7.56 "	2.38 "
2nd " (f_3)	35.4	3.75 "	1.53 "
3rd " (f_4)	47.3	0.505 "	0.271 "
68.7% burnt. t = 100 sec			
Fundamental (f_1)	12.34	30.0 "	6.49 "
1st overtone (f_2)	33.9	5.43 "	1.83 "
2nd " (f_3)	44.3	1.70 "	0.84 "
87.5% burnt. t = 127 sec			
Fundamental (f_1)	18.6	23.6 "	7.42 "
1st overtone (f_2)	41.3	4.92 "	1.91 "
93.8% burnt. t = 136 sec			
Fundamental (f_1)	21.4	20.9 "	7.84 "
1st overtone (f_2)	49.6	5.07 "	2.52 "
All-burnt. t = 145 sec			
Fundamental (f_1)	34.9	11.9 "	8.97 "
1st overtone (f_2)	73.8	2.86 "	2.77 "

TABLE 2

Estimated bending mode natural frequencies and forced vibration amplitudes of vehicle at gyro station for excitation at motor pivot for welded Black Knight structure (G4/3000 Series)[15]

Missile condition; time of flight on nominal trajectory; bending mode	Bending mode frequency c/s	Angular amplitude in radians of forced vibration at gyro station at resonance due to excitation at motor pivot of (a) 1 lb lateral force and (b) 1 lb ft couple assuming 1% of critical damping (ζ_n = 0.01)	
		(a) Lateral force of 1 lb	(b) 1 lb ft couple
Tanks full (t = 0)			
Fundamental (f_1)	8.17	35.1 × 10^{-6}	5.14 × 10^{-6}
1st overtone (f_2)	19.1	8.81 "	2.01 "
2nd " (f_3)	31.3	3.27 "	0.93 "
3rd " (f_4)	42.4	0.98 "	0.32 "
50% burnt (t = 72.5 sec)			
Fundamental (f_1)	10.63	29.8 "	5.33 "
1st overtone (f_2)	28.6	6.60 "	1.75 "
2nd " (f_3)	39.5	2.12 "	0.64 "
3rd " (f_4)	68.4	0.04 "	0.03 "
66.7% burnt (t = 96.7)			
Fundamental (f_1)	12.9	26.2 "	5.48 "
1st overtone (f_2)	30.2	5.36 "	1.38 "
2nd " (f_3)	50.5	0.60 "	0.23 "
83.3% burnt (t = 120.8)			
Fundamental (f_1)	16.4	21.7 "	5.91 "
1st overtone (f_2)	33.7	5.36 "	1.44 "
2nd " (f_3)	80.3	0.33 "	0.06 "
All-burnt (t = 145)			
Fundamental (f_1)	22.1	9.45 "	6.26 "
1st overtone (f_2)	59.7	1.28 "	1.83 "

FIG. I.

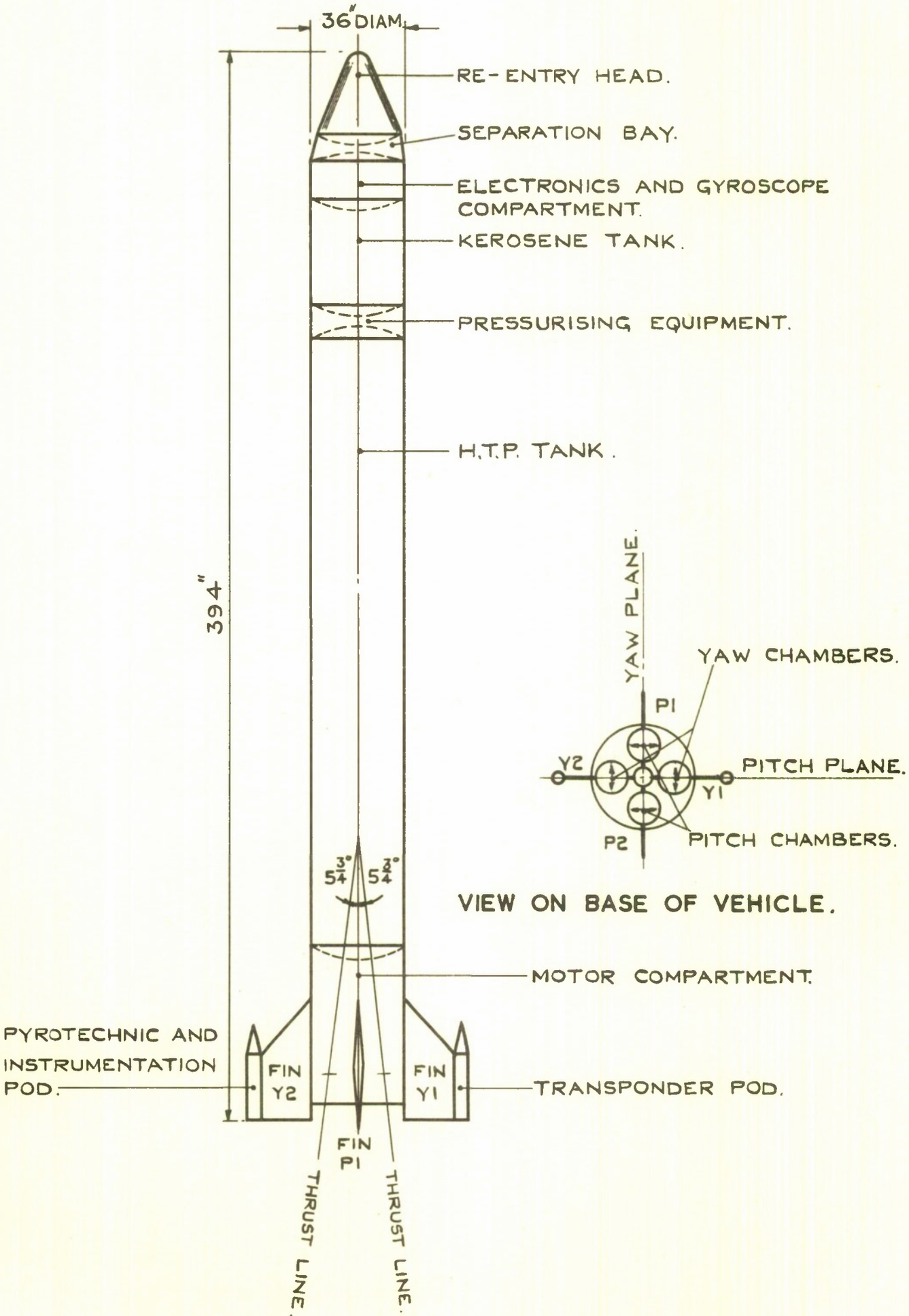

FIG. I. BLACK KNIGHT CONFIGURATION.

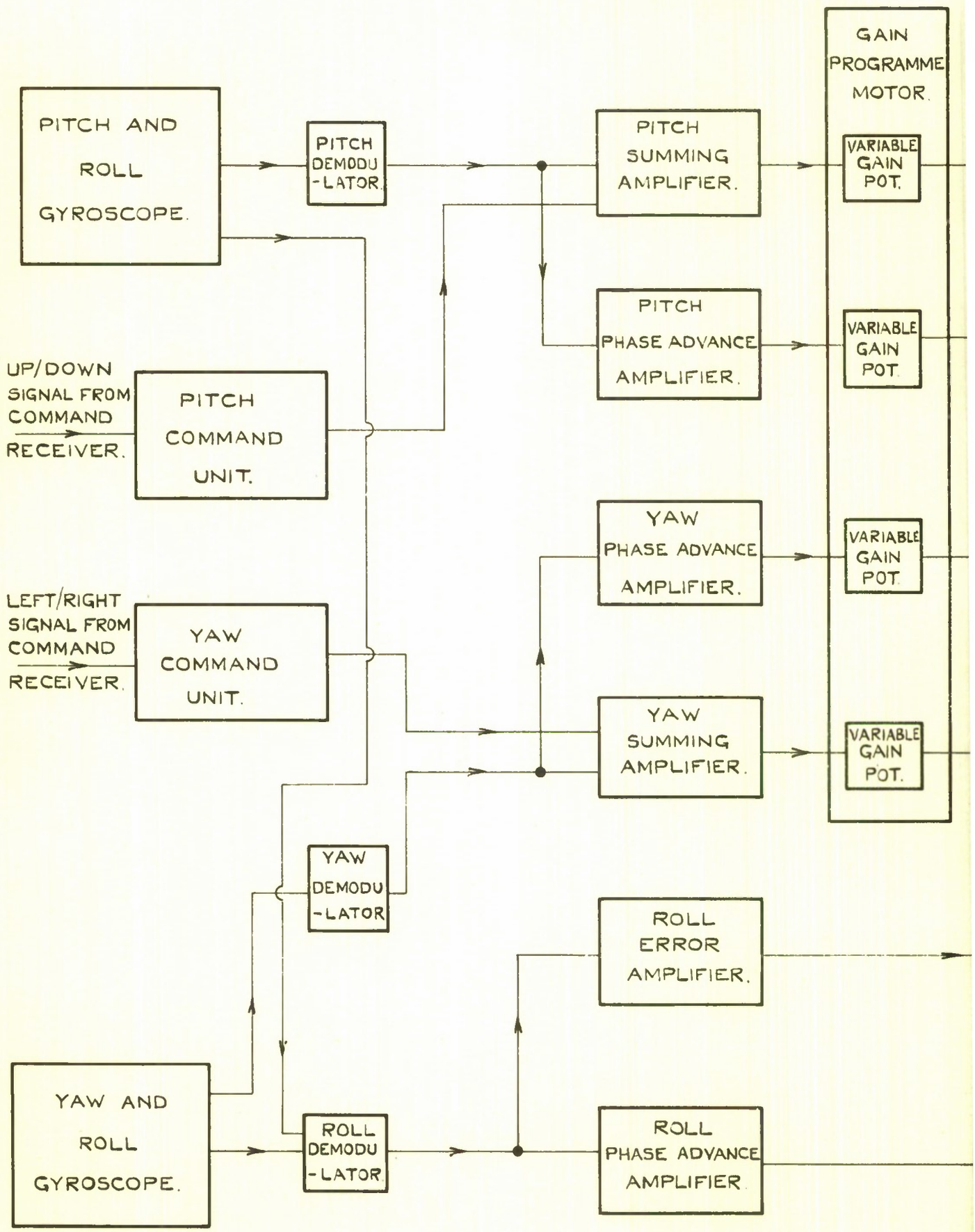

(1)

FIG. 2. BLACK KNIGHT CONTROL

FIG. 2.

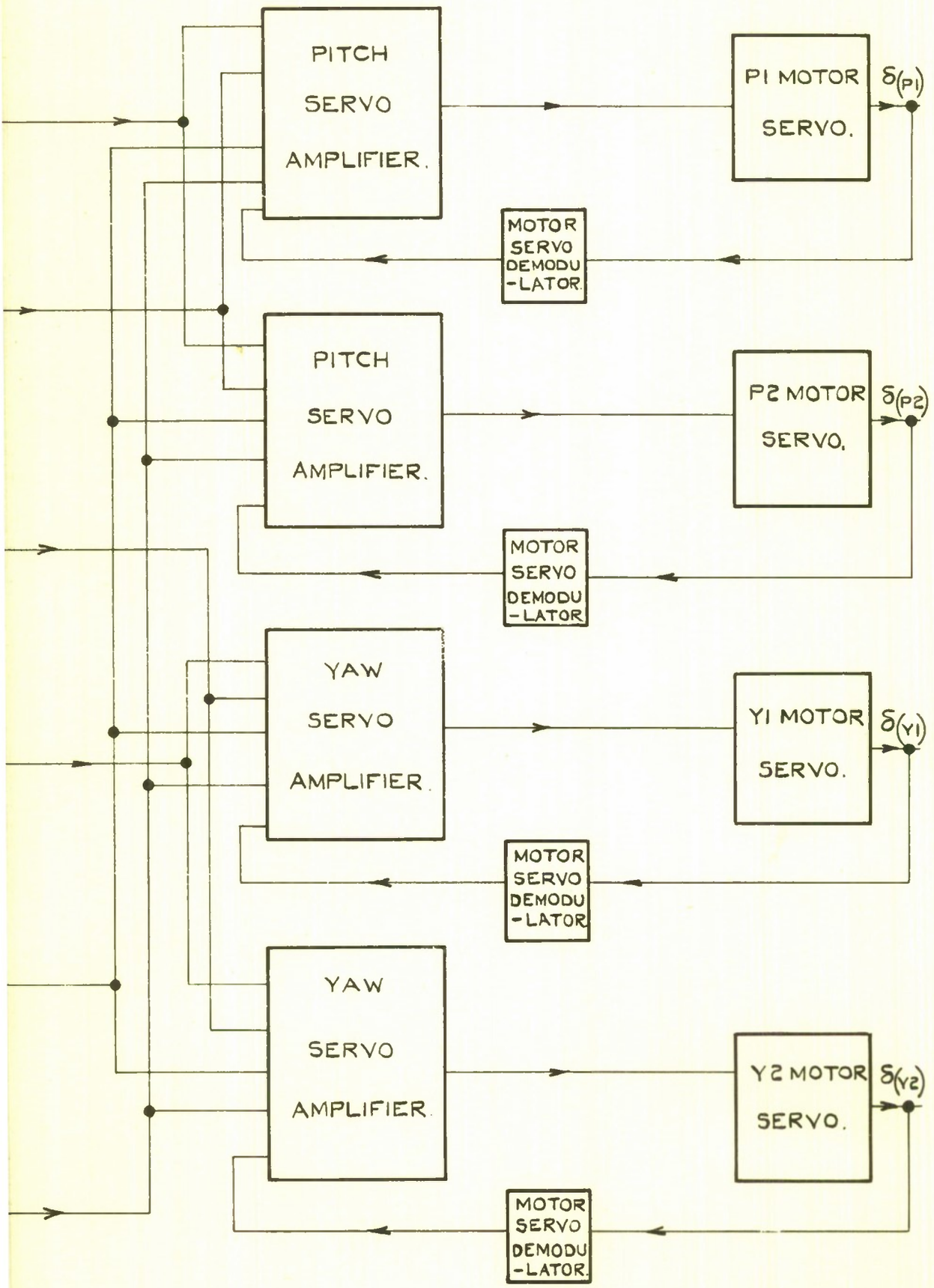

SYSTEM BLOCK DIAGRAM.

(2)

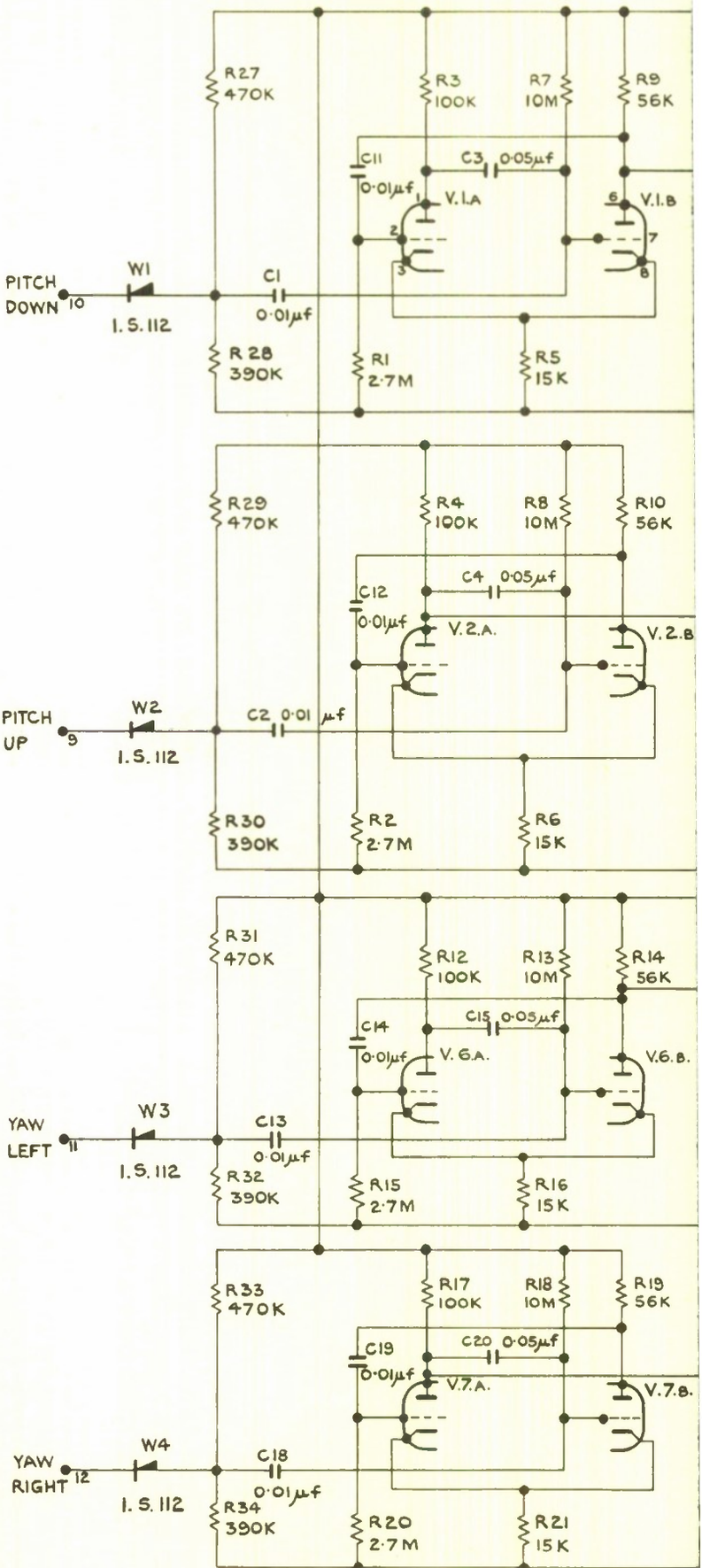

FIG. 3. COMBINED PITCH AN

FIG. 3.

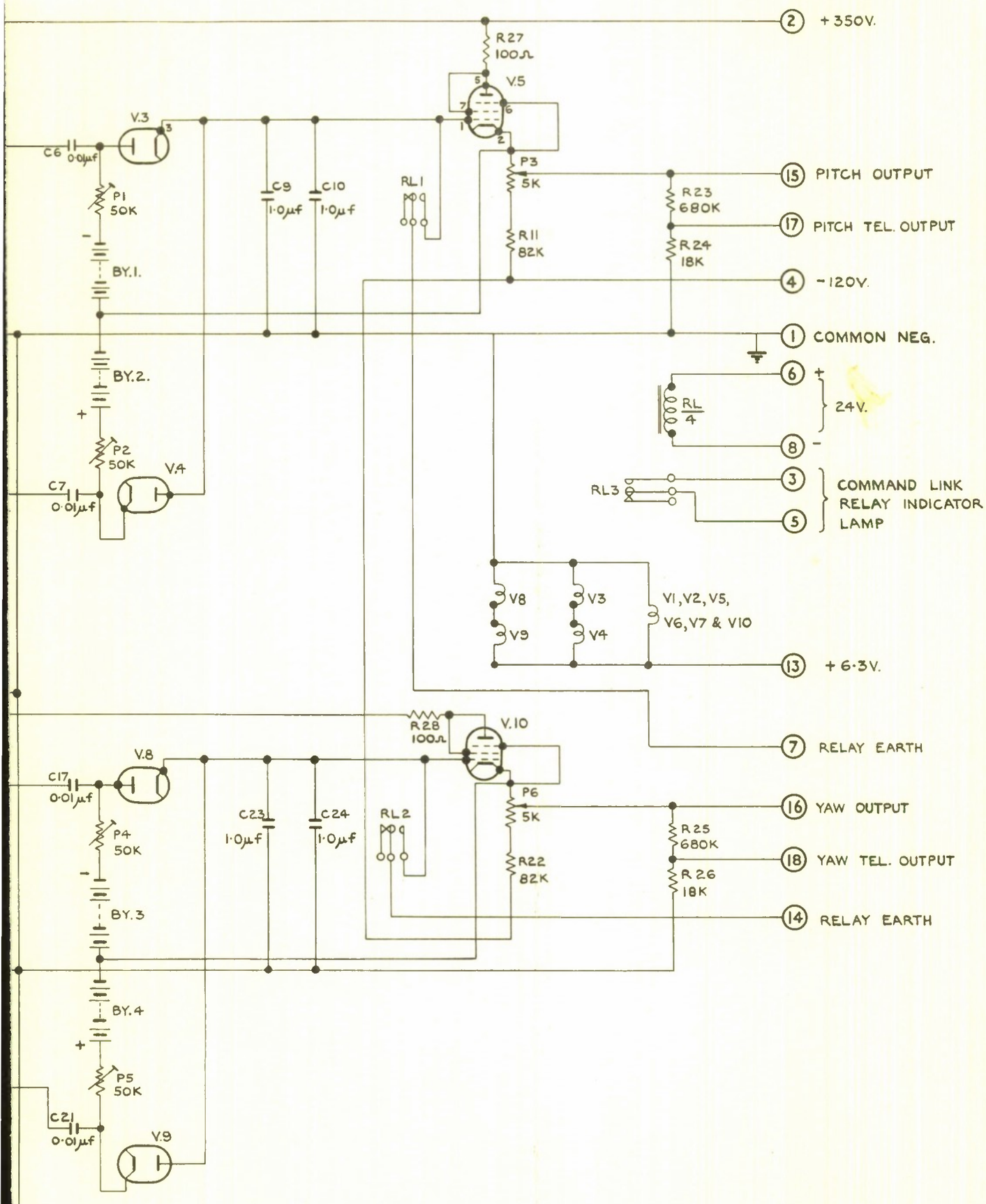

D YAW COMMAND UNIT CIRCUIT DIAGRAM.

(2)

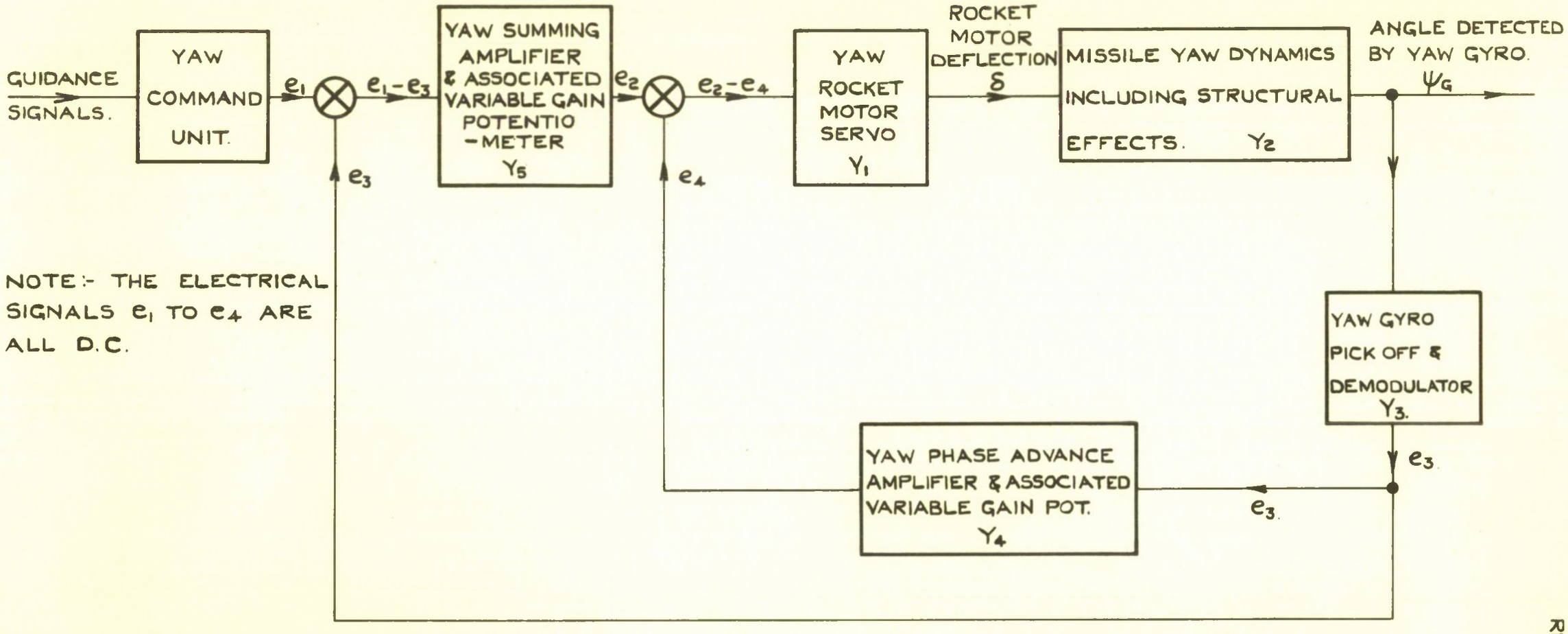

FIG. 4. BLOCK DIAGRAM OF THE HEADING CONTROL SYSTEM FOR THE YAW PLANE.

FIG. 5.

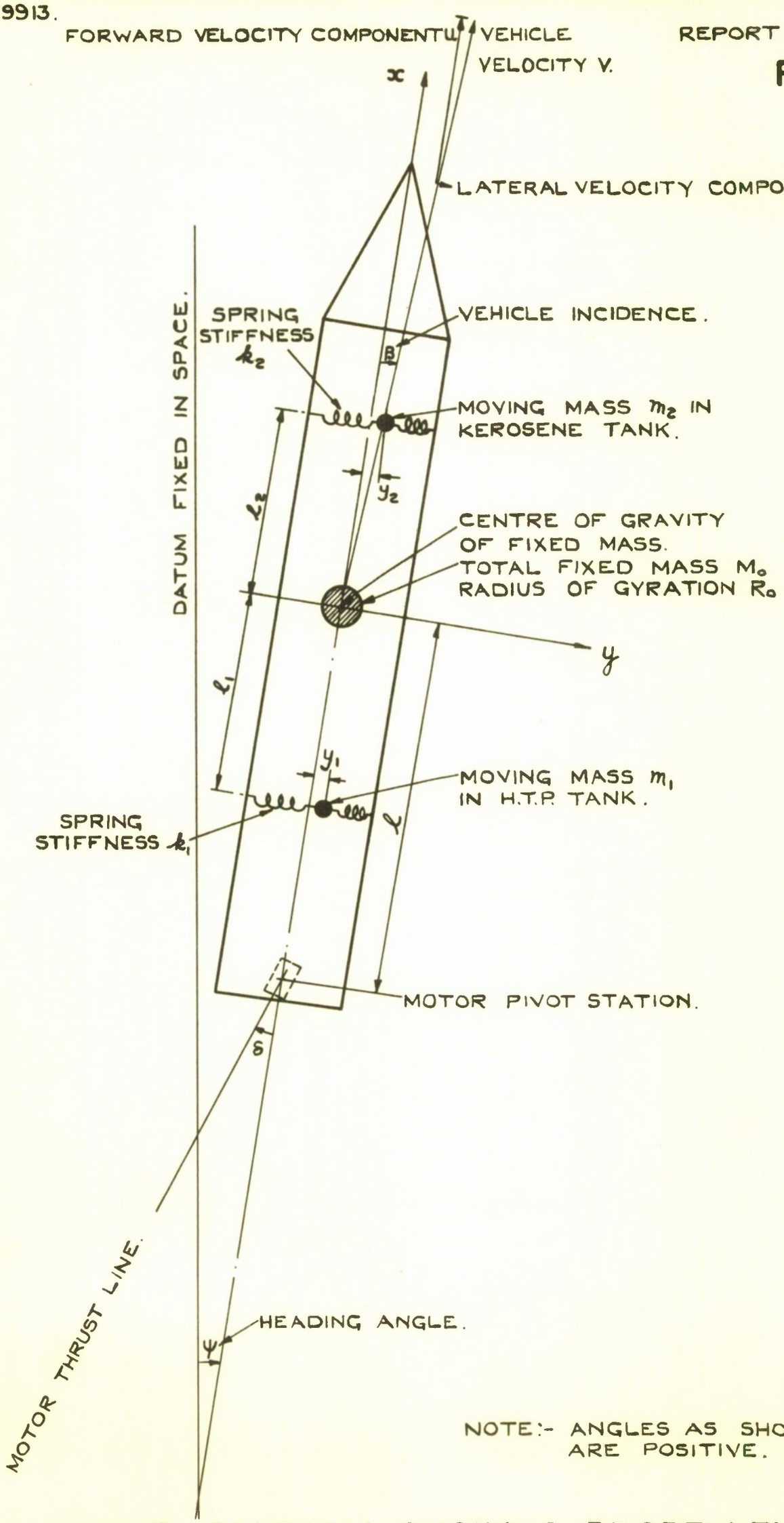

NOTE:- ANGLES AS SHOWN ARE POSITIVE.

FIG. 5. DIAGRAM SHOWING PROPELLENT SLOSHING MECHANICAL ANALOGUE.

REPORT G.W.24.

FIG. 6.

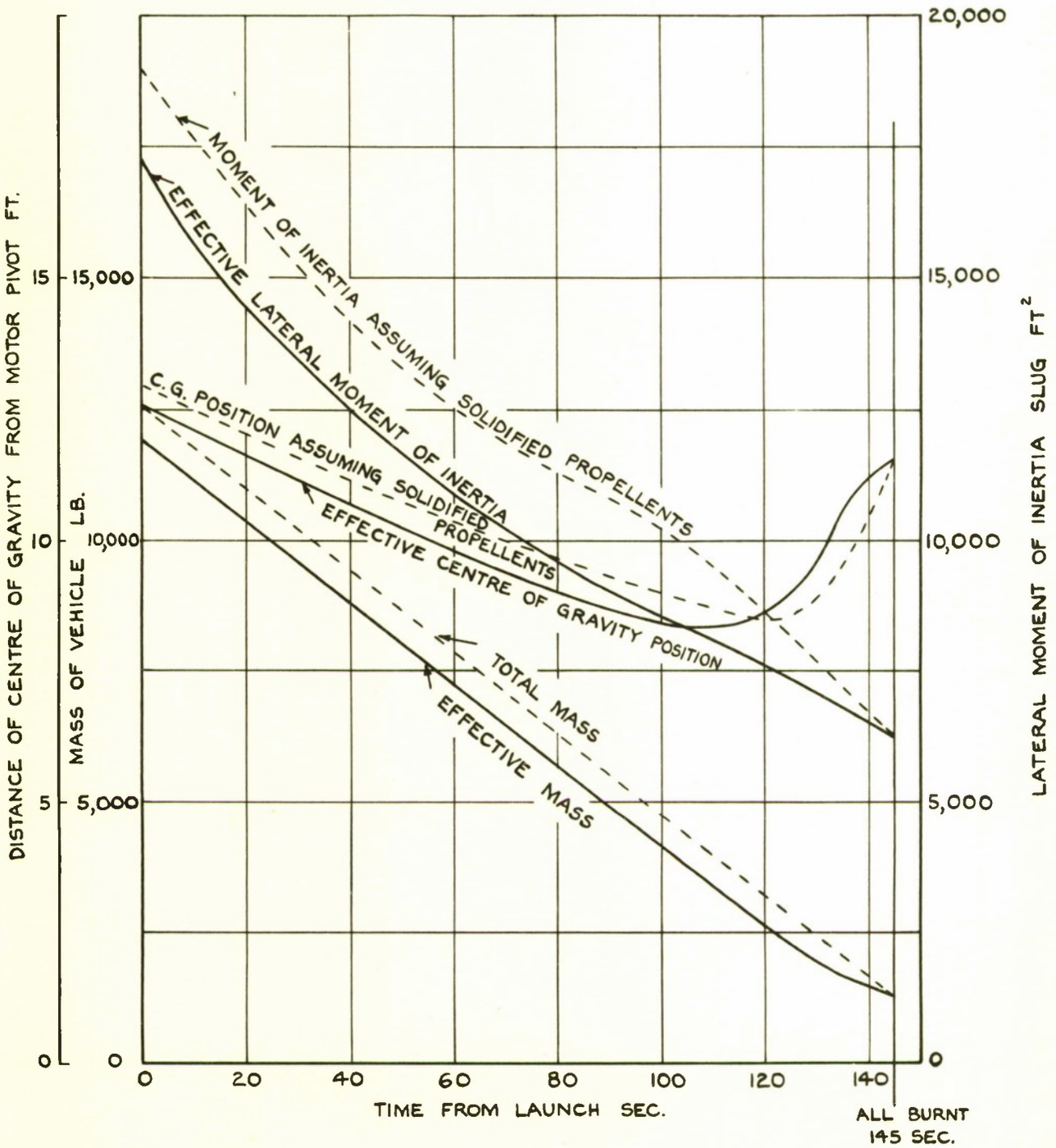

FIG. 6. ESTIMATED VARIATION WITH TIME OF VEHICLE MASS, LATERAL MOMENT OF INERTIA AND CENTRE OF GRAVITY POSITION.

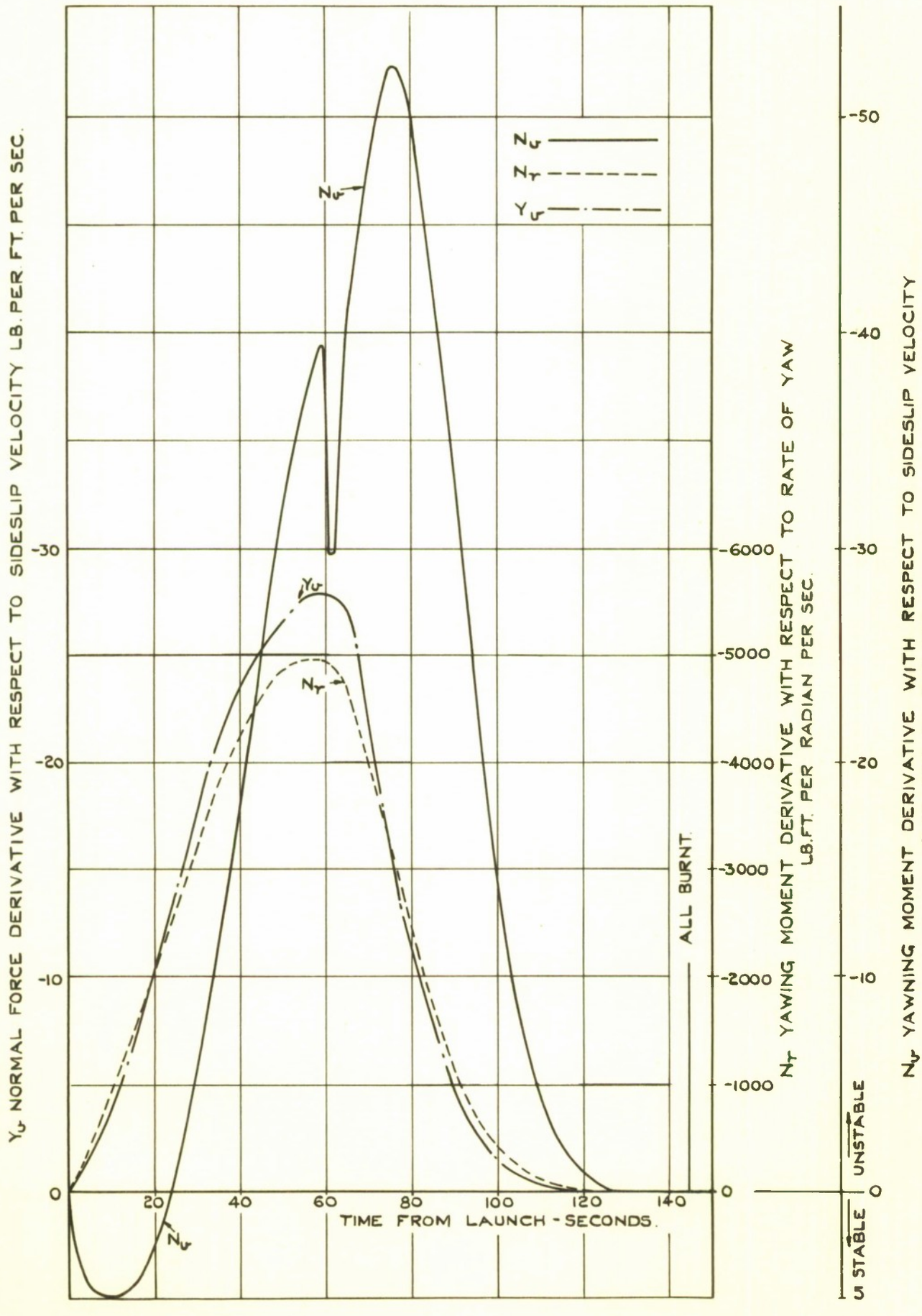

FIG.7. ESTIMATED VARIATION WITH TIME OF THE AERODYNAMIC DERIVATIVES N_v, N_r AND Y_v FOR ZERO INCIDENCE.

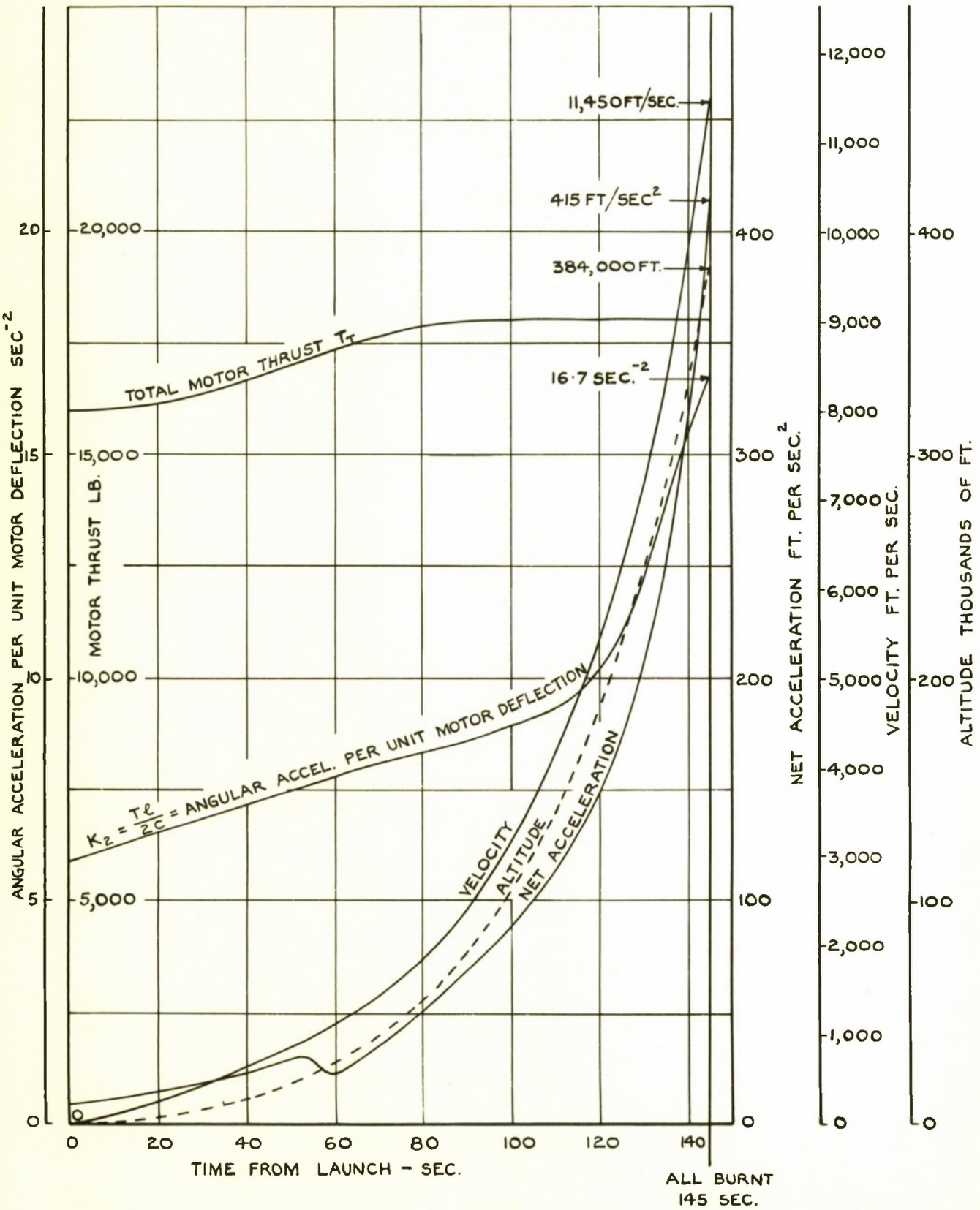

FIG. 8. ESTIMATED VARIATION WITH TIME OF TOTAL MOTOR THRUST, VEHICLE NET ACCELERATION, VELOCITY, ALTITUDE AND ANGULAR ACCELERATION PER UNIT MOTOR DEFLECTION.

FIG. 9.

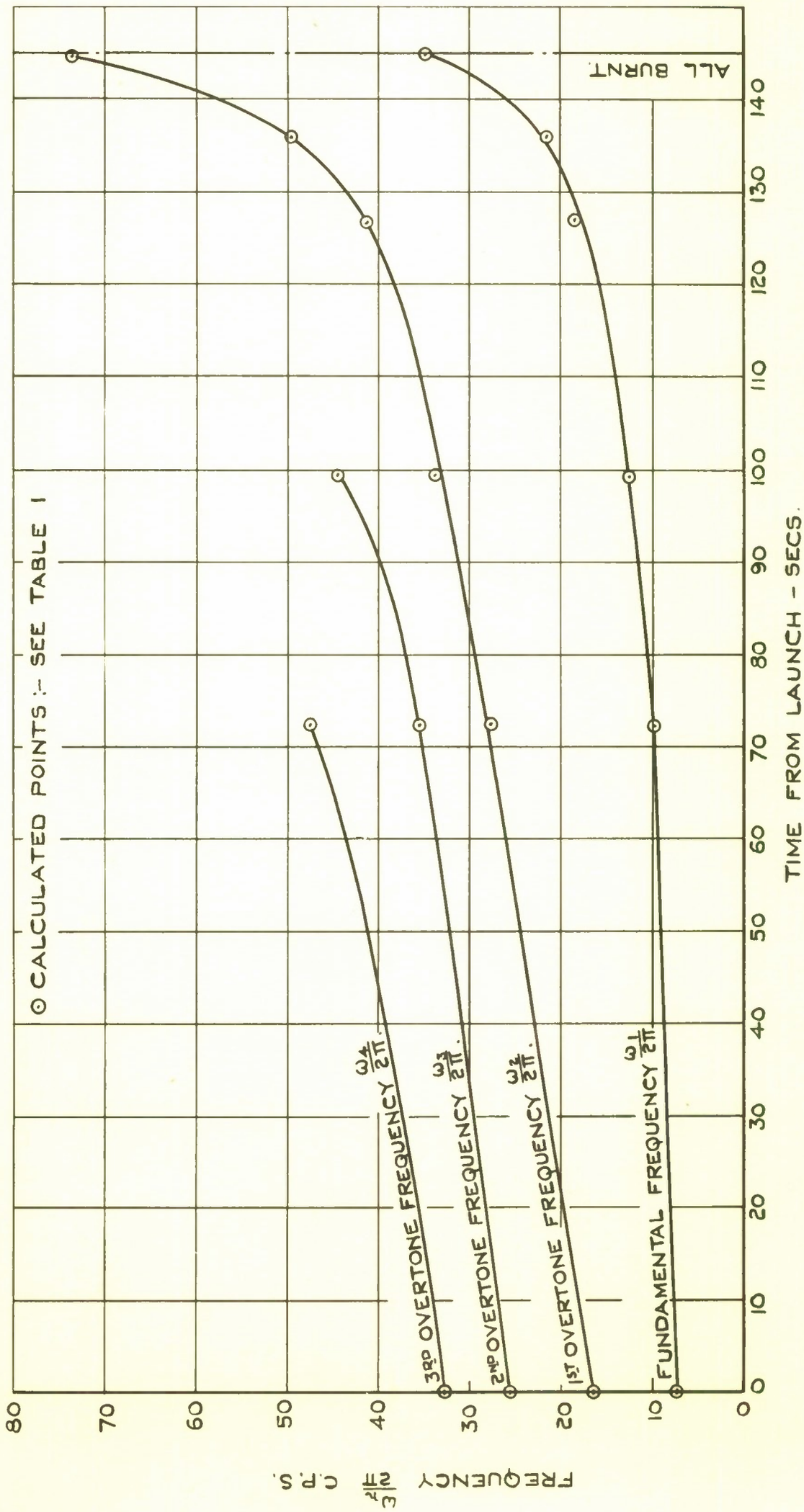

FIG. 9. VARIATION WITH TIME OF ESTIMATED BODY BENDING MODE NATURAL FREQUENCIES.

⊙ CALCULATED POINTS

[NOTE k_1 = 0·01 × MOTOR THRUST (FROM FIG. 8) × FUNDAMENTAL MODE DATA GIVEN IN SECOND COLUMN OF TABLE I]

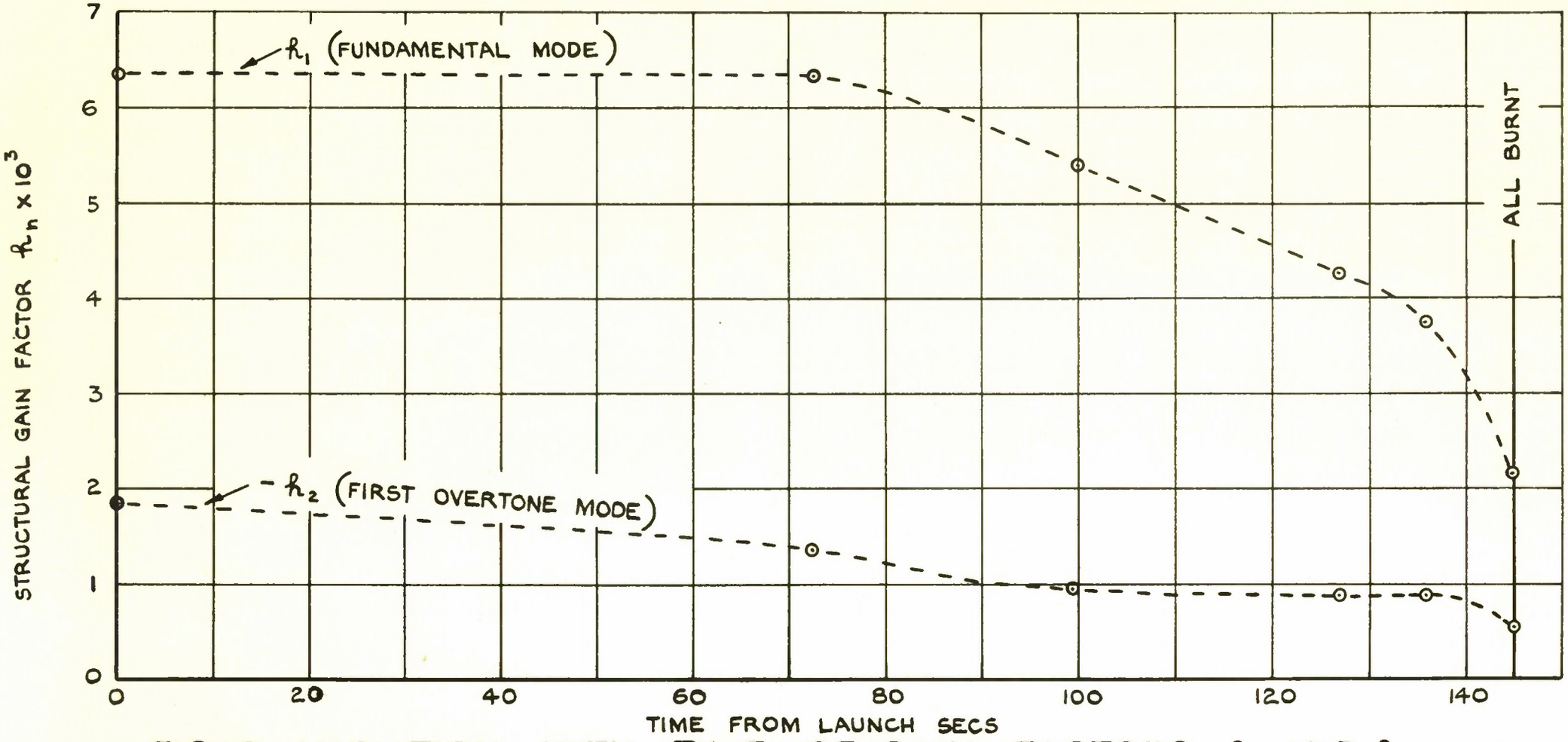

FIG. 10. VARIATION WITH TIME OF GAIN FACTORS k_1 AND k_2 ASSOCIATED WITH THE FIRST AND SECOND BODY BENDING MODES.

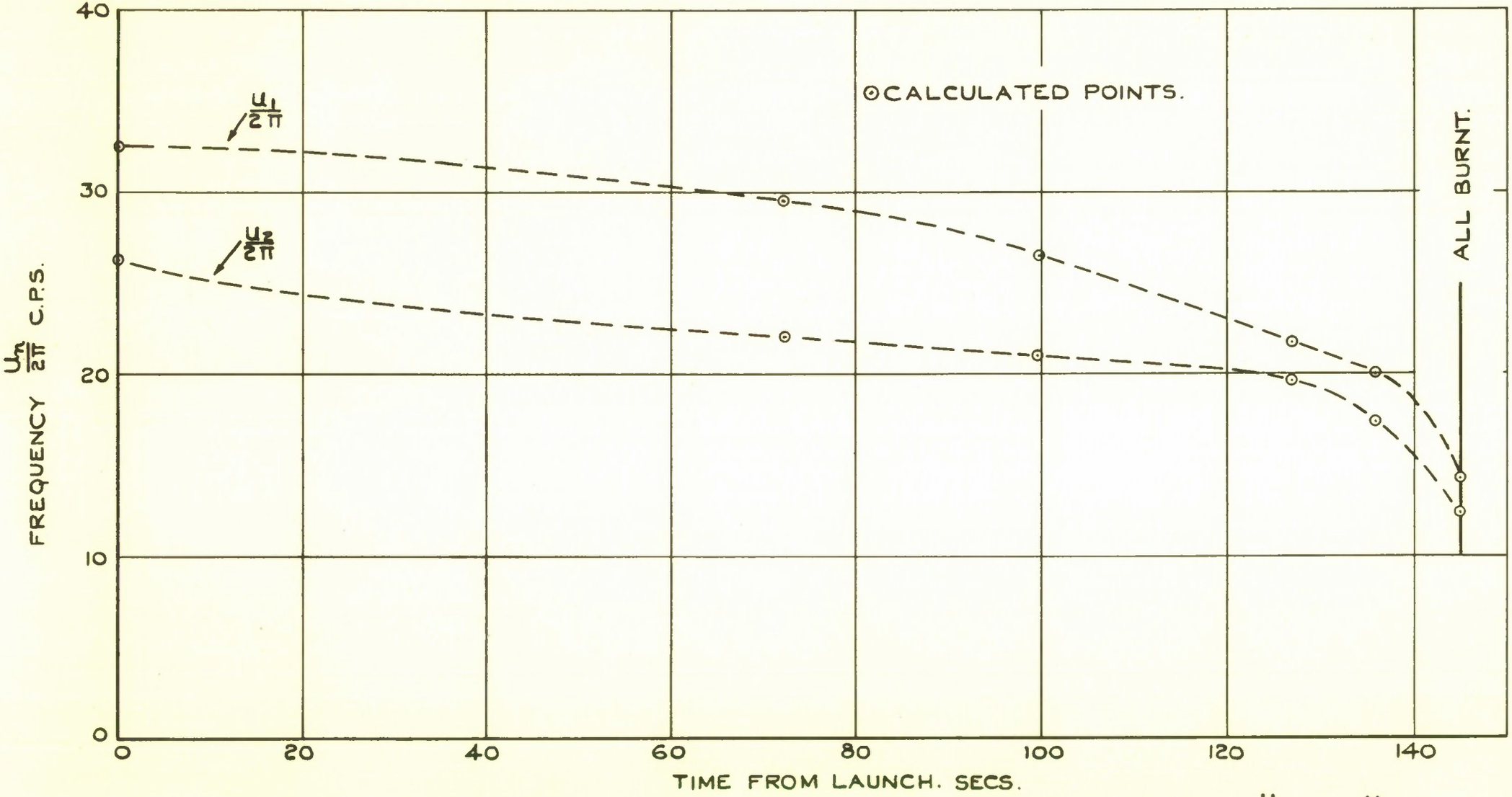

FIG. 11. VARIATION WITH TIME OF FREQUENCIES $\frac{u_1}{2\pi}$ & $\frac{u_2}{2\pi}$ AT WHICH EXCITATION OF FIRST & SECOND BENDING MODES IS EFFECTIVELY ZERO.

FIG. 12.

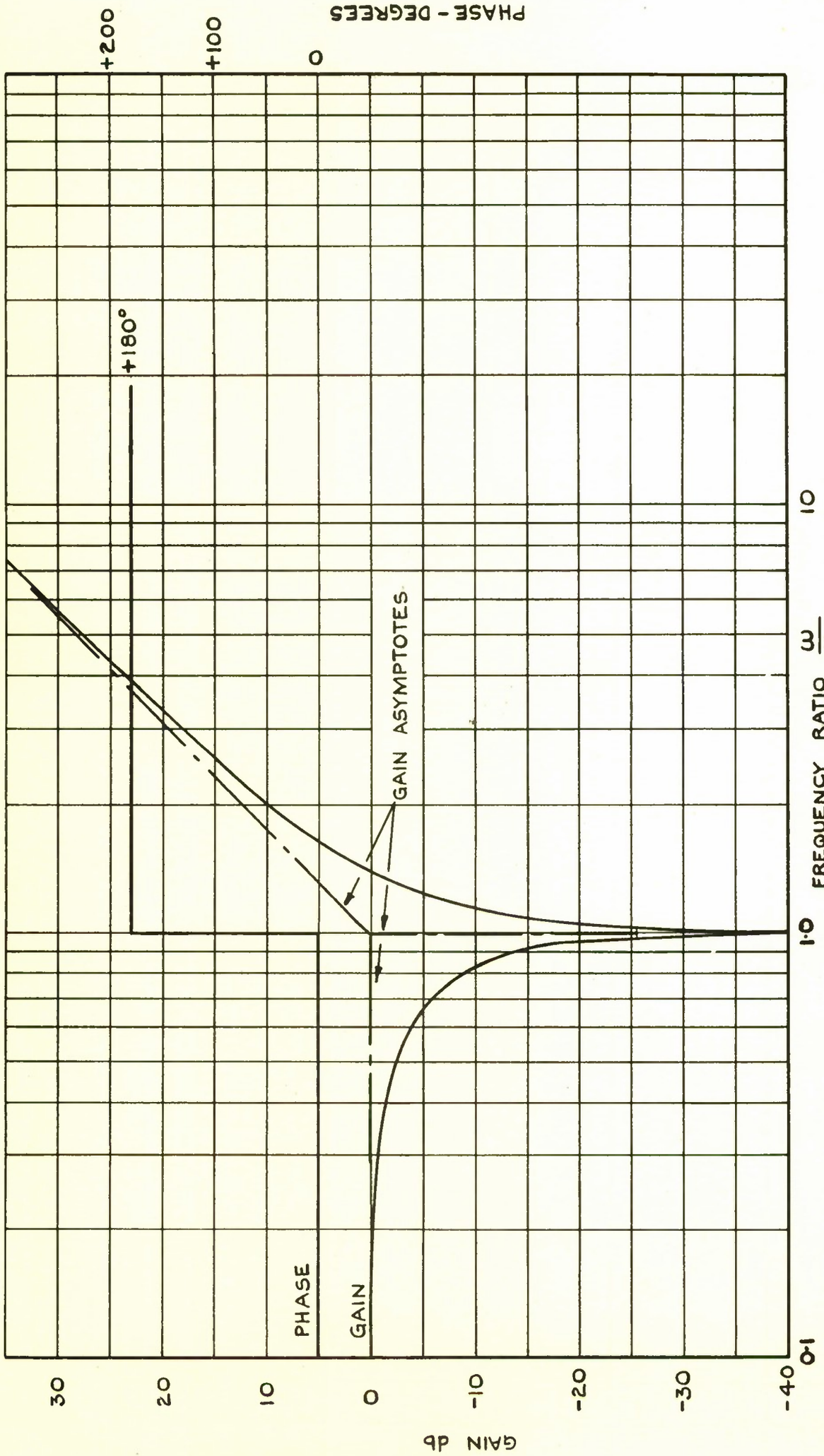

FIG. 12. FREQUENCY RESPONSE OF $\left(1+\frac{p^2}{\omega_n^2}\right)$ IN TERMS OF ω/ω_n.

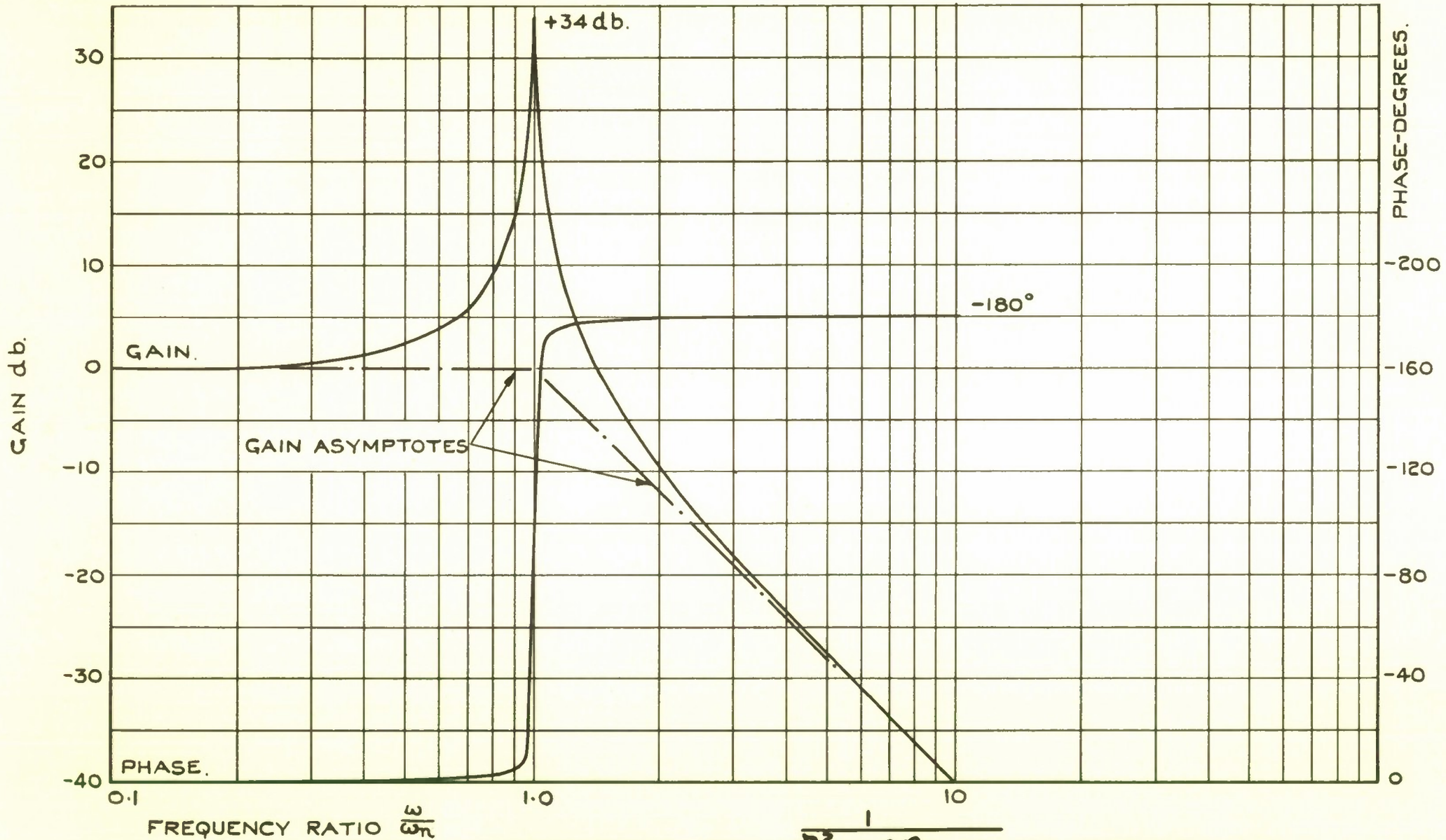

FIG. 13. FREQUENCY RESPONSE OF $\frac{1}{\frac{p^2}{\omega_n^2}+\frac{2\zeta_n}{\omega_n}p+1}$ IN TERMS OF $\frac{\omega}{\omega_n}$ FOR $\zeta_n = 0 \cdot 01$.

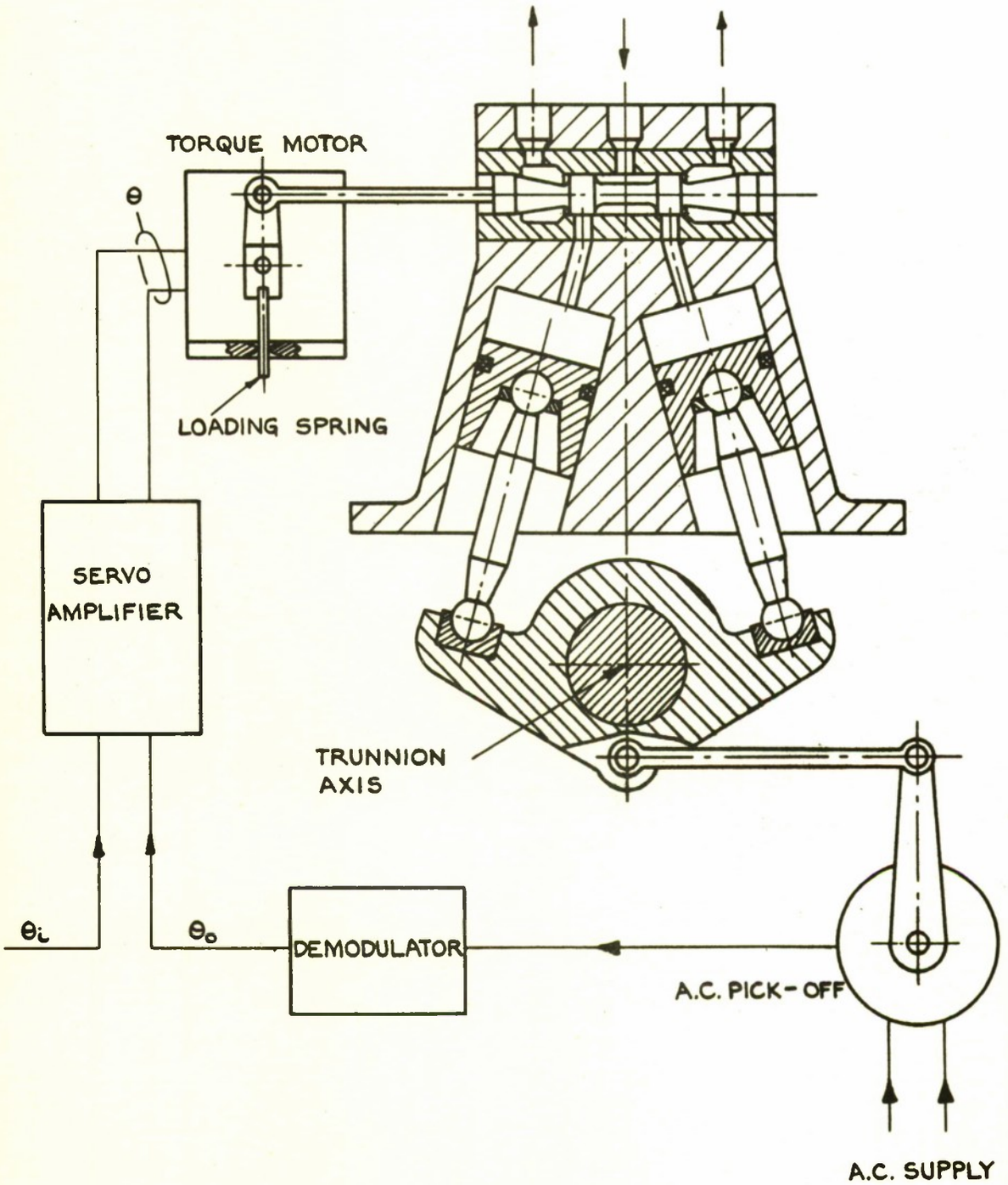

FIG. 14. HYDRAULIC SERVO SCHEMATIC LAYOUT.

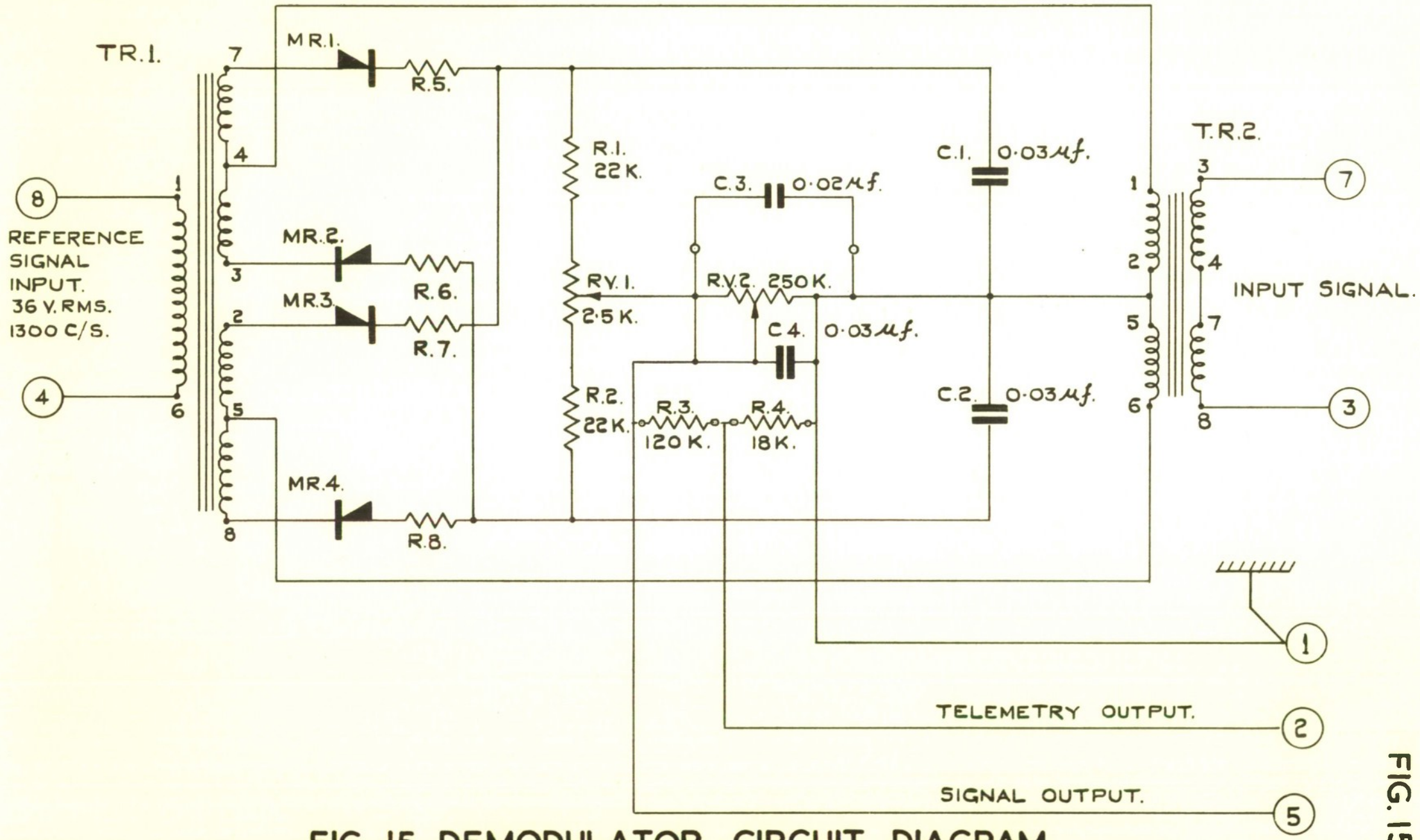

FIG. 15. DEMODULATOR CIRCUIT DIAGRAM.

FIG. 16.

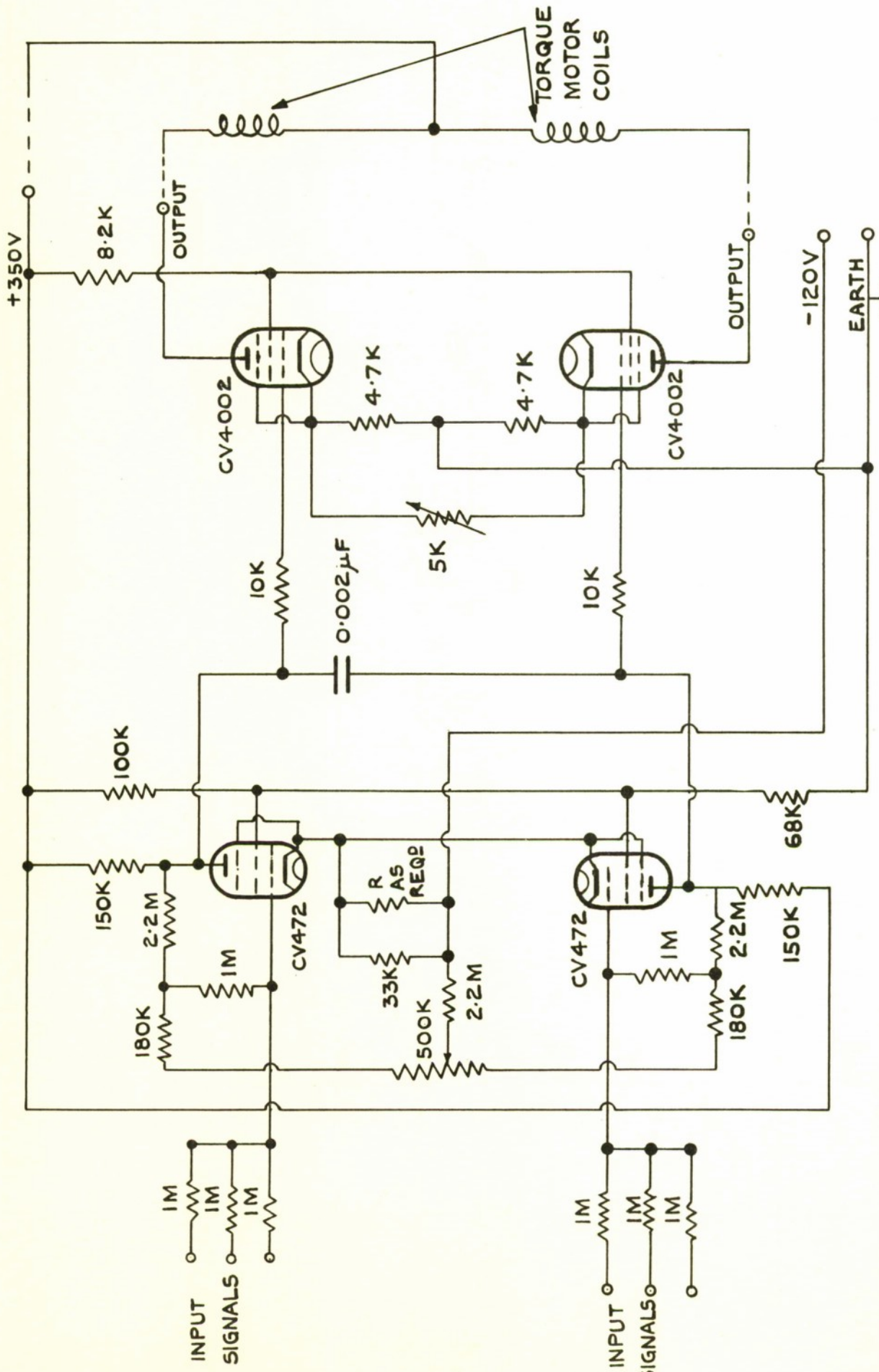

FIG. 16. SERVO AMPLIFIER CIRCUIT DIAGRAM.

FIG. 17.

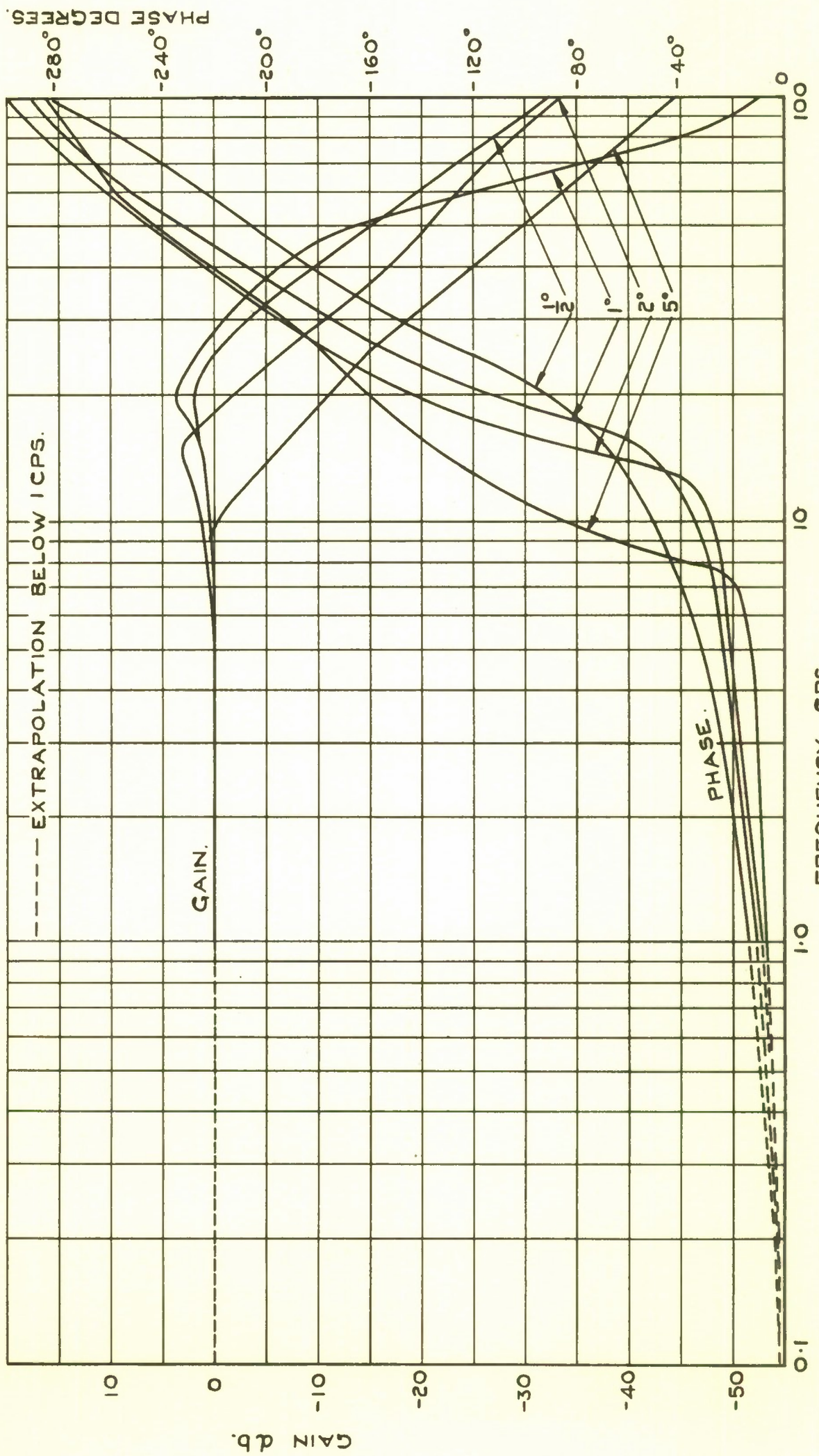

FIG. 17. EXPERIMENTAL FREQUENCY RESPONSE OF ROCKET MOTOR SERVO FOR DEMANDED AMPLITUDES OF 1/2°, 1°, 2° AND 5°.

FIG.18.

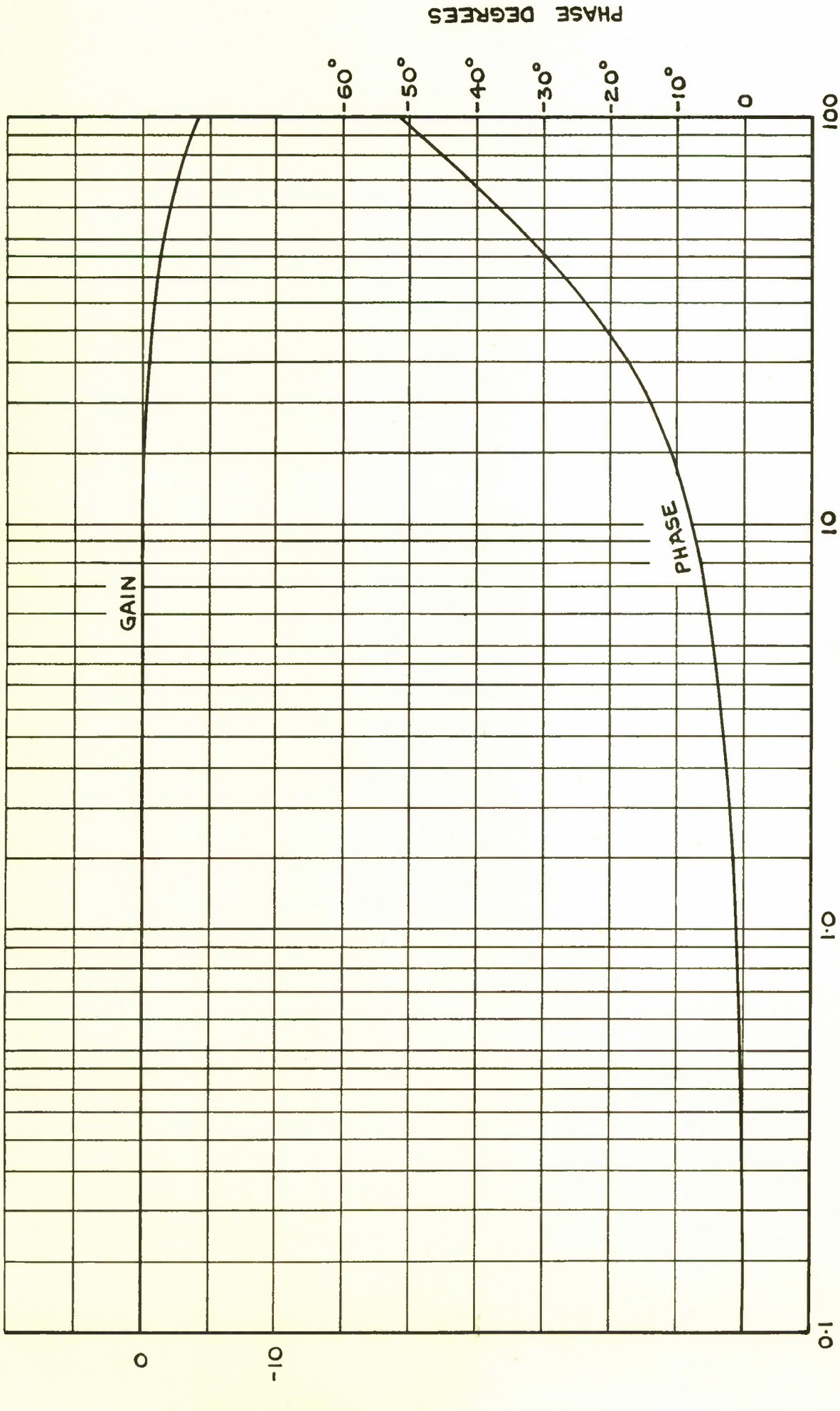

FIG.18. DEMODULATOR FREQUENCY RESPONSE CURVES.

A. INCLUDING GRAVITY —X—

B. NEGLECTING GRAVITY —⊙—

GAIN FACTORS $K_1 K_3 K_4 = 1$ AND $K_1 K_3 K_5 = 4$

FREQUENCIES MARKED AT PLOTTED POINTS (⊙X) IN CYCLES PER SEC.

NOTE CHANGE OF MAGNITUDE SCALE AT 2·0 ≡ +6 db

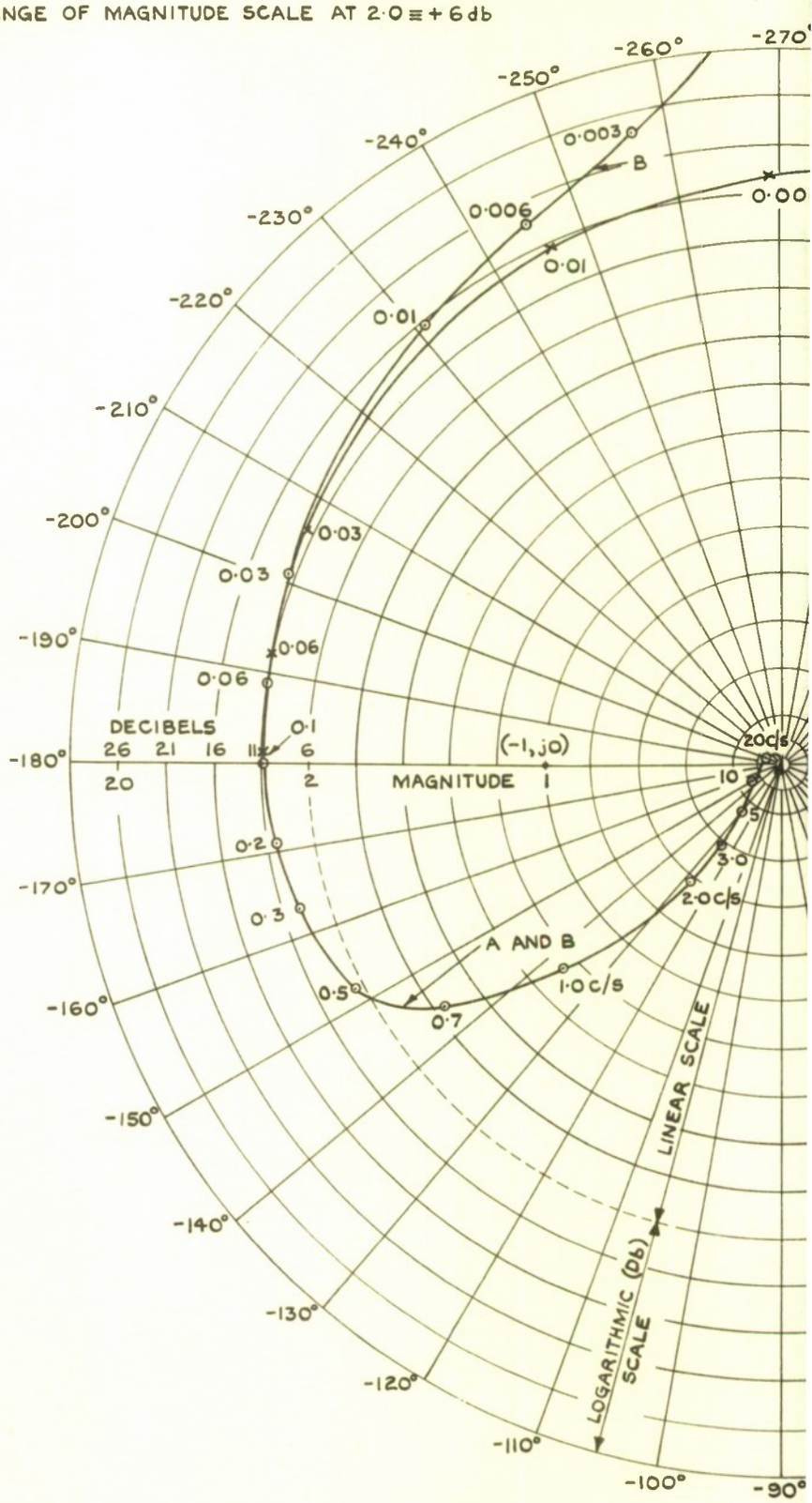

FIG.19. NYQUIST DIAGRAMS OF ELEM

ASSUM

(1)

FIG. 19.

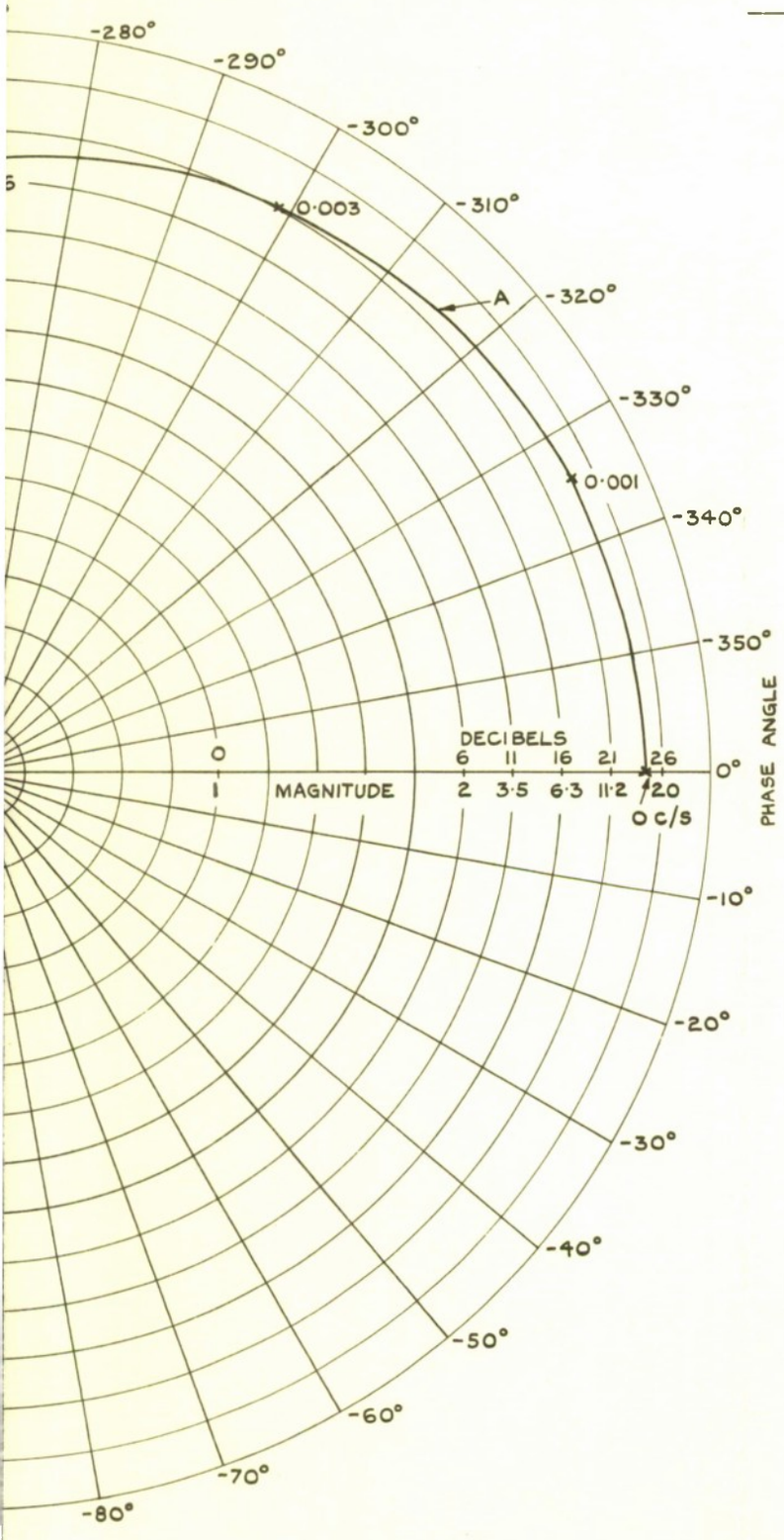

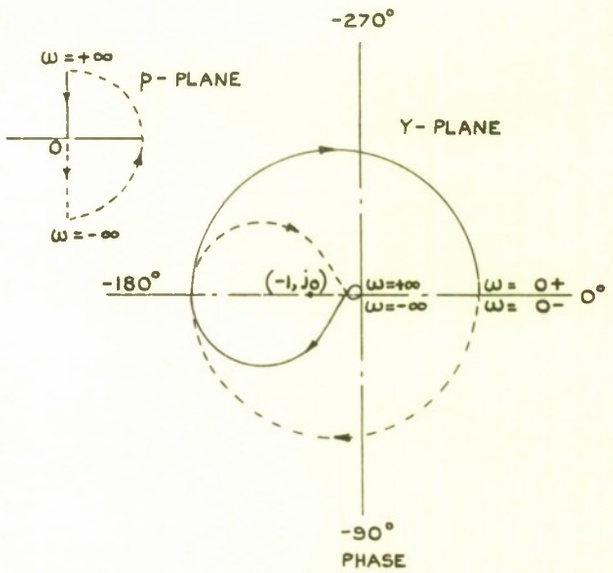

INSET A. RIGID MISSILE WITH GRAVITY INCLUDED.– COMPLETE NYQUIST DIAGRAM.

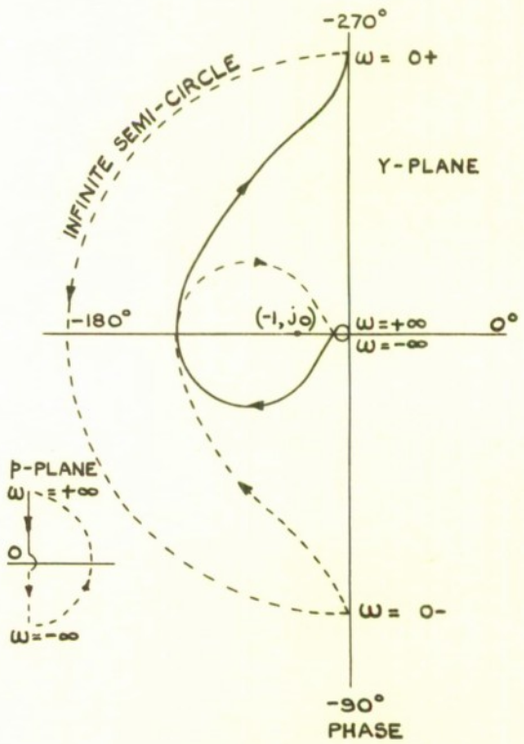

INSET B. RIGID MISSILE WITHOUT GRAVITY. – COMPLETE NYQUIST DIAGRAM.

MENTARY HEADING CONTROL SYSTEM AT t=80 SEC.
MING RIGID MISSILE.

(2)

GAIN FACTORS $K_1 K_3 K_4 = 1$ AND $K_1 K_3 K_5 = 4$
FREQUENCIES MARKED AT PLOTTED POINTS (x) IN CYCLES PER SEC.
NOTE CHANGE OF MAGNITUDE SCALE AT 2·0 ≡ + 6 db.

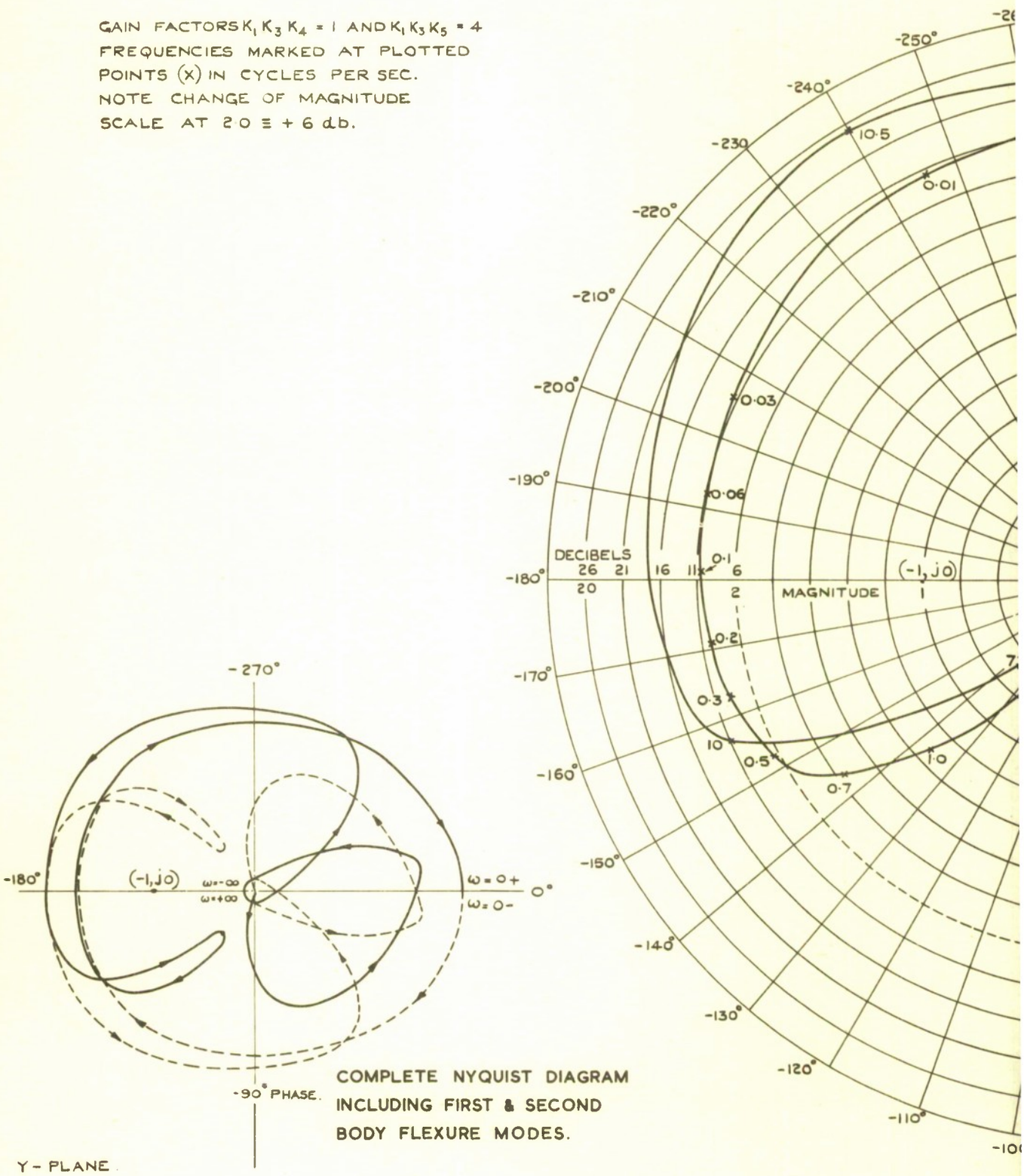

COMPLETE NYQUIST DIAGRAM INCLUDING FIRST & SECOND BODY FLEXURE MODES.

FIG. 20. NYQUIST DIAGRAM OF ELEMENTARY HEA
INCLUDING FIRST & SECOND BODY FLEXURE M

FIG. 20.

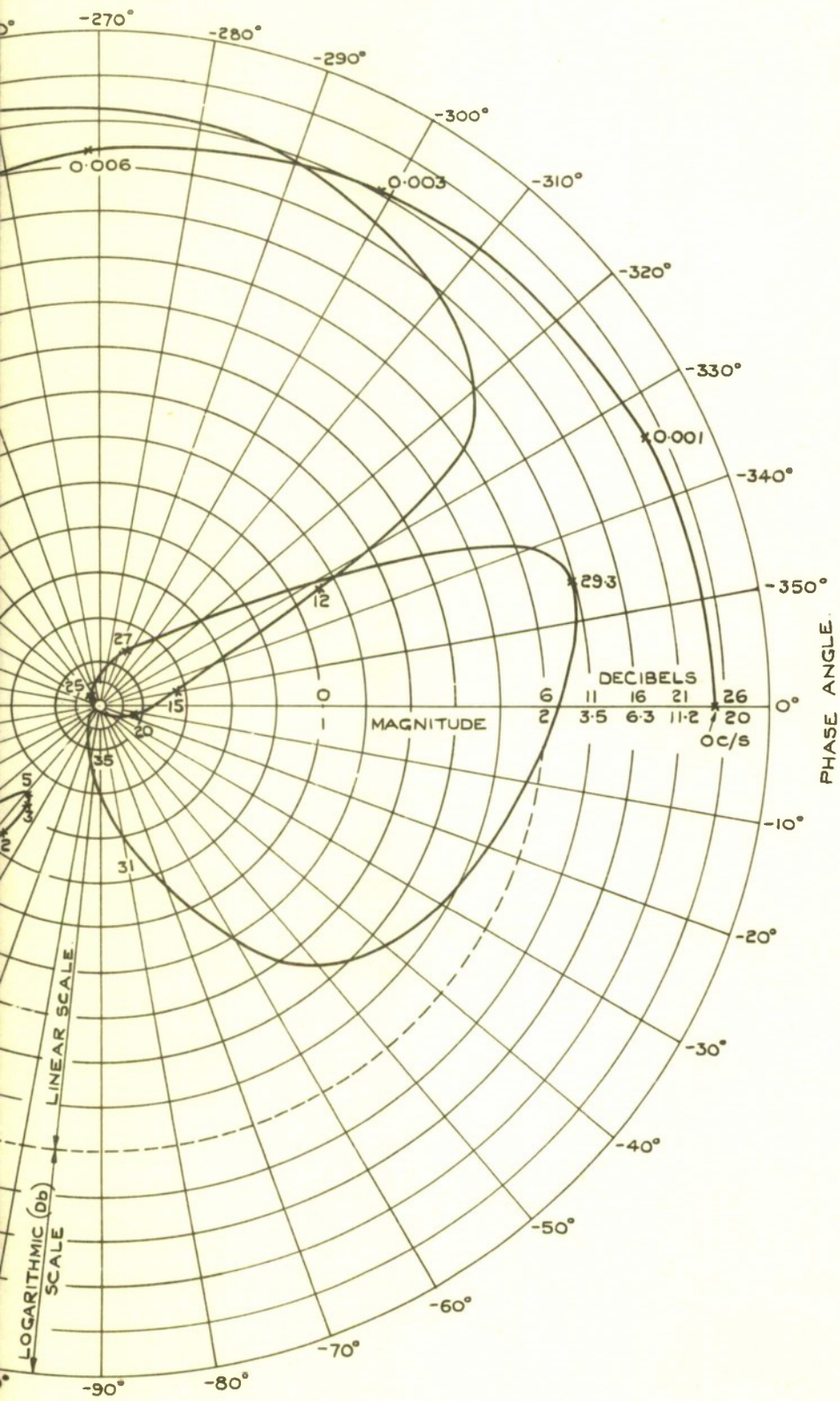

ADING CONTROL SYSTEM AT t=80SEC.
IODES BUT WITHOUT STABILISING FILTER.

(2)

FIG. 21.

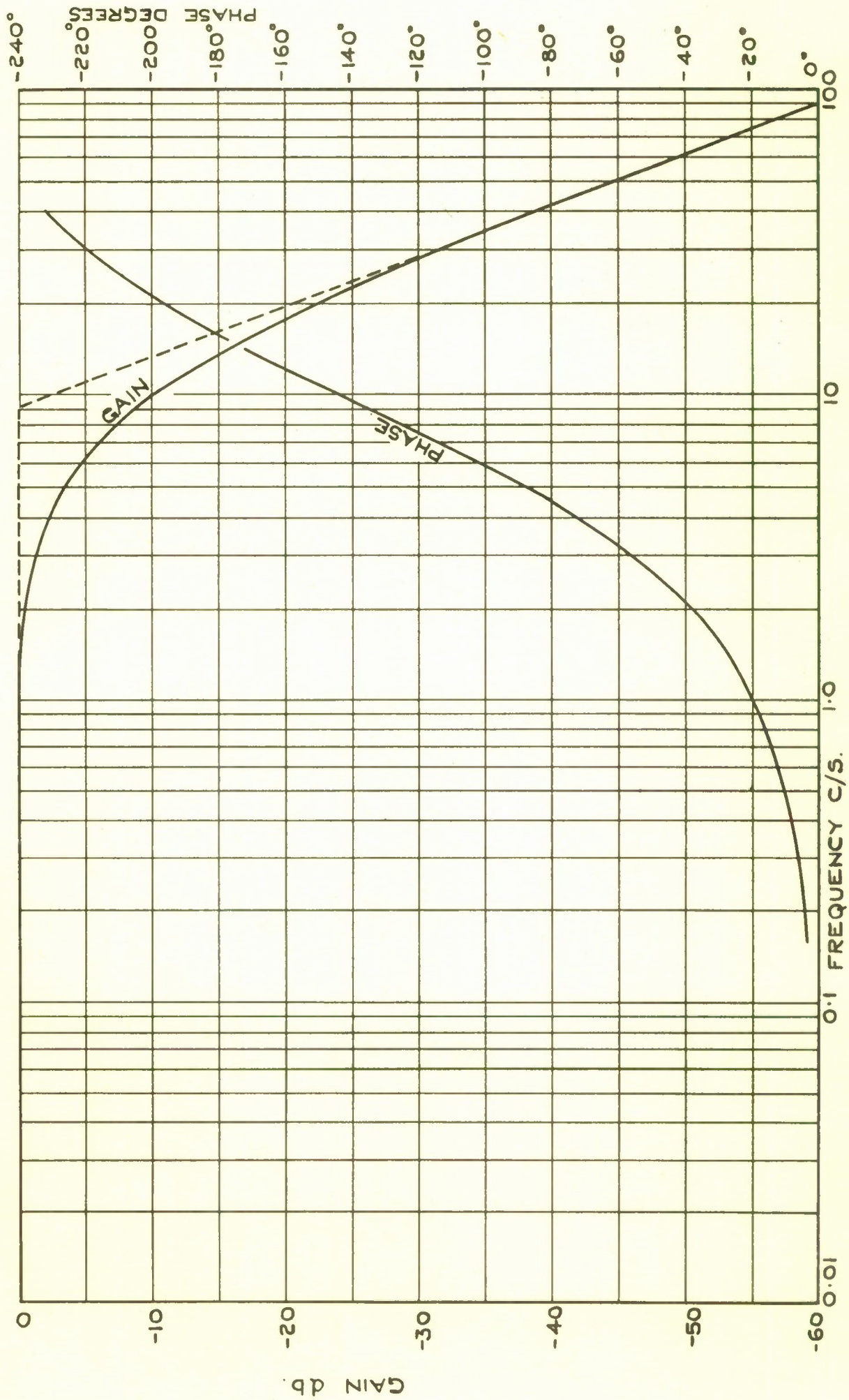

FIG. 21. FREQUENCY RESPONSE CURVES OF THIRD ORDER FILTER. TRANSFER FUNCTION IS $\frac{1}{(1+0{\cdot}018\,p)^3}$.

G.W/P.9930.

GAIN FACTORS $K_1 K_3 K_4 = 1$ AND $K_1 K_3 K_5 = 4$
NOTE CHANGE OF SCALE AT 2·0 ≡ 6 DB.

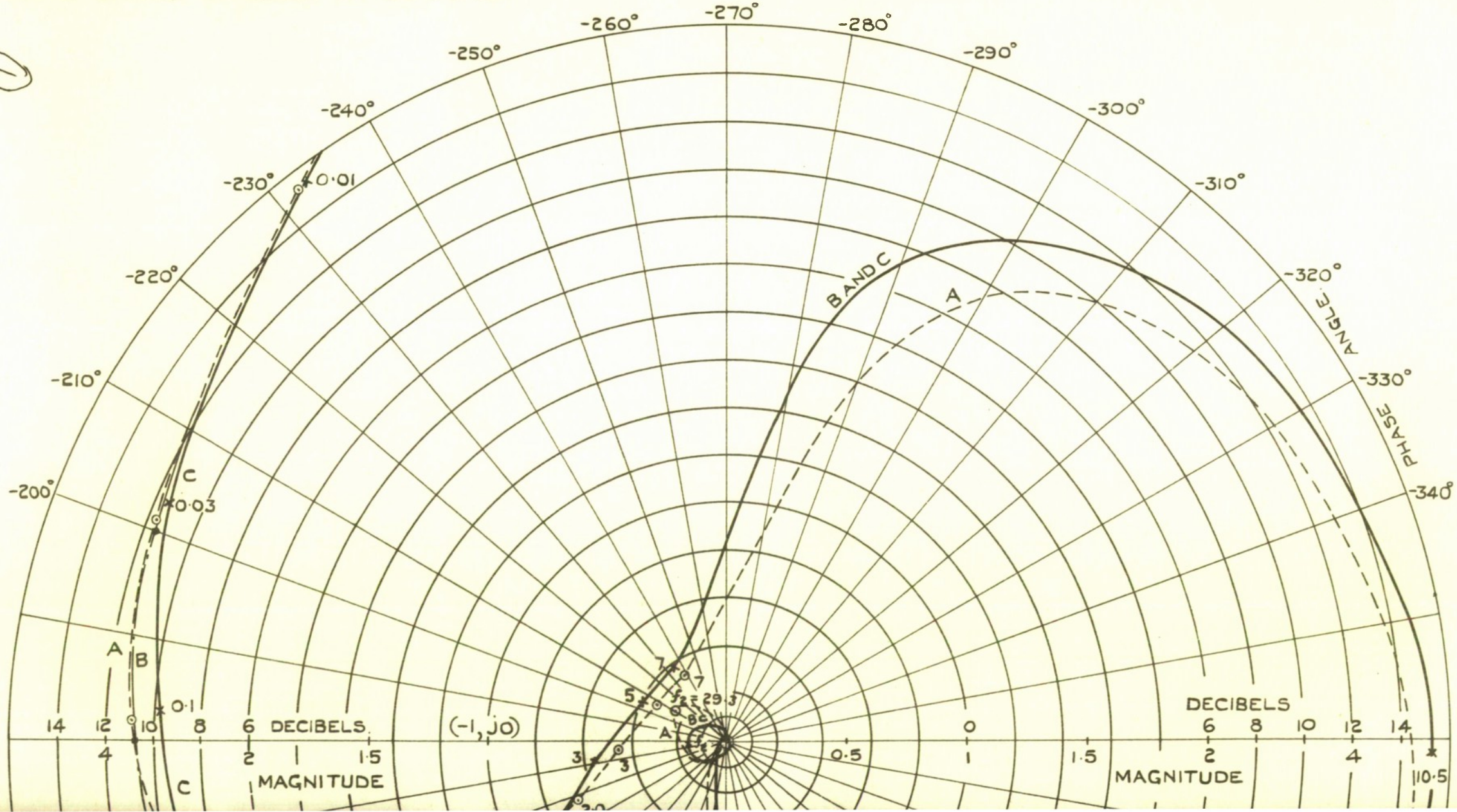

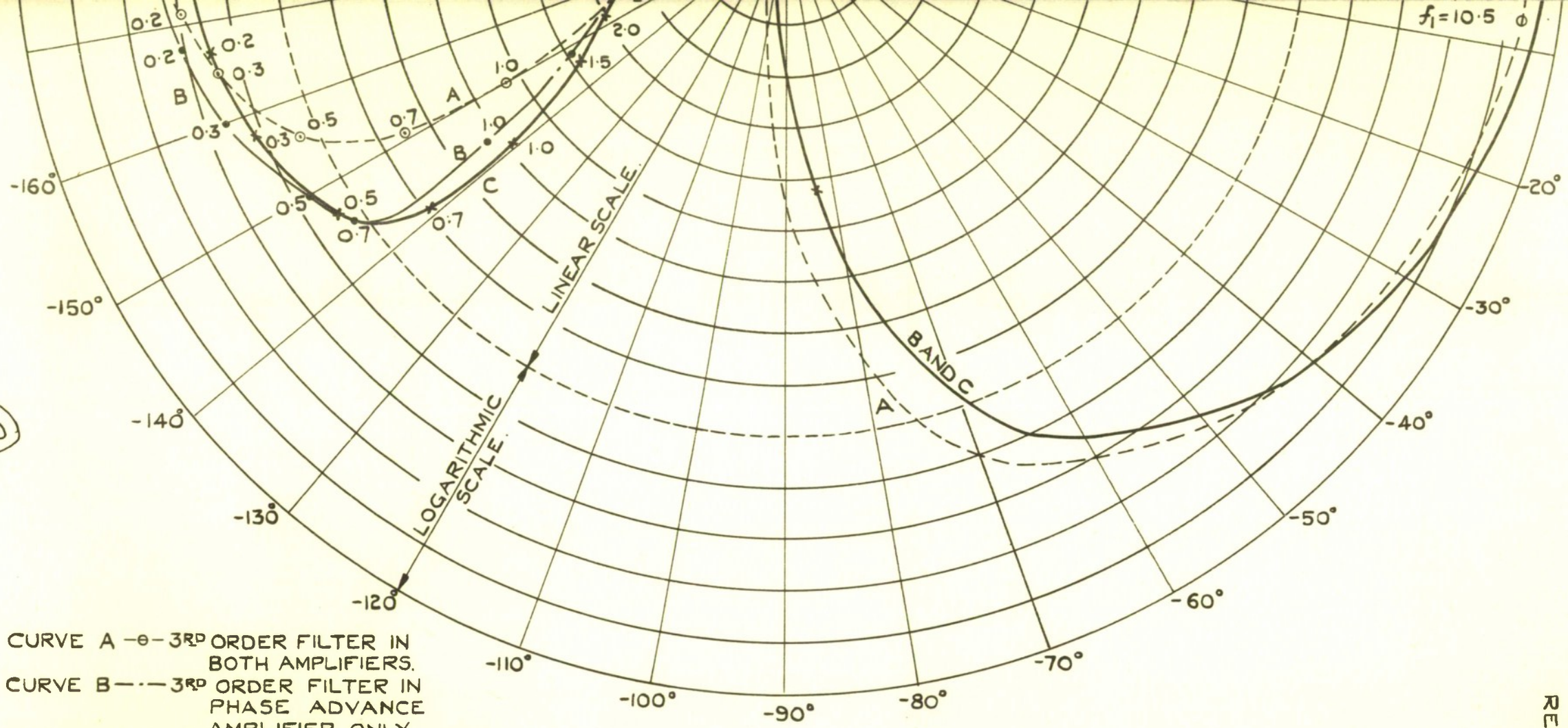

CURVE A —o— 3RD ORDER FILTER IN BOTH AMPLIFIERS.
CURVE B —·— 3RD ORDER FILTER IN PHASE ADVANCE AMPLIFIER ONLY.
CURVE C —×— ACTUAL PHASE ADVANCE AMPLIFIER CIRCUIT.
FREQUENCIES IN CYCLES/SEC.

FIG. 22. NYQUIST DIAGRAMS OF HEADING CONTROL SYSTEM, INCLUDING BODY FLEXURE MODES & STABILISING FILTER, AT t = 80 SEC.

REPORT GW. 24.
FIG. 22.

FIG. 23.

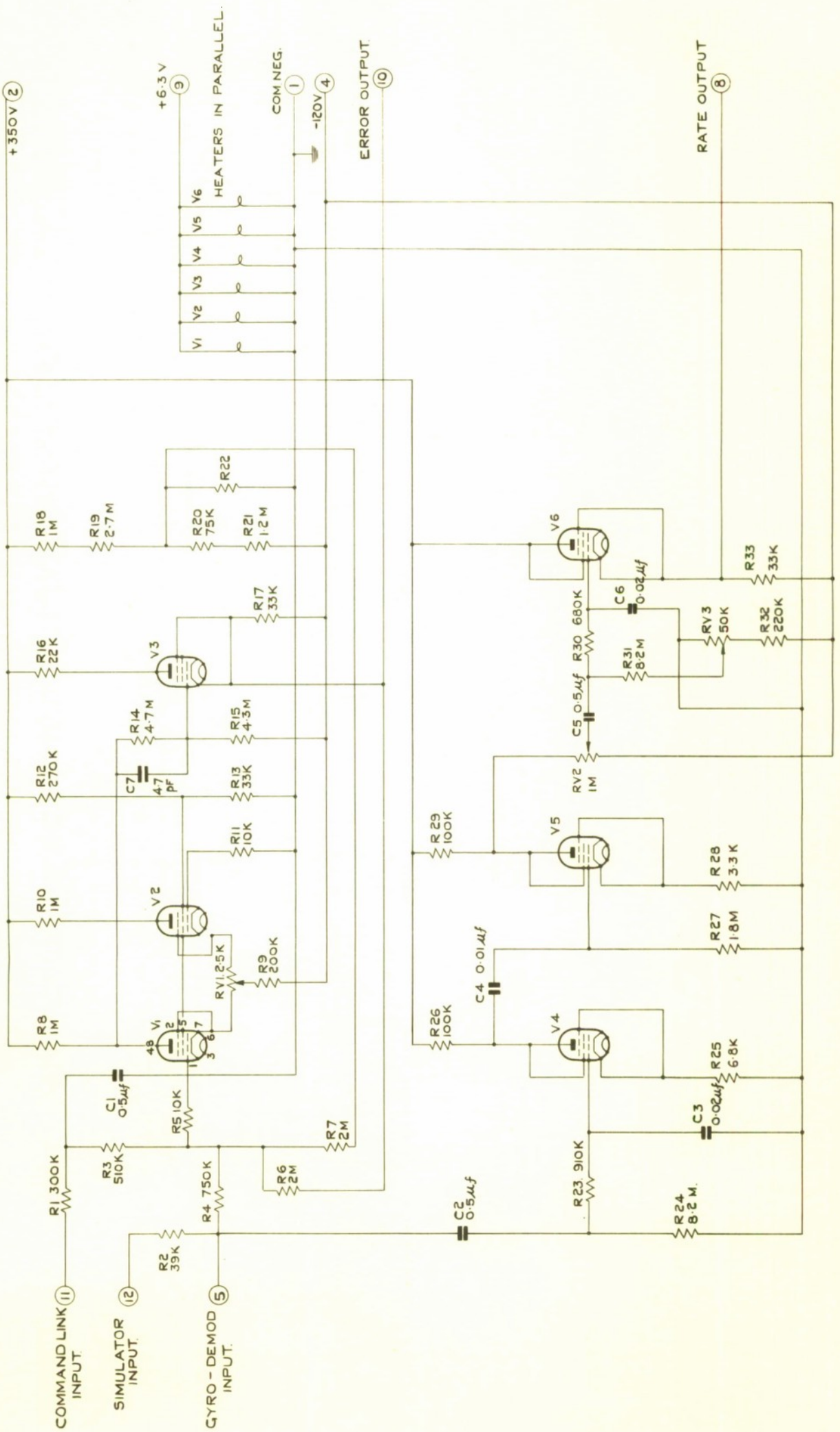

FIG. 23. CIRCUIT DIAGRAM OF LATERAL SUMMING & PHASE ADVANCE AMPLIFIERS.

FIG.24.

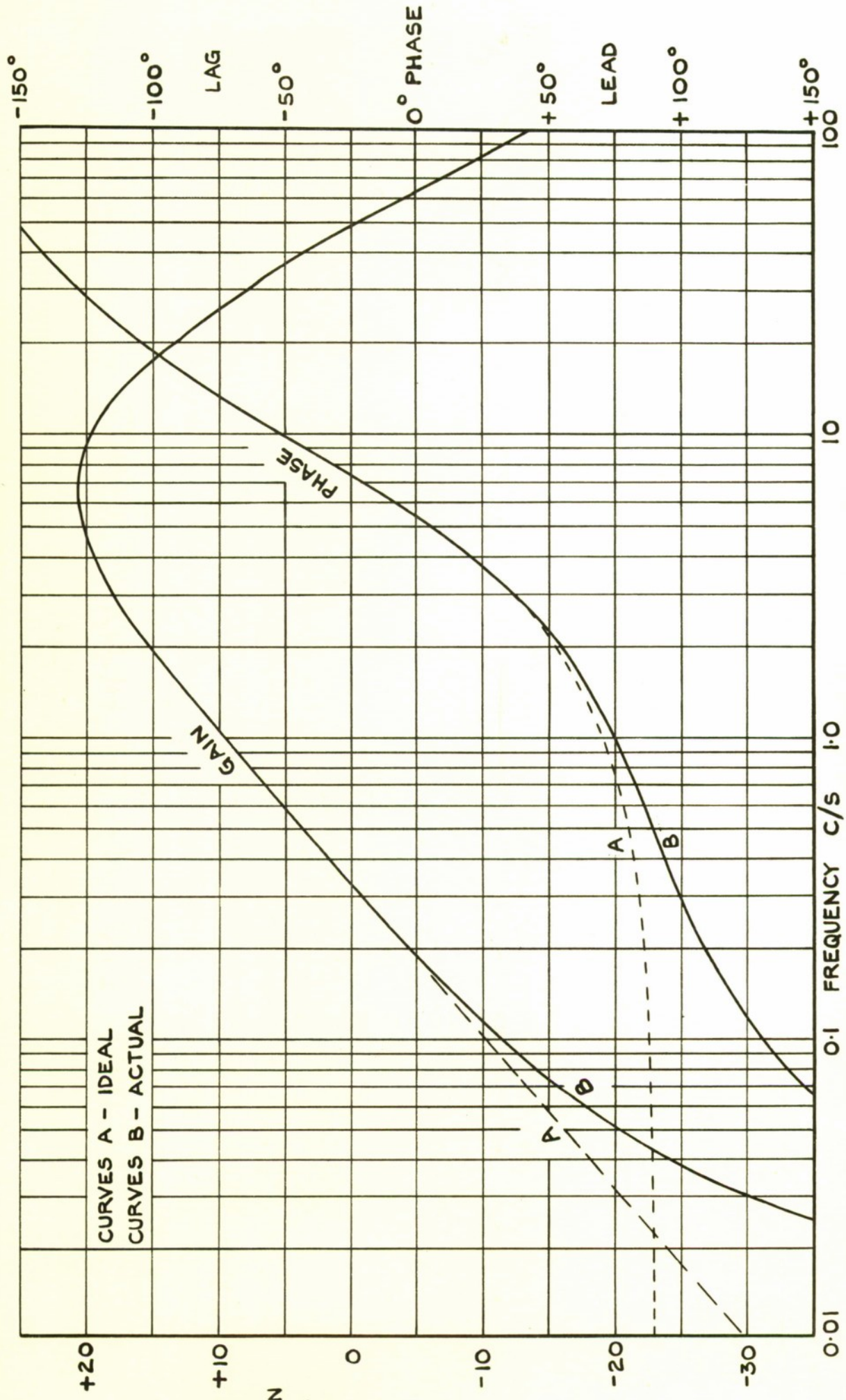

FIG. 24. FREQUENCY RESPONSE CURVES OF THE LATERAL PHASE ADVANCE AMPLIFIER.

GAIN FACTORS

$K_1 K_3 K_4 = 0.25$ AND $K_1 K_3 K_5 = 1$

NOTE CHANGE OF SCALE

AT 1·0 ≡ 0DB

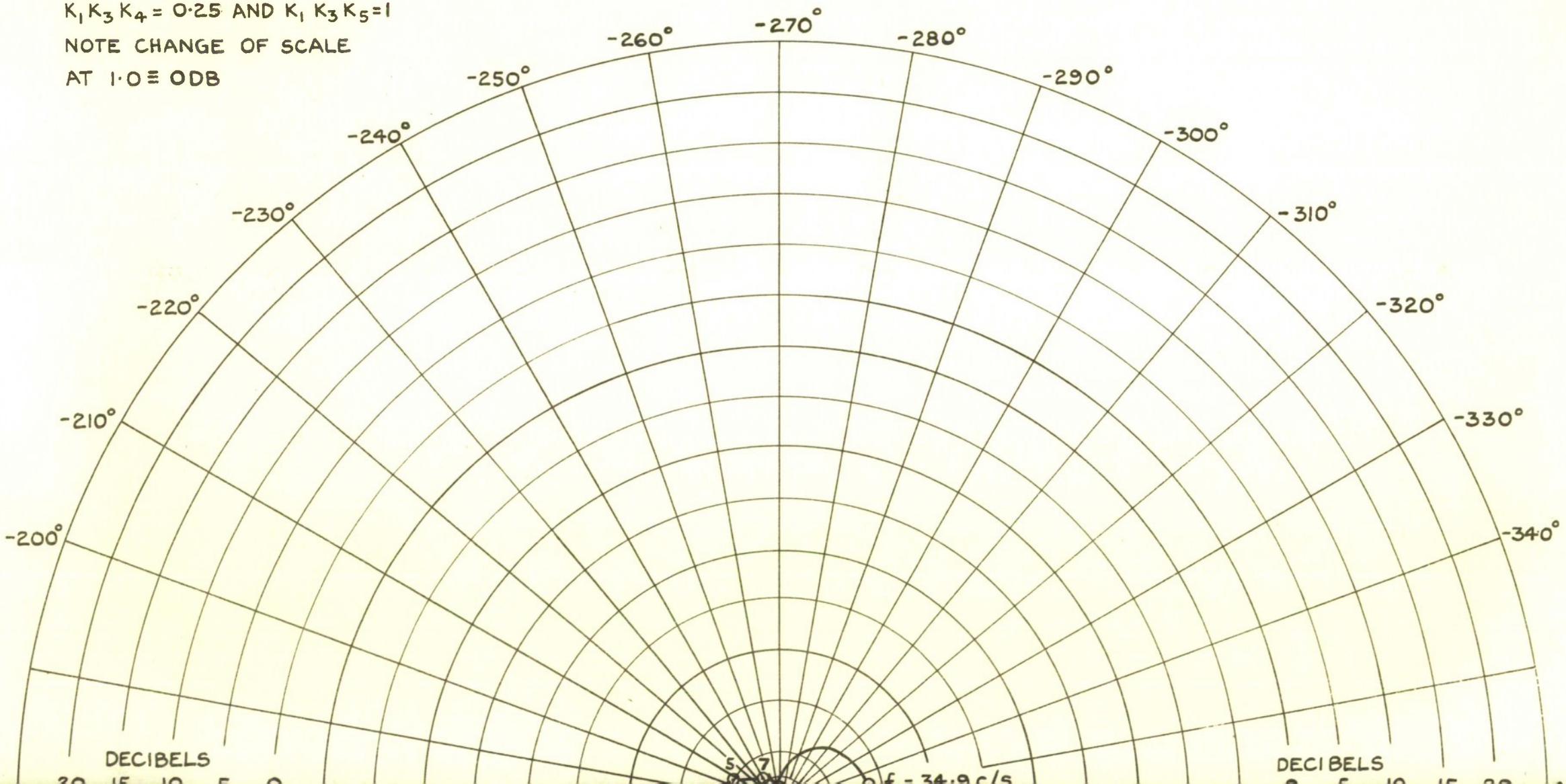

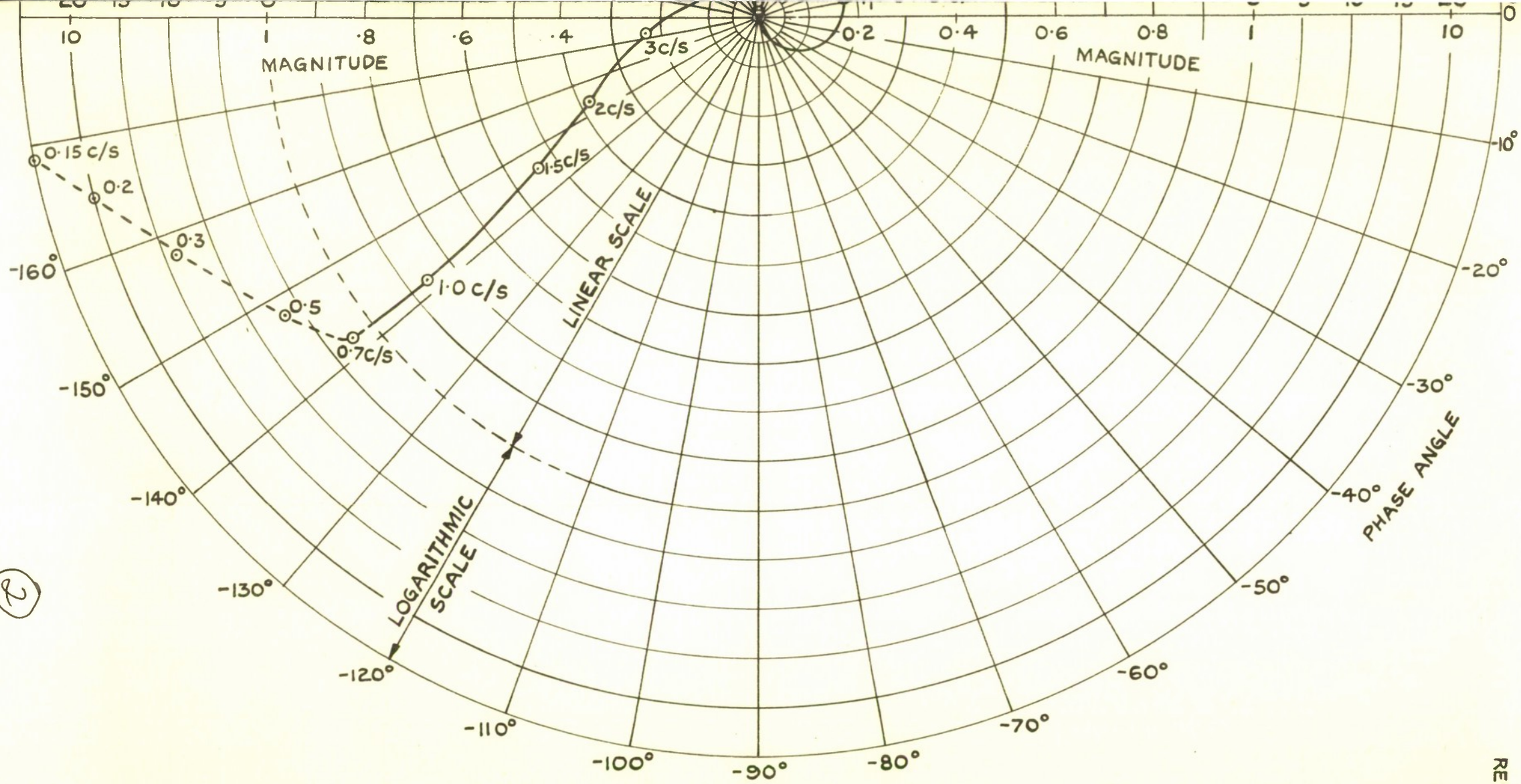

(2)

FIG. 25. NYQUIST DIAGRAM OF HEADING CONTROL SYSTEM AT t = 145 SEC.

REPORT G.W. 24.
FIG. 25.

G.W/P.9934.

GAIN FACTORS $K_1K_3K_4 = 1$ AND $K_1K_3K_5 = 4$.
NOTE CHANGE OF SCALE AT
1·0 ≡ 0 DB.

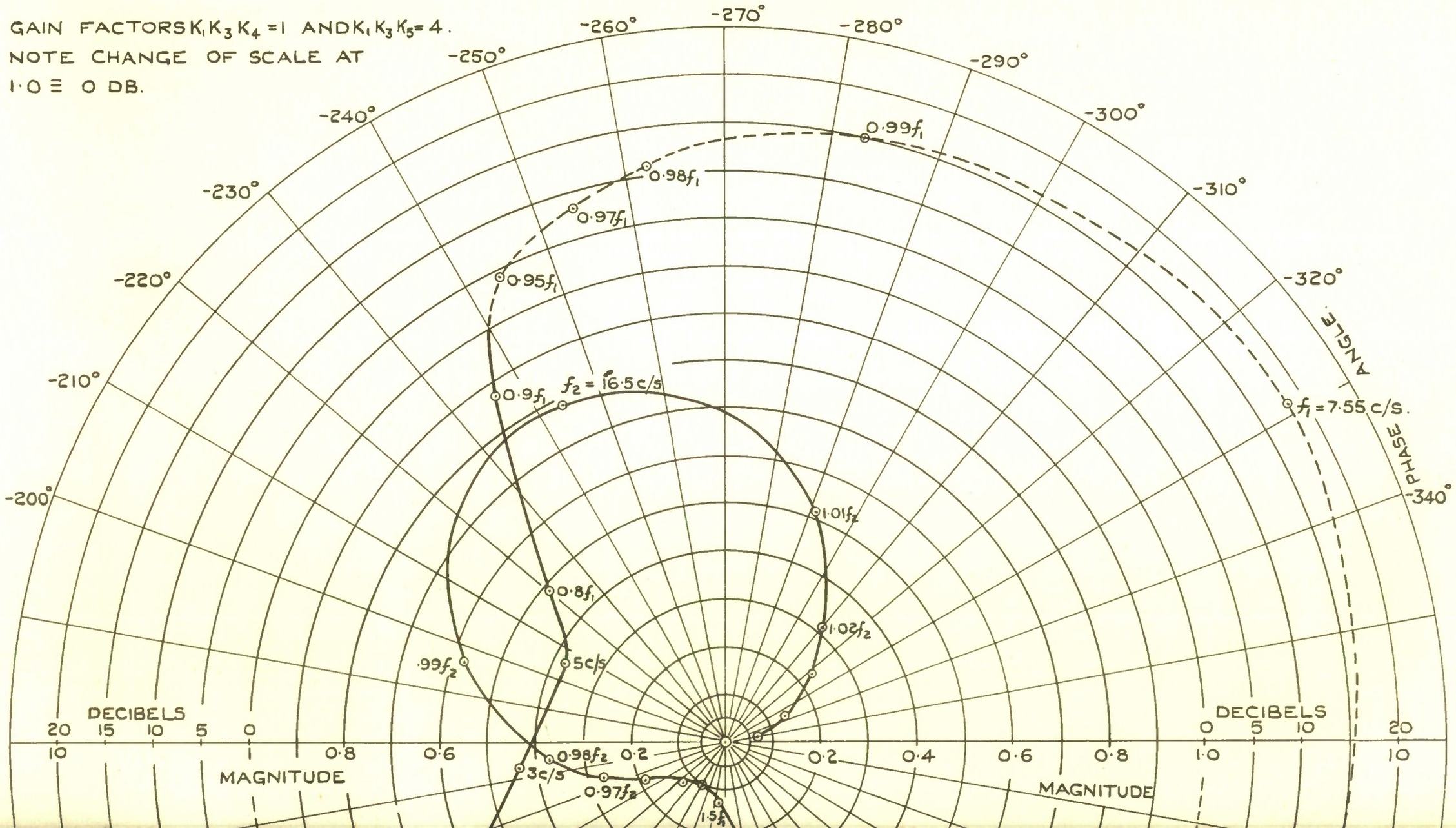

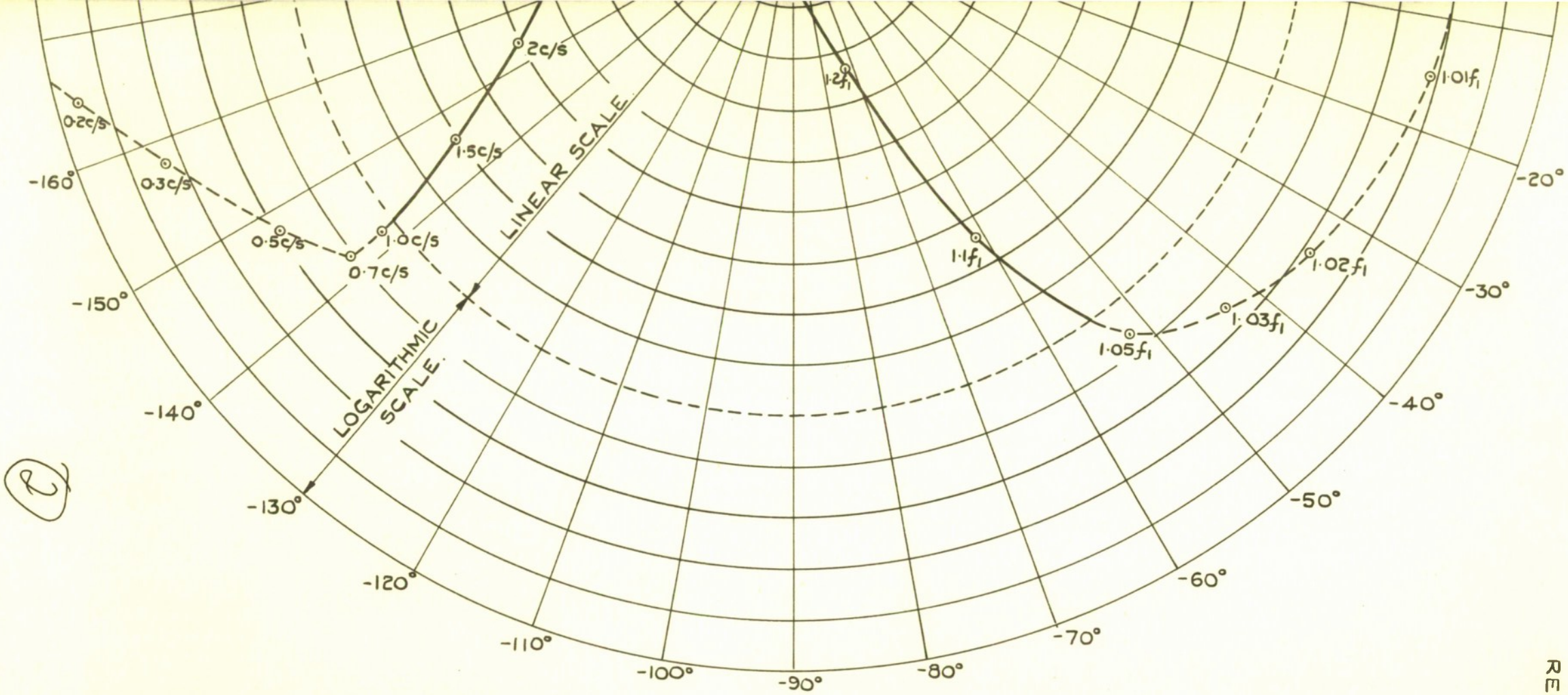

FIG. 26. NYQUIST DIAGRAM OF HEADING CONTROL SYSTEM AT TAKE-OFF $t = 0$.

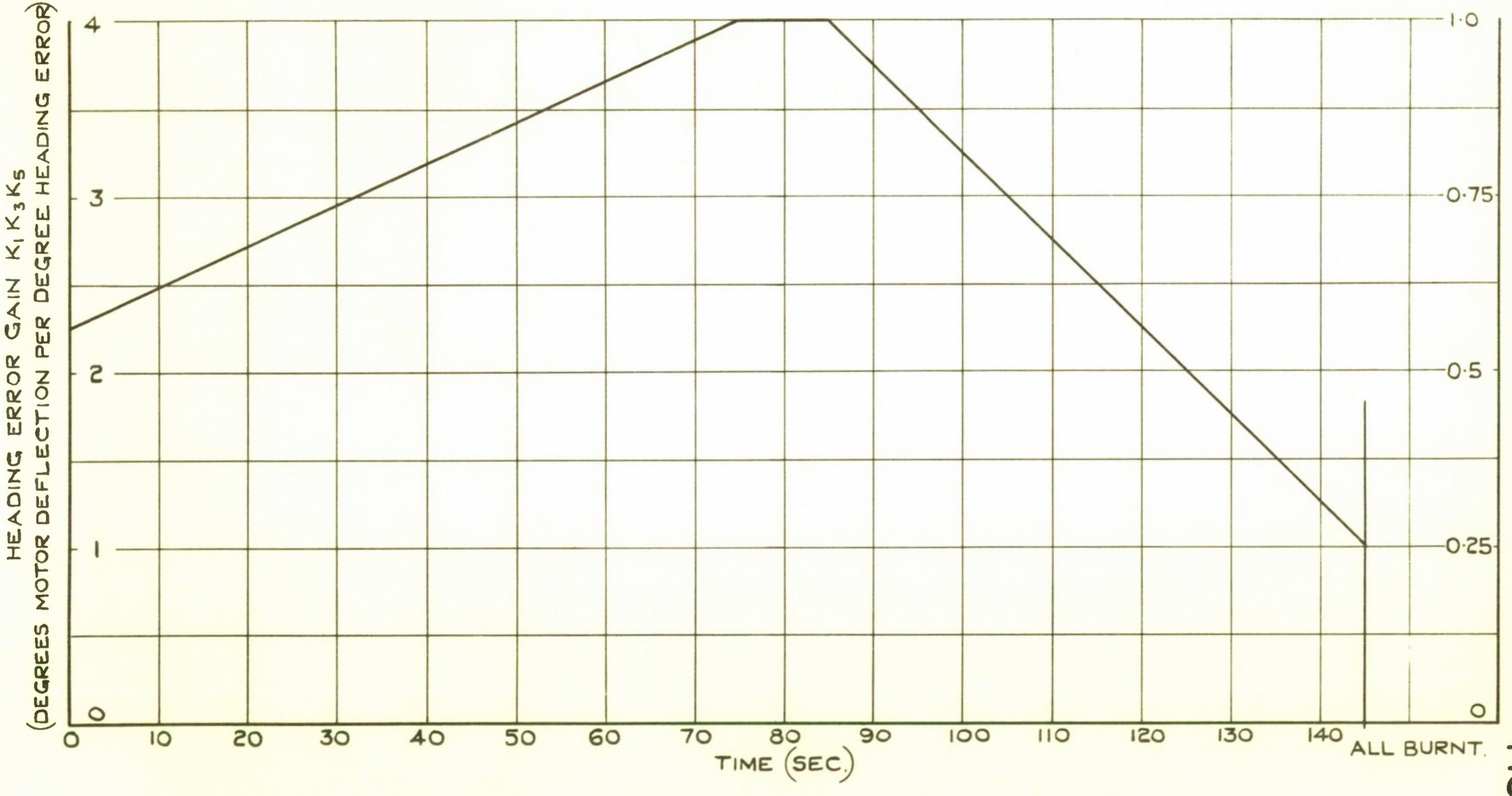

FIG. 27.

FIG. 27. PROPOSED VARIATION OF GAIN DURING FLIGHT.

GW/P.9936.

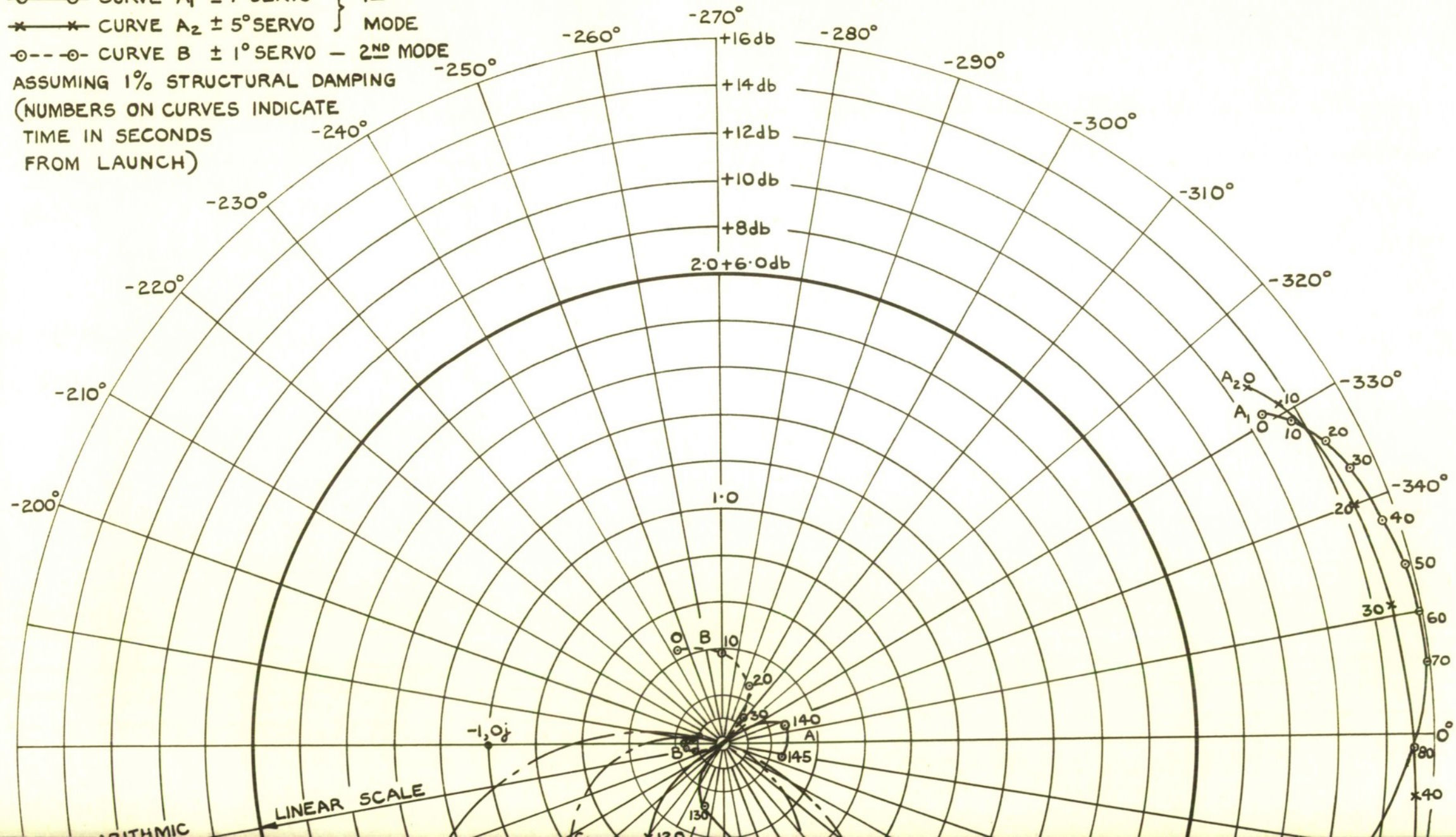
CURVE A_1 ± 1° SERVO } 1ST
CURVE A_2 ± 5° SERVO } MODE
CURVE B ± 1° SERVO — 2ND MODE
ASSUMING 1% STRUCTURAL DAMPING
(NUMBERS ON CURVES INDICATE
TIME IN SECONDS
FROM LAUNCH)
-270°
-260°
-280°
-250°
-290°
-240°
-300°
-230°
-310°
-220°
-320°
-210°
-330°
-200°
-340°
0°
+16db
+14db
+12db
+10db
+8db
2·0+6·0db
1·0
LINEAR SCALE
-1,0j
A2
A1
B
LOGARITHMIC

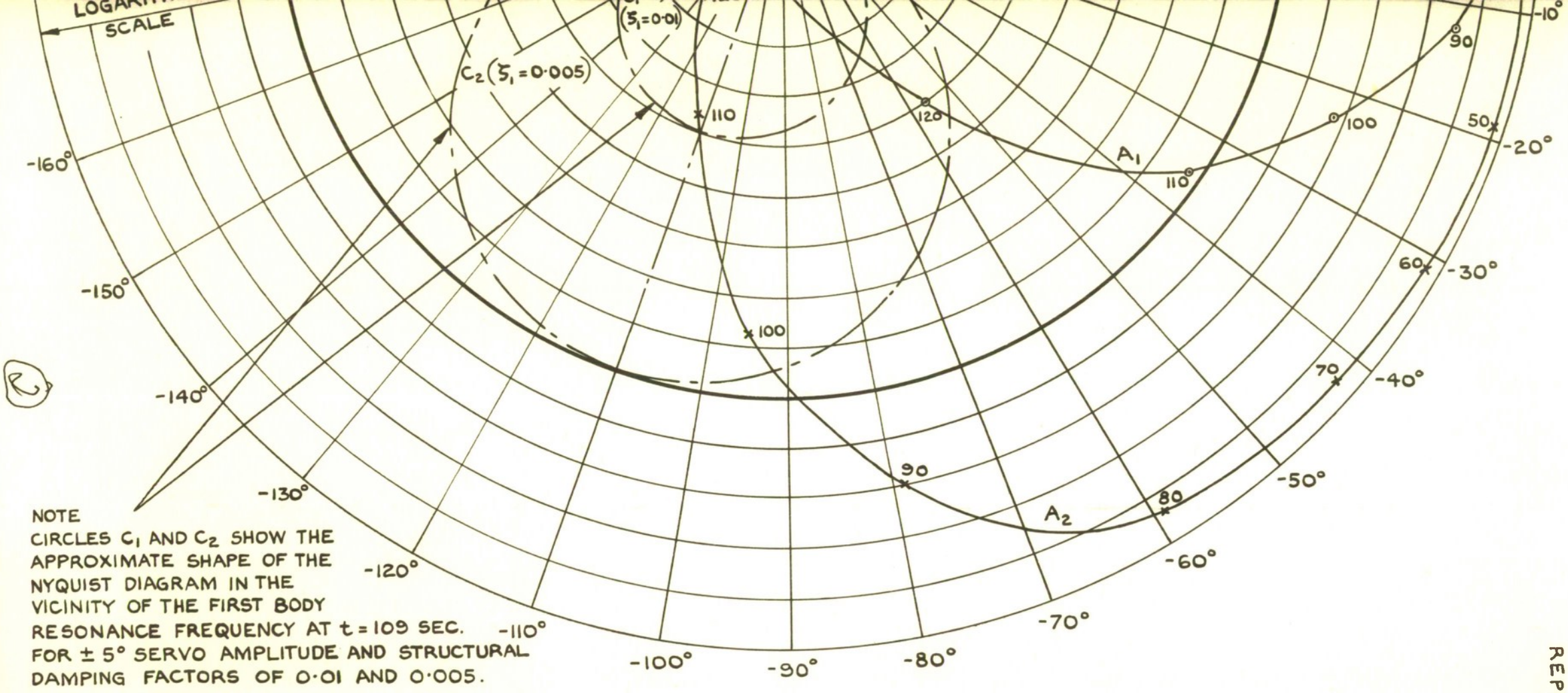

NOTE
CIRCLES C_1 AND C_2 SHOW THE APPROXIMATE SHAPE OF THE NYQUIST DIAGRAM IN THE VICINITY OF THE FIRST BODY RESONANCE FREQUENCY AT $t = 109$ SEC. FOR $\pm 5°$ SERVO AMPLITUDE AND STRUCTURAL DAMPING FACTORS OF 0·01 AND 0·005.

FIG. 28. LOCI SHOWING THE VARIATION WITH TIME OF THE FEEDBACK GAIN AND PHASE AT BODY FLEXURE FREQUENCIES

(SEE TABLE 1)

REPORT G.W.24.
FIG. 28.

(1)

G.W/P.9937.

GAIN FACTORS $K_1K_3K_4 = 0.56$ AND $K_1K_3K_5 = 2.25$
ASSUMED STRUCTURAL DAMPING 0·3 %
NOTE CHANGE OF SCALE AT 1·0.

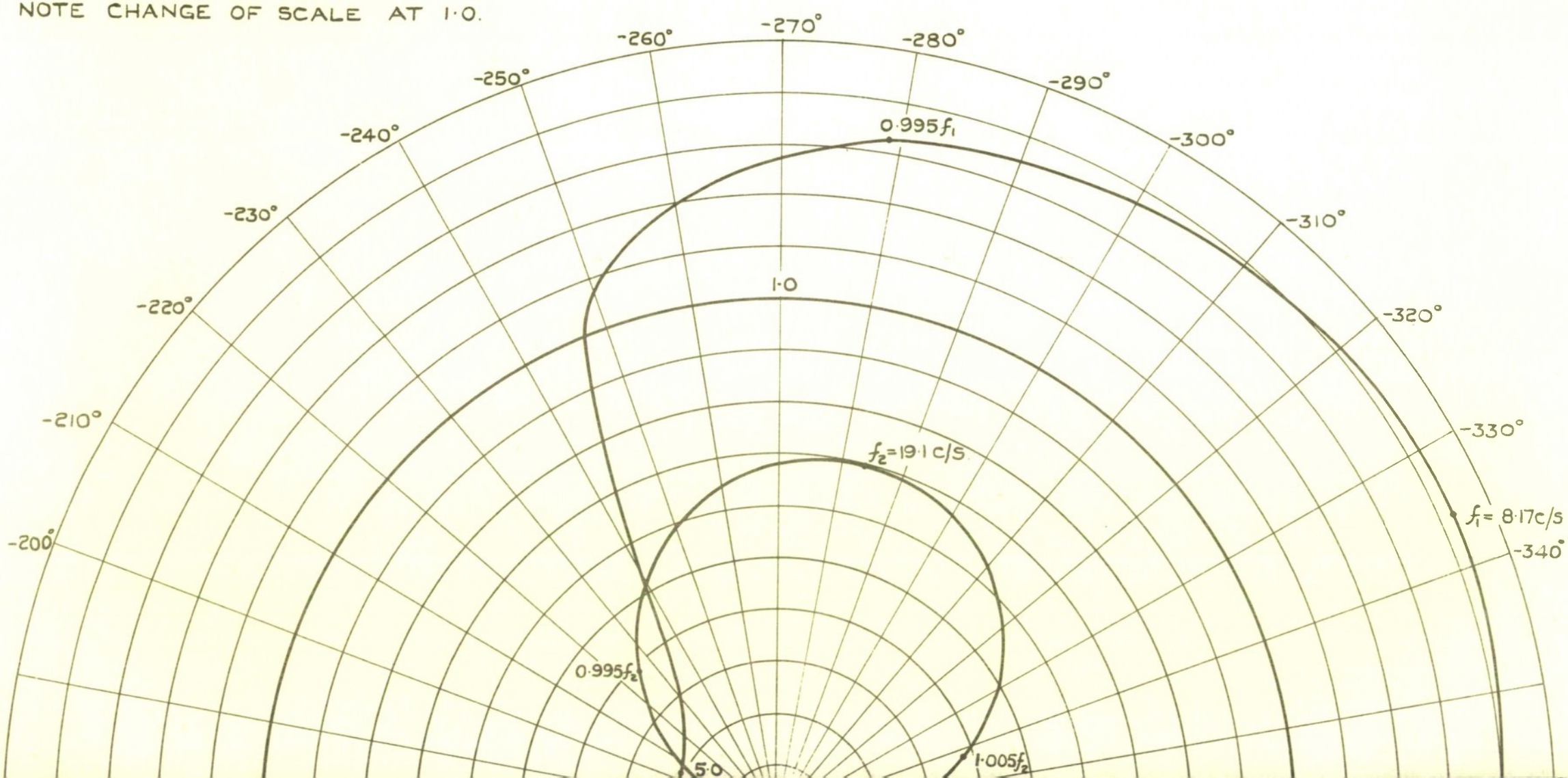

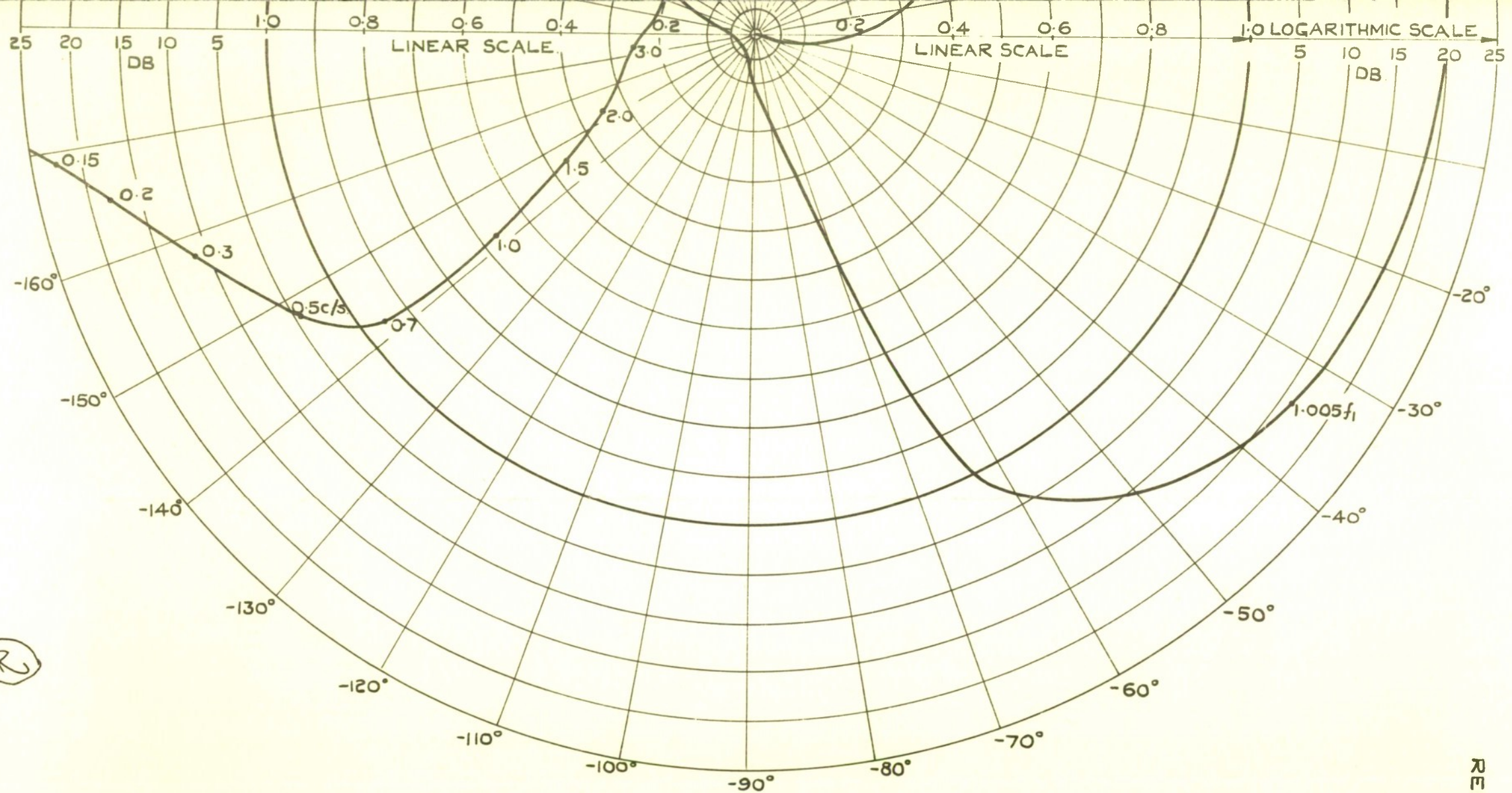

(2)

FIG. 29. NYQUIST DIAGRAM OF HEADING CONTROL SYSTEM AT TAKE-OFF WITH REVISED BODY FLEXURE MODES.
(SEE TABLE 2.)

REPORT G.W. 24.
FIG. 29.

CURVE A ± 1° SERVO CHARACTERISTICS.

CURVE B ± 5° SERVO CHARACTERISTICS.

ASSUMED STRUCTURAL DAMPING 0·5%
(NUMBERS ON CURVES INDICATE TIME FROM TAKE-OFF IN SECONDS.)

G.W/P.9938.

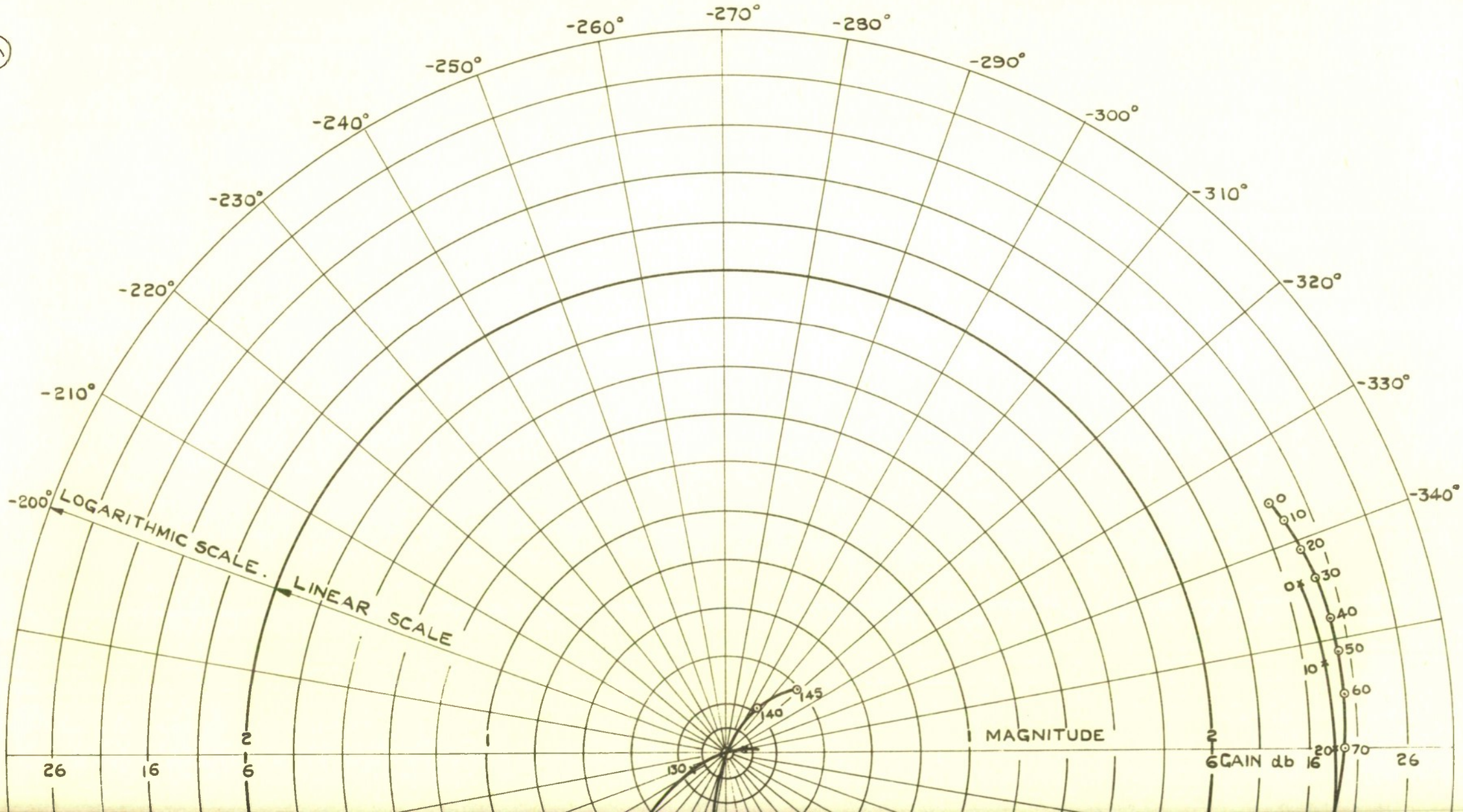

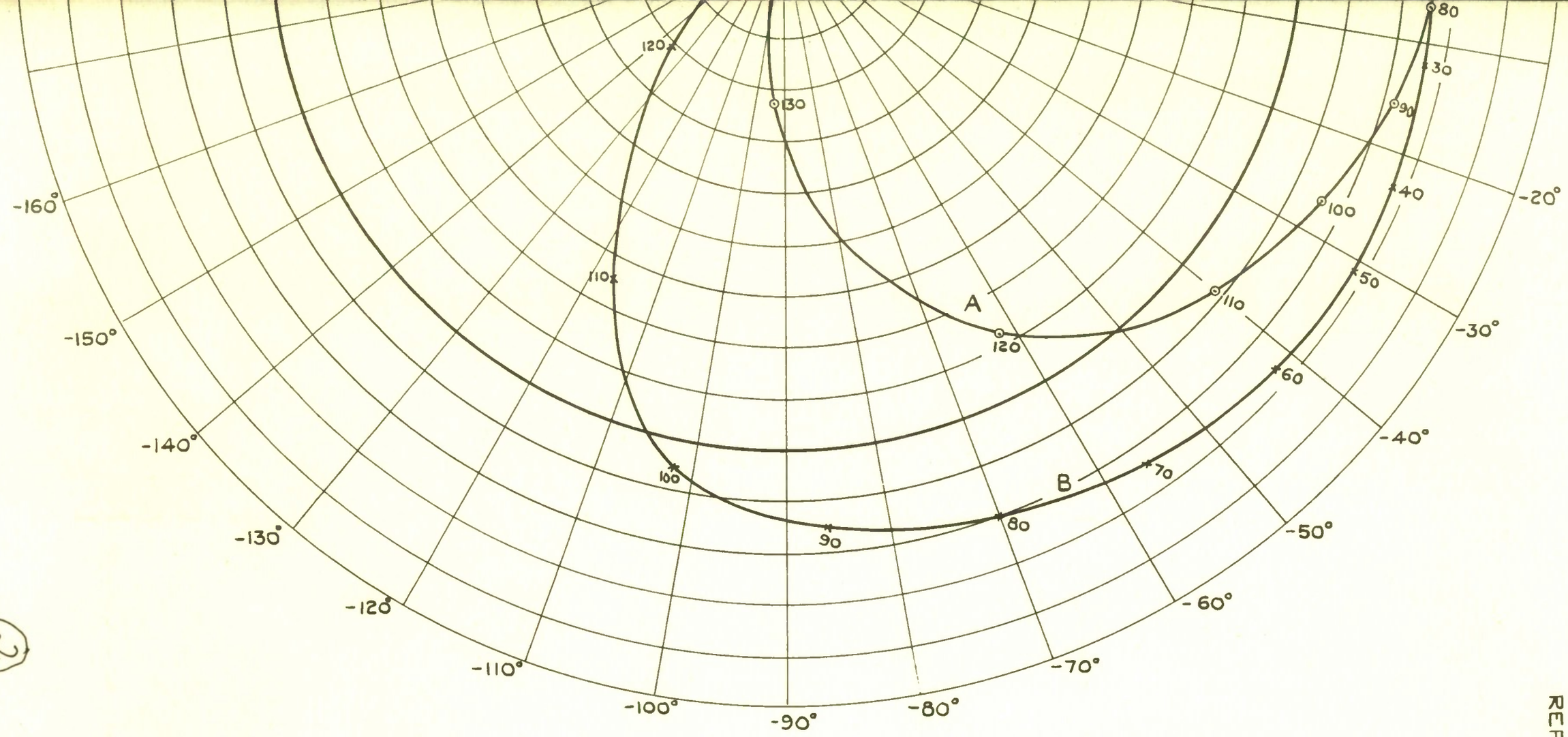

FIG.30. LOCI SHOWING THE VARIATION WITH TIME OF THE FEEDBACK GAIN & PHASE AT FUNDAMENTAL BENDING FREQUENCY OF WELDED BODY.
(SEE TABLE 2.)

REPORT G.W.24.
FIG.30.

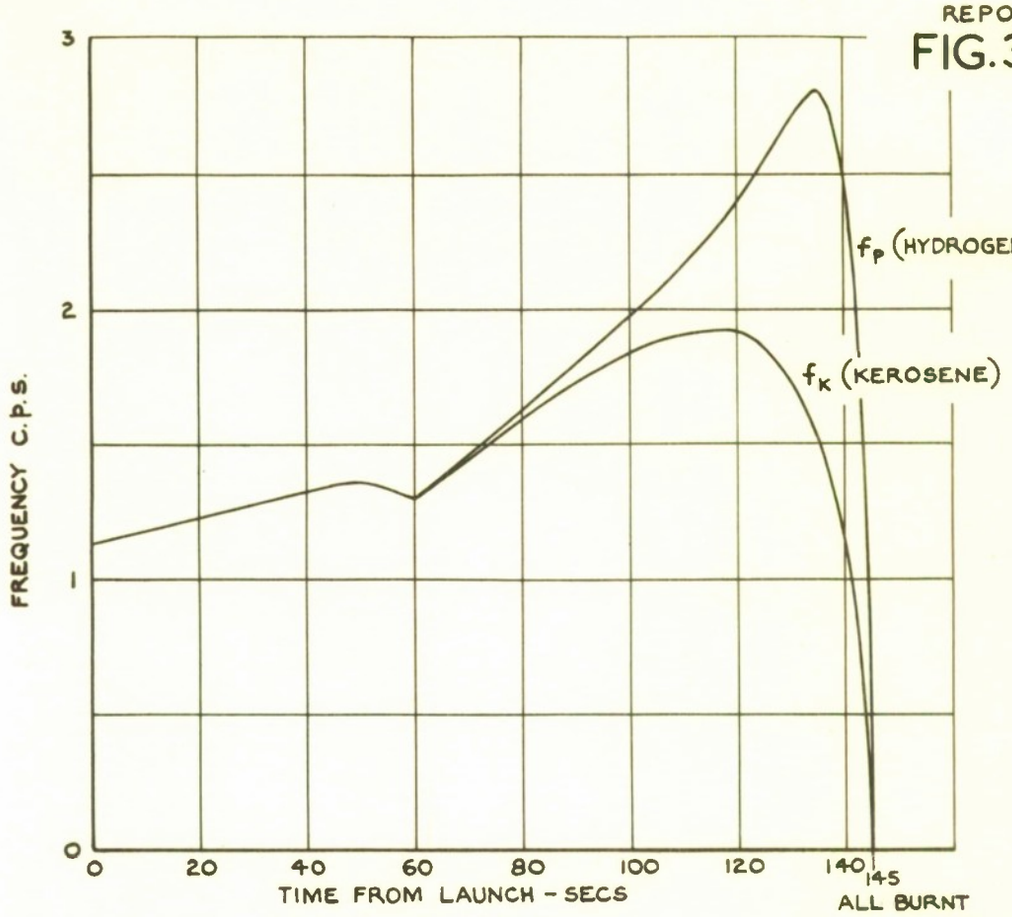

FIG. 31. VARIATION WITH TIME OF FUNDAMENTAL PROPELLENT SLOSHING FREQUENCIES.

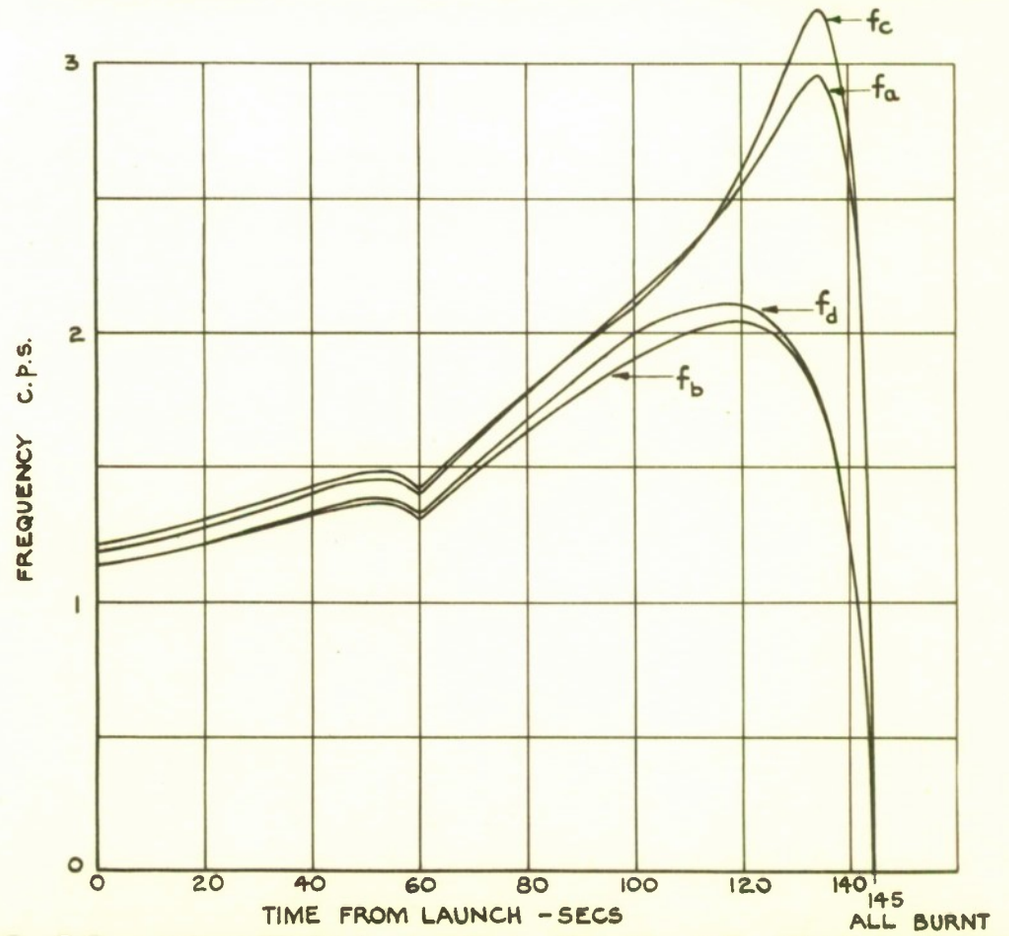

FIG. 32. VARIATION WITH TIME OF FREQUENCIES f_a, f_b, f_c AND f_d AT WHICH THE MISSILE TRANSFER FUNCTION, INCLUDING PROPELLENT SLOSHING, HAS POLES AND ZEROS.

FIG. 33.

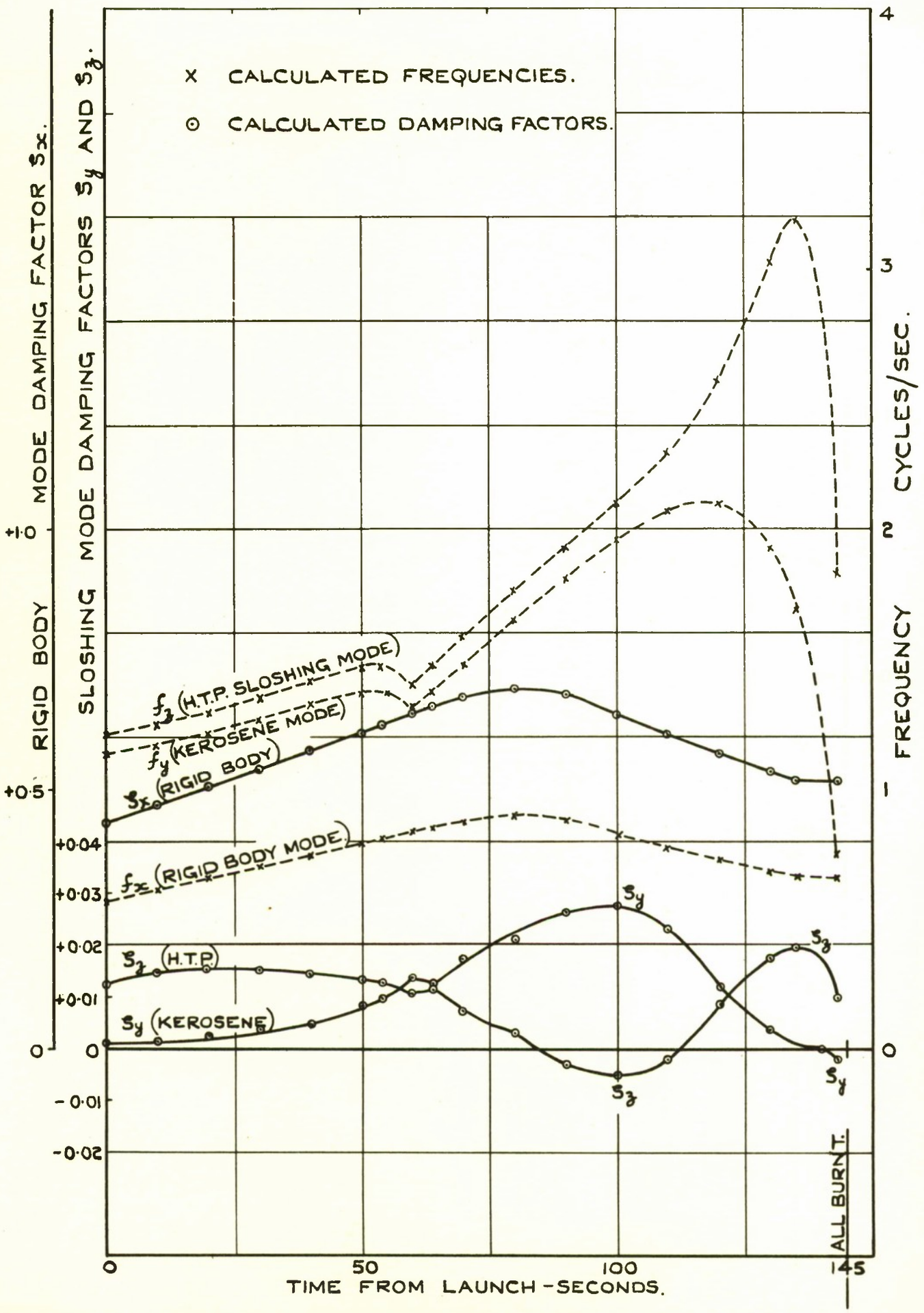

FIG. 33. VARIATION OF FREQUENCIES & DAMPING FACTORS ASSOCIATED WITH PROPELLENT SLOSHING UNDER CLOSED LOOP CONDITIONS, NEGLECTING COMPONENT LAGS.

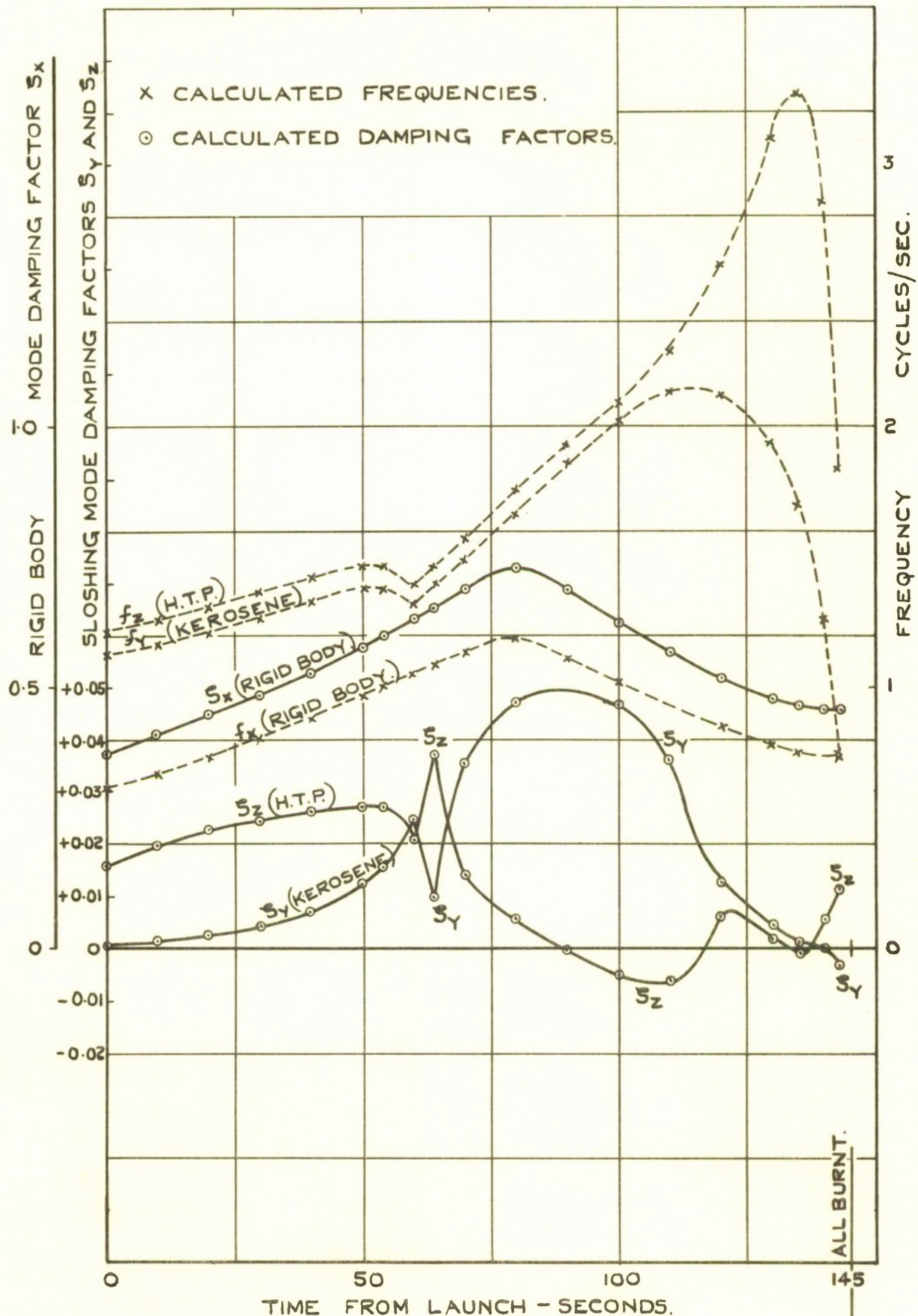

FIG.34. VARIATION OF FREQUENCIES & DAMPING FACTORS ASSOCIATED WITH PROPELLENT SLOSHING UNDER CLOSED LOOP CONDITIONS INCLUDING EFFECT OF COMPONENT LAGS.

GAIN FACTORS $K_1 K_3 K_6 = 1{\cdot}7$ AND $K_1 K_3 K_7 = 0{\cdot}1$.

CURVE A — ½° SERVO AMPLITUDE, t > 120 SEC.
CURVE B — 1° SERVO AMPLITUDE, t > 120 SEC.
CURVE C — 5° SERVO AMPLITUDE, t > 120 SEC.
CURVE D — ½° SERVO AMPLITUDE, t = 50 SEC.
FREQUENCIES IN CYCLES / SEC.

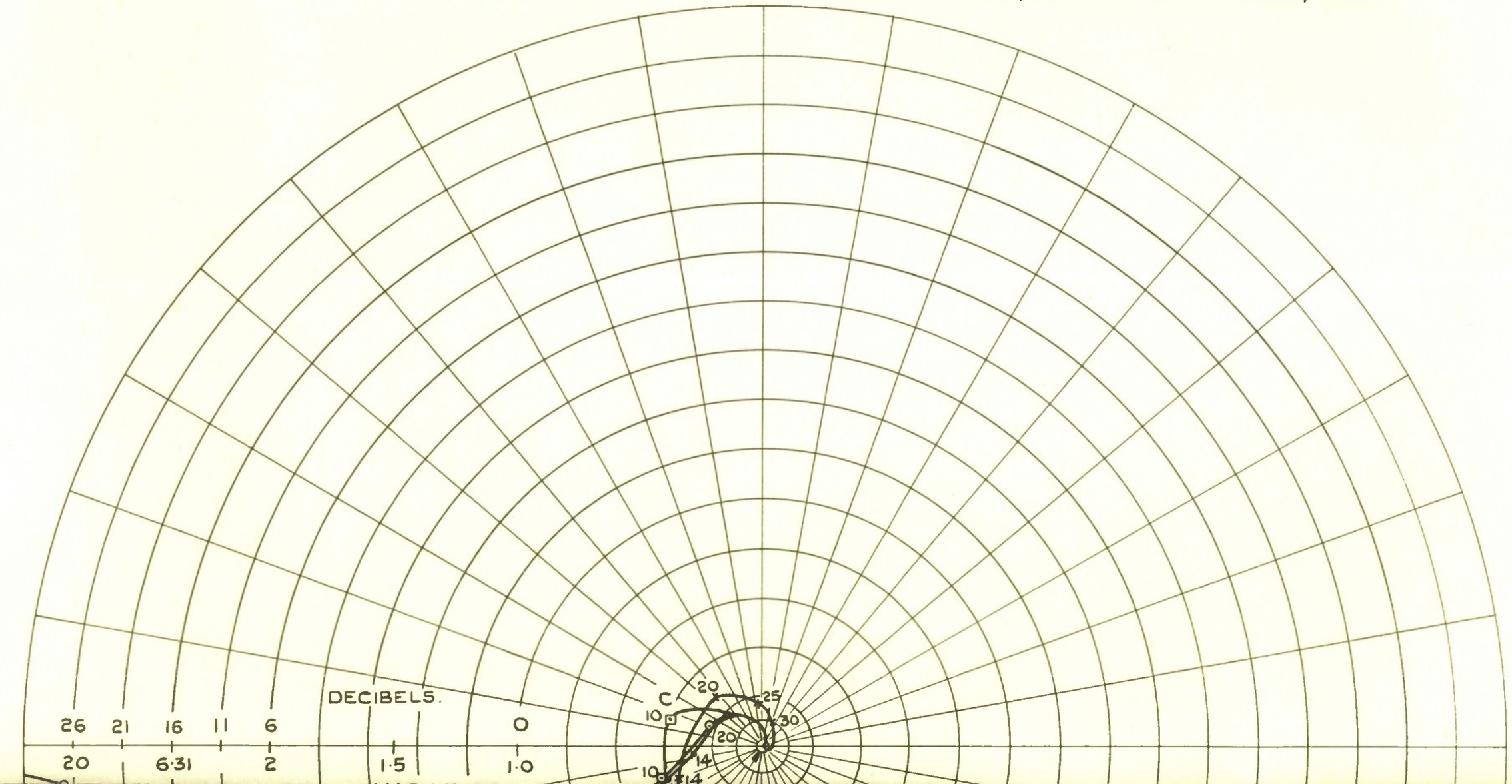

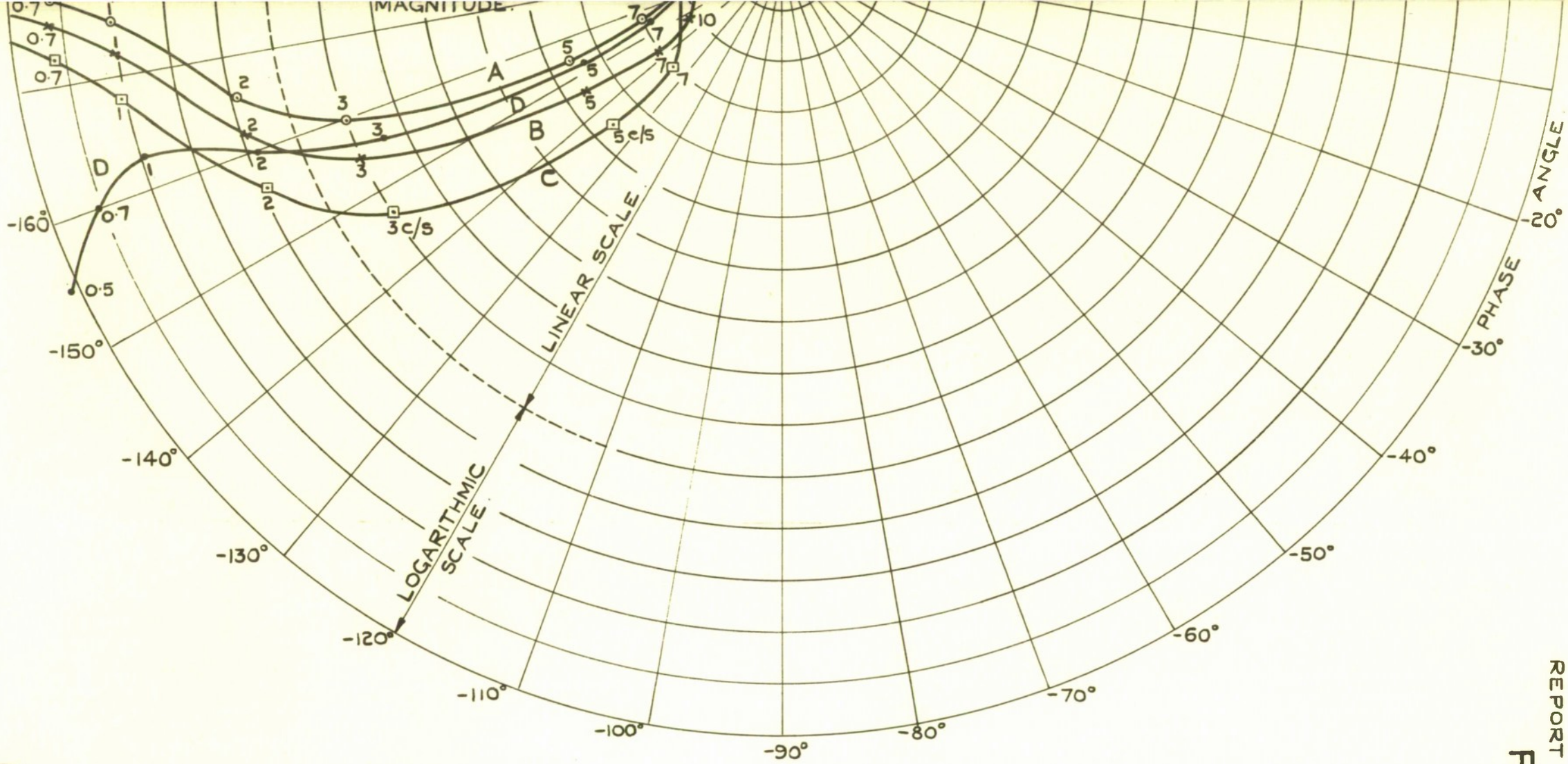

REPORT G.W. 24.

FIG. 35.

FIG. 35. NYQUIST DIAGRAMS OF THE RIGID BODY ROLL STABILISATION SYSTEM.

GAIN FACTORS $K_1K_3K_6 = 1{\cdot}7$ AND $K_1K_3K_7 = 0{\cdot}1$.

$\frac{1}{2}^\circ$ SERVO AMPLITUDE $t > 120$ SEC.

CURVE A —o— WITHOUT FILTER.
CURVE B —x— WITH LOW PASS FILTER IN PHASE ADVANCE CIRCUIT. (TIME CONSTANTS 1 AND 3 MILLISECONDS.)

G.W/P 9943.

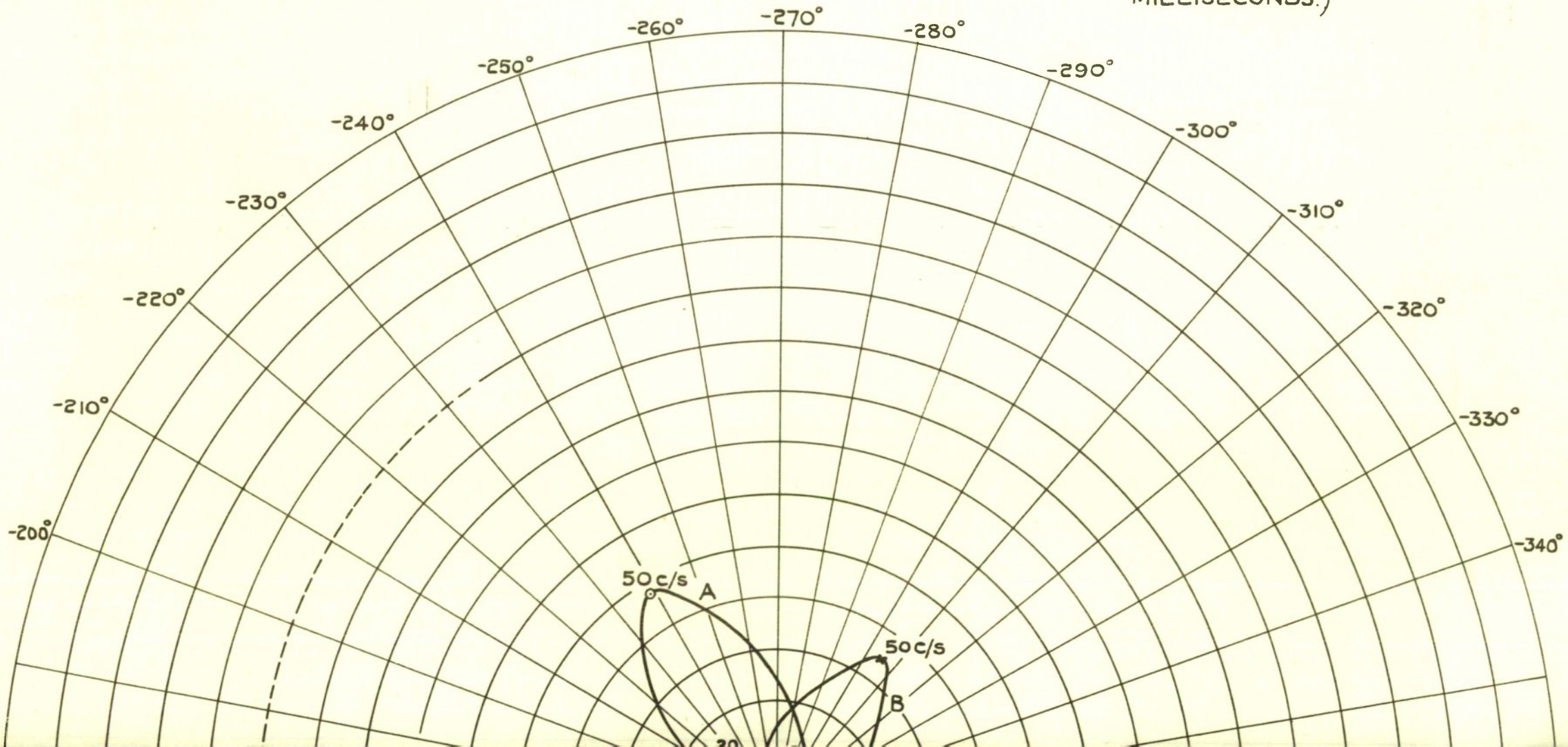

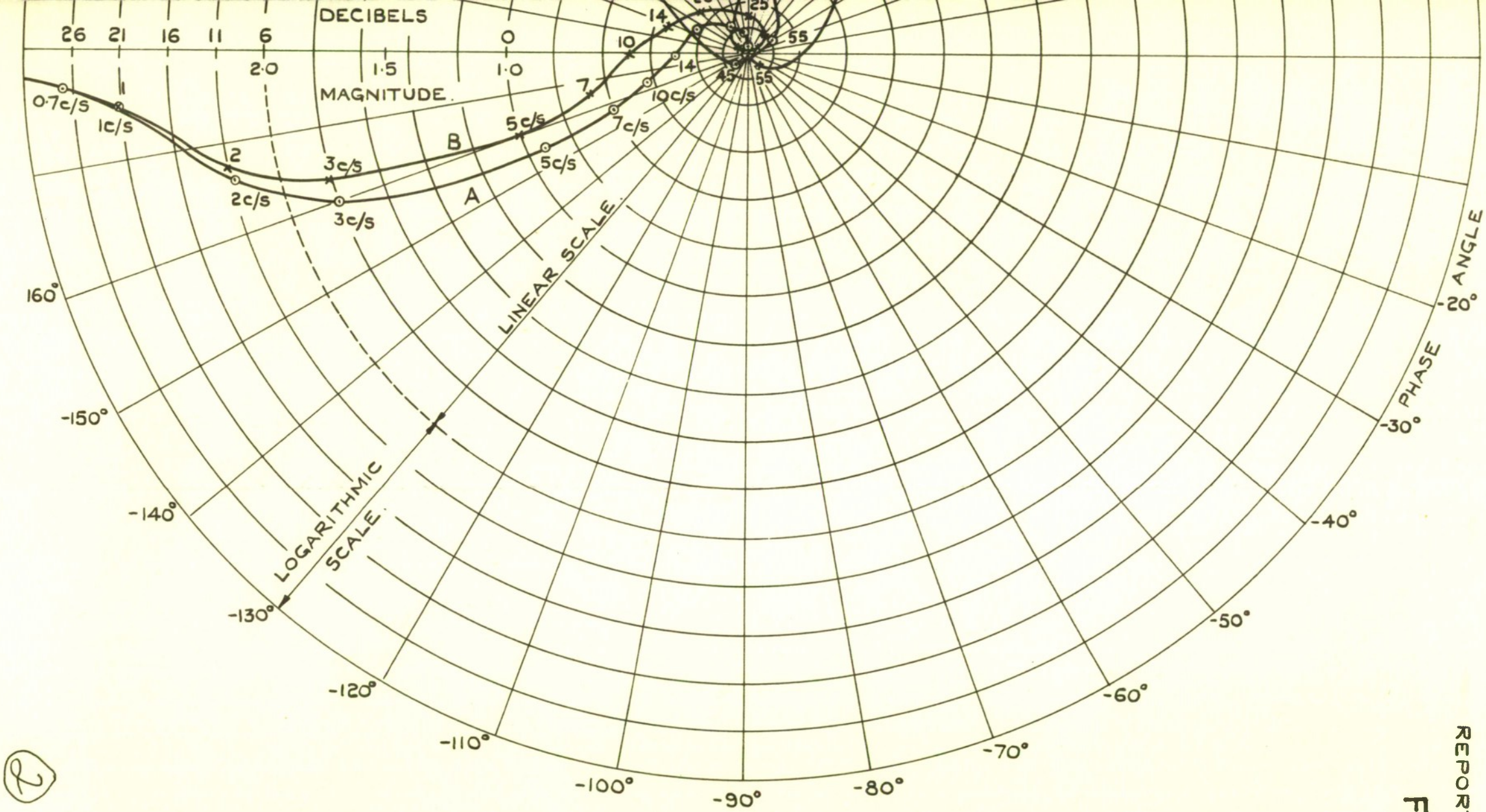

(2)

FIG. 36. NYQUIST DIAGRAMS OF THE ROLL STABILISATION SYSTEM INCLUDING ORIGINAL ESTIMATE OF FUNDAMENTAL TORSIONAL MODE.

REPORT G.W.24.

FIG. 36.

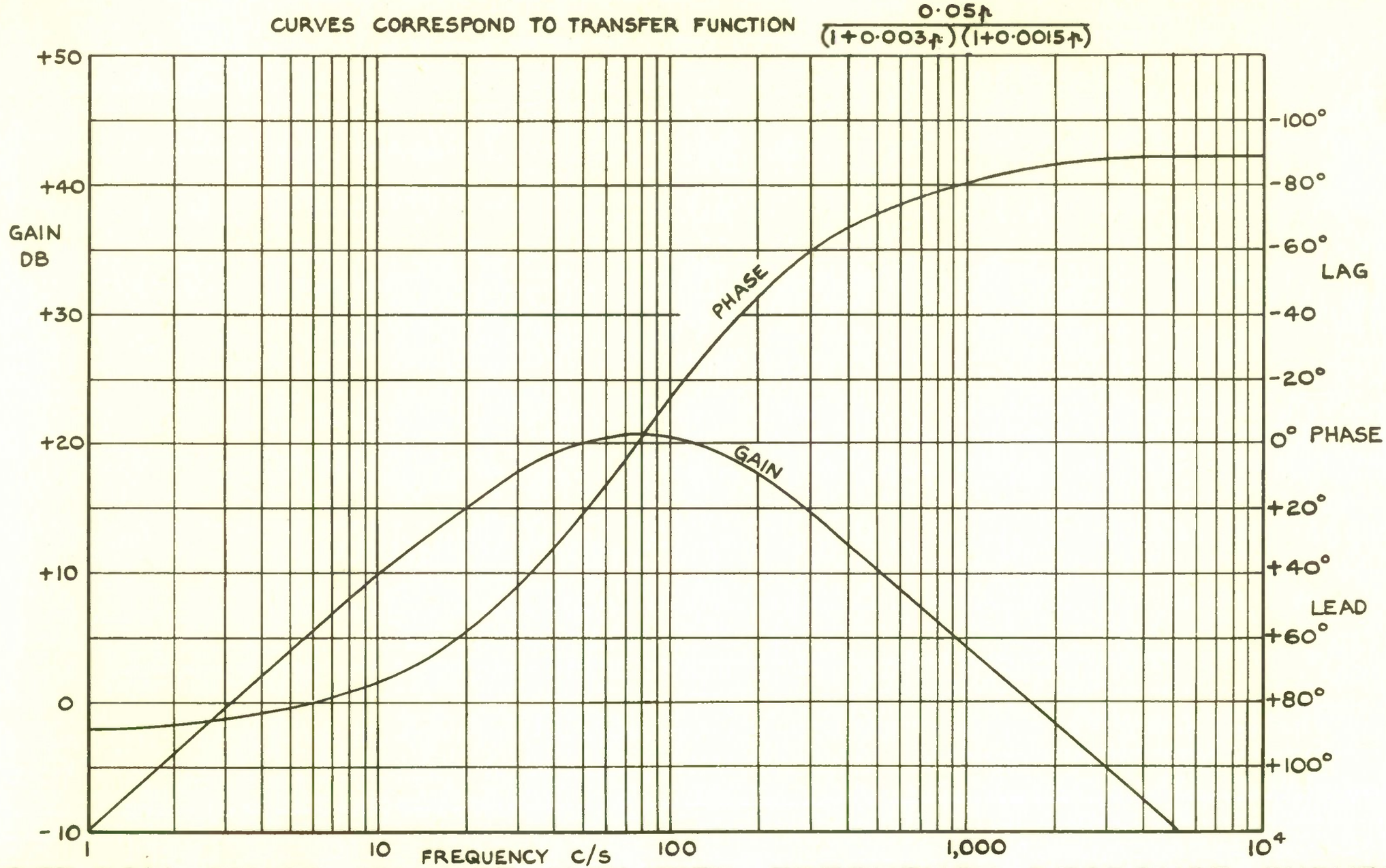

FIG.37. ROLL PHASE ADVANCE AMPLIFIER FREQUENCY RESPONSE CURVES.

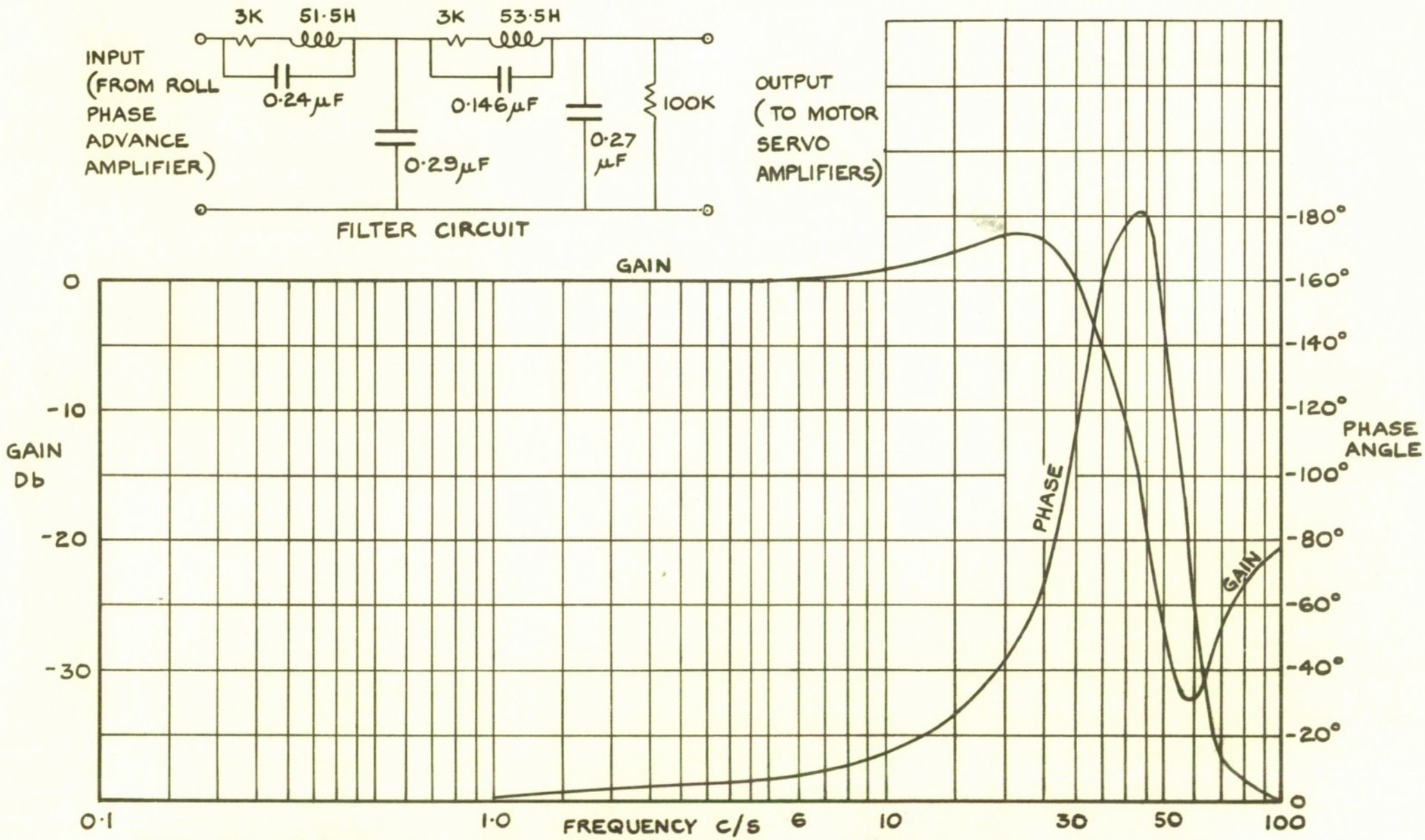

FIG. 38. CIRCUIT AND FREQUENCY RESPONSE CURVES OF TWO STAGE LC LOW-PASS FILTER.

GAIN FACTORS
$K_1 K_3 K_6 = 0.8$
$K_1 K_3 K_7 = 0.1$
$\frac{1}{2}°$ SERVO AMPLITUDE
$t > 120$ SEC.

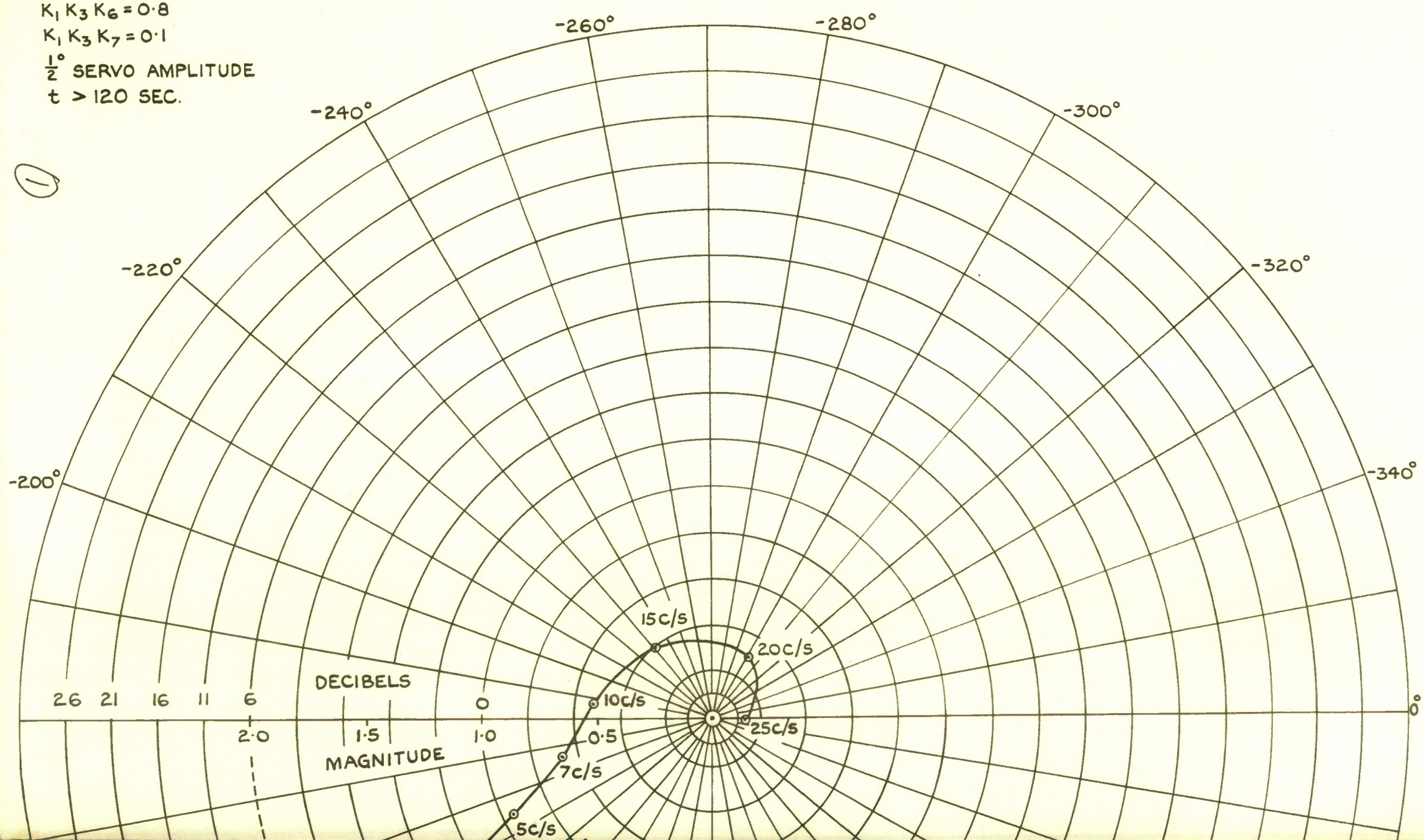

GW/P. 9946.

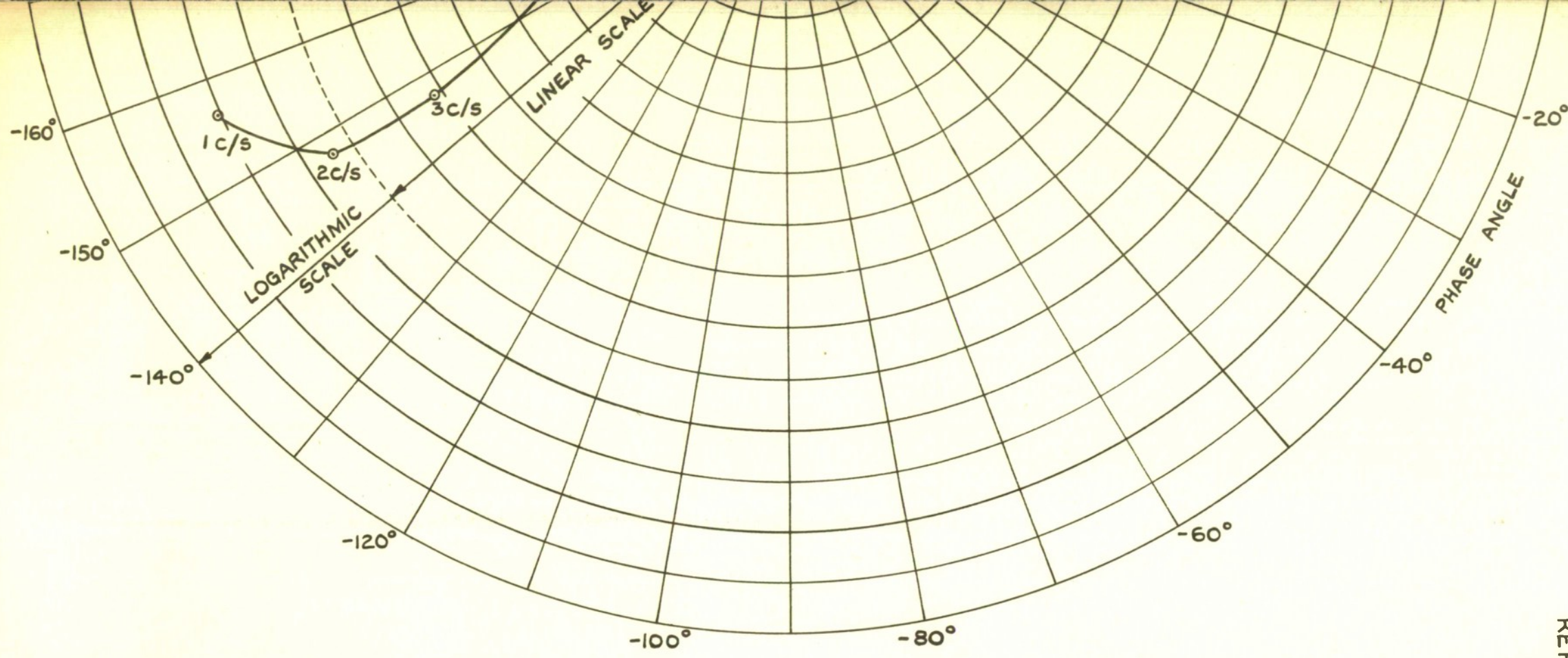

FIG. 39. NYQUIST DIAGRAM OF THE ROLL STABILISATION SYSTEM INCLUDING TWO-STAGE LC FILTER.

REPORT G.W. 24.
FIG. 39.

(2)

Information Centre
Knowledge Services
[dstl] Porton Down
Salisbury
Wilts
SP4 0JQ
22060-6218
Tel: 01980-613753
Fax 01980-613970

Defense Technical Information Center (DTIC)
8725 John J. Kingman Road, Suit 0944
Fort Belvoir, VA 22060-6218
U.S.A.

AD#: AD324796

Date of Search: 11 December 2008

Record Summary: DSIR 23/28861
Title: The BLACK KNIGHT test vehicle control system (RAE REP GW24)
Availability Open Document, Open Description, Normal Closure before FOI Act: 30 years
Former reference (Department) ARC 23024
Held by The National Archives, Kew

This document is now available at the National Archives, Kew, Surrey, United Kingdom.

DTIC has checked the National Archives Catalogue website (http://www.nationalarchives.gov.uk) and found the document is available and releasable to the public.

Access to UK public records is governed by statute, namely the Public Records Act, 1958, and the Public Records Act, 1967.
The document has been released under the 30 year rule.
(The vast majority of records selected for permanent preservation are made available to the public when they are 30 years old. This is commonly referred to as the 30 year rule and was established by the Public Records Act of 1967).

This document may be treated as UNLIMITED.